Journal of Advanced Ceramics
2021, **10**(5): 885–932
https://doi.org/10.1007/s40145-021-0528-4

ISSN 2226-4108
CN 10-1154/TQ

Review

The latest process and challenges of microwave dielectric ceramics based on pseudo phase diagrams

Hongcheng YANG[a,b], Shuren ZHANG[a,b], Hongyu YANG[a,b], Qingyu WEN[a,b], Qiu YANG[a,b], Ling GUI[a,b], Qian ZHAO[a,b], Enzhu LI[a,b,*]

[a]*National Engineering Research Center of Electromagnetic Radiation Control Materials, University of Electronic Science and Technology of China, Chengdu 610054, China*
[b]*Key Laboratory of Multi-Spectral Absorbing Materials and Structures of Ministry of Education, University of Electronic Science and Technology of China, Chengdu 610054, China*

Received: April 28, 2021; Revised: June 4, 2021; Accepted: June 6, 2021

Abstract: The explosive process of 5G communication evokes the urgent demand of miniaturized and integrated dielectric ceramics filter. It is a pressing need to advance the development of dielectric ceramics utilization of emerging technology to design new materials and understand the polarization mechanism. This review provides the summary of the study of microwave dielectric ceramics (MWDCs) sintered higher than 1000 ℃ from 2010 up to now, with the purpose of taking a broad and historical view of these ceramics and illustrating research directions. To date, researchers endeavor to explain the structure–property relationship of ceramics with multitude of approaches and design a new formula or strategy to obtain excellent microwave dielectric properties. There are variety of factors that impact the permittivity, dielectric loss, and temperature stability of dielectric materials, covering intrinsic and extrinsic factors. Many of these factors are often intertwined, which can complicate new dielectric material discovery and the mechanism investigation. Because of the various ceramics systems, pseudo phase diagram was used to classify the dielectric materials based on the composition. In this review, the ceramics were firstly divided into ternary systems, and then brief description of the experimental probes and complementary theoretical methods that have been used to discern the intrinsic polarization mechanisms and the origin of intrinsic loss was mentioned. Finally, some perspectives on the future outlook for high-temperature MWDCs were offered based on the synthesis method, characterization techniques, and significant theory developments.

Keywords: high-temperature microwave dielectric ceramics (MWDCs); pseudo phase diagram; developments and challenges; composition–structure–property relationship

1 Introduction

Over the past half century, semiconductor integration technology has become one of the most far-reaching and significant technological innovations in human society. The rapid development of this technology has enabled mankind to enter today's information society. However, semiconductor devices as active devices are only part of the electronic components. Another part of

* Corresponding author.
E-mail: lienzhu@uestc.edu.cn

the huge amount and a wide variety of components with different functions are passive devices. The core materials of these components are various types of functional ceramic materials. Microwave dielectric ceramics (MWDCs) are the pivotal component of a passive device, which are mainly used as filters, resonators, RF antennae, frequency discriminators in electronic countermeasures, navigation, radar, home satellite live television receivers, and hand-held mobile phones. The applications of MWDCs in different frequency are directly plotted in Fig. 1. However, the development of microwave ceramics had gone through a sluggish procession because of the lack of suitable materials for dielectric resonator. The discovery of rutile (also known as titanium dioxide ceramics) in the 1970s makes it possible to synthesis dielectric resonator [1]. Various literature has been reported to explore the potential candidates of MWDCs after that, from single oxide, binary oxide, to ternary oxide. According to the data in the Web of Science, over 1000 papers were published about MWDCs around the world after 2000. Figure 2 presents the trend of published papers where more than 30% of investigations belong to China.

To evaluate the dielectric properties of ceramics, the relative permittivity (ε_r), dielectric loss (loss tangent or quality factor ($Q\times f$ value)), and temperature coefficient of resonant frequency (τ_f) are the three pivotal characteristics. As early as in 2006, the direction of development of microwave dielectric materials has been highlighted by Ohsato *et al*. [2], including high Q and low ε_r ceramics for millimeter-wave application, high Q and high ε_r ceramics for base station, and high ε_r ceramics for miniaturization of mobile phone. Up to now, researchers have explored hundreds of ceramics to enrich the database of MWDCs, but only a dozen of those ceramics with unique properties have been commercially used to fabricate relevant devices because most of the ceramics lack stability or generate large loss in the electronic components. Booming development of millimeter technology and 5G communication have rendered a new round of requirement of MWDCs of low permittivity with a stable dielectric loss in the scope

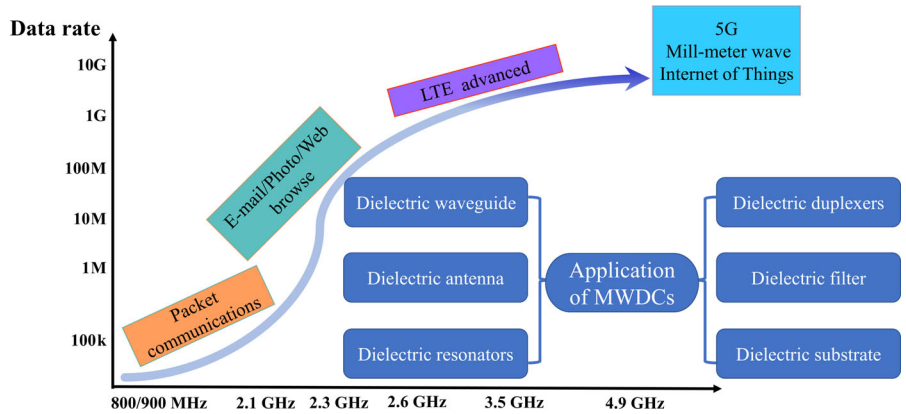

Fig. 1 Applications of MWDCs in different frequencies.

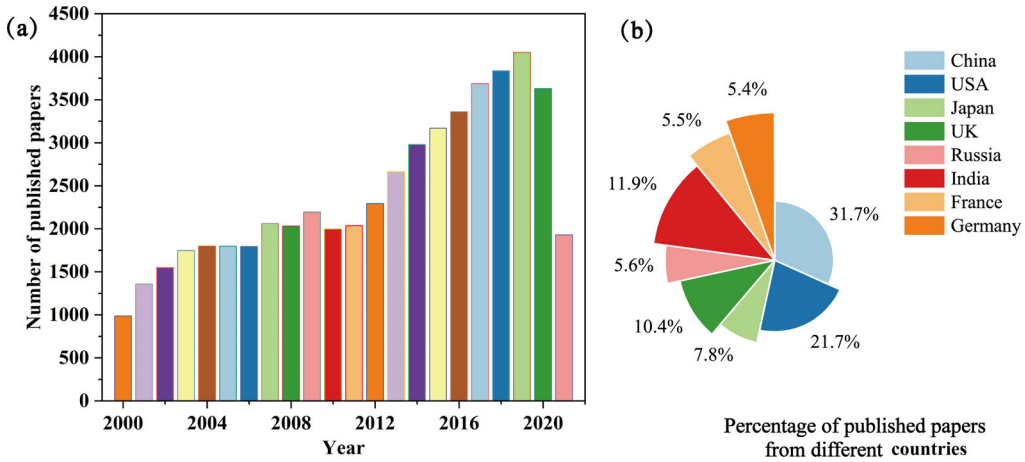

Fig. 2 (a) Number of published papers about MWDCs from 2000 and (b) percentage of published papers from different countries.

of frequency up to 100 GHz. Especially, the emergency of COVID-19 makes video conferencing and telecommuting as a daily part in our lives. Consequently, the unprecedented growth of global data volume and huge demand for high data rates urge researchers to search more alternative materials for commercial electronic market. It is also a very significant issue for the industry to yield ceramics with ultra-low permittivity which are suitable for 5G and 6G communication system. However, it is still a "try and error" state in our experiments for discovering materials or optimizing the properties of the reported ceramics. The main difficulty in the development of MWDCs is to understand the fundamental relationship of composition–structure–property and draw general trends throughout the field, after normalizing and comparing the various results. Despite long-term sustained attempts, there is no systematic or comprehensive theory which can provide common guidance in the experiments and drive currently reported ceramics toward commercialization applications.

With the exploration of MWDCs clusters and the development of modern experiment techniques, investigations about MWDCs have been largely scoped by the designs and search for new systems and reoptimizing their properties. It is paramount that an MWDCs candidate has an appropriate dielectric constant, low dielectric loss, and near-zero temperature coefficient of resonant frequency for applications. Generally, to tune the microwave dielectric properties, there are two parts that should be taken into consideration (extrinsic and intrinsic parts). Extrinsic part is usually regarded as the influence originated from the synthesis method and raw materials. MWDCs usually prepare by solid state reaction method, and the sintering conditions directly influence the microstructure and compactness of ceramics, which subsequently affect the microwave dielectric properties. Meanwhile, the selectivity of size distribution, purity, non-stoichiometric ratio, species of different compounds, and pretreatment of raw materials based on their physical and chemical properties are crucial for reaching optimal microwave dielectric properties. For example, the procedures to reduce pores are designed for ceramics containing the volatile element, evolving non-stoichiometric ratio in the chemical formula, and providing the compensation atmosphere of volatile element. The relevant attempts are mostly discussed for the rock salt structure ceramics such as $Li_2Mg_3TiO_6$. Besides, various synthesis methods, namely sol–gel method, sink plasma sintering method, and high energy ball-milling method are gradually used for preparing the MWDCs, and numbers of studies analyze the discrepancy of microwave dielectric properties obtained with different methods. The intrinsic part stems from anharmonic lattice vibration, which primarily generates large dielectric loss. As yet, there is no technology or theory that could feasibly adjust the anharmonic lattice vibration to reduce dielectric loss. In the experiment, after carefully controlling the sintering conditions and selecting raw materials, the most pragmatic approach to optimize the properties is cation substitution with the consideration of the radii and the electronegativity of cations, contributing to reducing the dielectric loss or modifying the temperature coefficient of resonant frequency. Near-zero temperature coefficient of resonant frequency is also obtained by designing co-exited phase system with introduction of two ceramics with opposite τ_f values, but the composite ceramics may lead to a poor $Q\times f$ value. More recently, the strategy of tri-layer structures of $Zn_{1.01}Nb_2O_6/TiO_2/Zn_{1.01}Nb_2O_6$ [3], $MgTiO_3/TiO_2/MgTiO_3$ [4], and $Zn_3Nb_2O_8/TiO_2/Zn_3Nb_2O_8$ [5] were verified as a method to obtain the temperature-stable ceramics with low dielectric loss.

Currently, the database of MWDCs is enriched by insightful information about the structure and properties, and the growing number of literature converts from description of phenomena to explanation of the theoretical mechanism of the dielectric materials. Thorough and comprehensive investigation of ceramics is gradually presented to estimate the extrinsic and intrinsic influence on the microwave dielectric properties. For instance, the common discussion of polarization mechanism is usually based on the ionic polarization, where the Clausius–Mossotti (C–M) equation is applied to evaluate the discrepancy of theoretical ε_r and measured ε_r. The popularization of Rietveld-refinement in the literature supports the analysis of lattice parameters, packing fraction, and chemical bond characteristic obtained by the complex chemical bond theory (P–V–L) theory. Especially, disassembling the crystal into the sum of sample binary compound based on the crystal parameters and coordinate numbers of each ions [6], the investigations about application of P–V–L theory into multi-type structure emerge in abundance. The origin of dielectric loss is quantified by lattice vibrational spectroscopy, and the contribution of each chemical bond to the microwave dielectric

properties is verified by P–V–L theory. For some unique ceramics, researchers bend themselves to exploring the underlying mechanism for the observed phenomenon. The influence of long-range movement of charged defects in the grain and grain boundary was estimated by the impedance analysis, terahertz (THz) time-domain spectroscopy analysis, and the electron paramagnetic resonance spectra, which can explain the defect generation mechanism in doped $Li_2ZnTi_3O_8$ ceramics. The analysis of disordered–ordered crystal structure evolution and super-lattice in rock salt ceramics and complex perovskite ceramics gives evidence to explain the ultra-low dielectric loss. Both the development of experimental and theoretical method allows us to summarize the relevant experimental probes of different systems and propose the challenges and prospects of MWDCs.

While many great review and perspective articles have been published about MWDCs, they have finished the review by classified MWDCs based on the criteria of sintering temperature, dielectric constant, and crystal structure [1,7–9]. Furthermore, the early works before 2010 are mainly concentrated on the description of phase composition, micrographic images, and variation of microwave dielectric properties. The topic about the MWDCs sintered lower than 950 ℃ is especially focused owing to the advantages of low-temperature co-fired ceramics (LTCC) technology where this approach guarantees the integration of electronic components. Considering either the timespan or topic covered, the mentioned ceramics, in this review, are all sintered higher than 1000 ℃. The LTCC system including ceramics with a few sintering aids, glass–ceramics system, or glass-free system is not referred. To follow the development of new analysis methods, MWDCs, beginning with the first reported properties and upgrading the relevant references after 2010, were included. Additionally, because of so various structures and properties of MWDCs, pseudo phase diagram was used to classify the ceramics according to the composition, which will serve as the basis and link for each pseudo phase diagram of diversity composition. The organization of this review consists of a brief section detailing the phase evolution or structure transformation of oxide ceramics in the designed pseudo phase diagram, and then the chronological experimental probes for a unique system are summarized.

2 Phase diagram

The phase diagram is a visual representation of the phase equilibrium, which defines the composition of multiphase system. It is an efficient and convenient technique to analyze the composition and their proportion, which plays a significant role in guiding the research and exploration of materials to reduce the manpower and material resources effectively. This section provides a broad context by summarizing the ceramics system based on pseudo phase diagram, and all the composition in the following pseudo phase diagram is in molar ratio. The endpoint of each pseudo phase diagram contains more than one component, and the labelled ceramics are the primary system reported by researchers. The summary of investigations in the same general formal is listed in detail.

2. 1 Silicate and germanate

There is a low ε_r (< 10) for silicates, owing to the low ionic polarizability of Si^{4+} and half covalent bond in Si–O. In the binary silicate, the $CaSiO_3$, Mg_2SiO_4, Zn_2SiO_4, and Re_2SiO_5 are the main representatives, where $CaSiO_3$ usually appeared as the crystalized phase in $CaO–B_2O_3–SiO_2$ glass. Ternary silicate such as diopside-type $CaMgSi_2O_6$, melitile-type $A_2BC_2O_7$ and $AB_2C_2O_7$ (A = Sr, Ca, Ba; B = Mg, Zn, Co, Mn, Cu), and cuspidine-type $Ca_3SnSi_2O_9$ were highlighted by researchers, due to the diverse crystal structures in those systems. With the wake of exploration of new ceramics, the germanate gradually occurred as a candidate material with low dielectric loss despite of the expensive cost of GeO_2 as raw material. The pseudo phase diagram of the silicate and germanate is presented in Fig. 3, where the primary phases of binary and ternary silicate and germanate are listed in the phase diagram.

2.1.1 Binary silicate ceramics

Synthesis of dense SiO_2 ceramic is challengeable because of its complexity in polymorphs and phase transitions. Until 2012, microwave dielectric properties of SiO_2 ceramic were reported as $\varepsilon_r \approx 3.81$, $Q \times f$ value ≈ 80,400 GHz, and $\tau_f \approx -16.1$ ppm/℃, sintered at 1650 ℃ for 3 h [10]. After that, Li *et al*. [11] illustrated that $0.84SiO_2–0.16TiO_2$ composite ceramics possessed satisfied properties of $\varepsilon_r \approx 5.91$, $Q \times f$ value ≈ 39,680 GHz, and $\tau_f \approx -4.5$ ppm/℃, sintered at 1275 ℃ for 3 h.

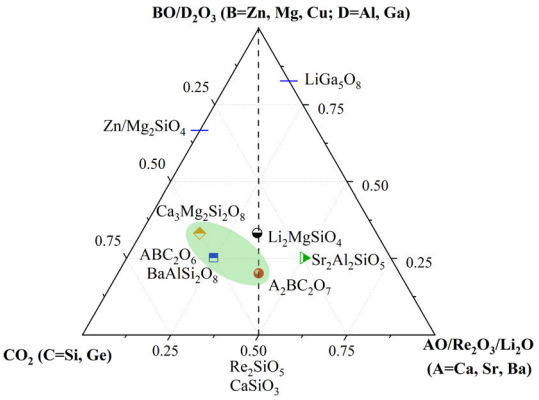

Fig. 3 Pseudo phase diagram of the silicate and germinate.

Comparing to the difficulty of preparing compact SiO_2 ceramic, the restriction of preparing dense $CaSiO_3$ ceramic stemmed from the narrow sintering temperature range of pure $CaSiO_3$ and the porous microstructure [12]. Commonly, $CaSiO_3$ was reported as a main phase in the $CaO–B_2O_3–SiO_2$ glass–ceramic system, which primarily determined the properties. There are two main phases of $CaSiO_3$, containing low-temperature wollastonite (α-$CaSiO_3$) and high-temperature preudo-wollastonite (β-$CaSiO_3$). Through a sol–gel method, the microwave dielectric properties of α-$CaSiO_3$ are: $\varepsilon_r \approx 6.69$, $Q\times f$ value ≈ 25,398 GHz, sintered at 1320 ℃ [13]. In order to improve the microwave dielectric properties, $(Ca_{1-x}Mg_x)SiO_3$ ceramics with x = 0.1, 0.5, 0.9 were verified as single phases, and properties of $\varepsilon_r \approx 6.49$, $Q\times f$ value ≈ 62,420 GHz, and $\tau_f \approx –43.3$ ppm/℃ were obtained when sintered at 1320 ℃ with x = 0.1 [14]. Besides, the investigation of $CaSiO_3–Al_2O_3$ ceramics revealed that the secondary phases of $Ca_2Al_2SiO_7$ and $CaAl_2Si_2O_8$ would deteriorate the microwave dielectric properties with excessive Al_2O_3 [15,16]. According to Hu *et al*. [17], the phase transformation of $CaSiO_3$ was inhibited with the increase of SiO_2 content, and α-$CaSiO_3$–2 wt% Al_2O_3–2.5 wt% TiO_2 shows excellent properties of $\varepsilon_r \approx 7.88$, $Q\times f$ value ≈ 24,412 GHz, and $\tau_f \approx –0.52$ ppm/℃ [18]. To obtain compact ceramics, SnO_2-doped α-$CaSiO_3$ ceramics with $\varepsilon_r \approx 9.27$, $Q\times f$ value ≈ 53,000 GHz, and $\tau_f \approx –52$ ppm/℃ sintered at 1450 ℃ were reported in a relative density higher than 97% [19].

With a $Q\times f$ value larger than 100,000 GHz, another class of binary silicate can be written as A_2SiO_4 (A = Ba, Sr, Ca, Mg, Zn) [20–23]. Forsterite Mg_2SiO_4 is extensively explored because of its superior microwave dielectric properties ($\varepsilon_r \approx 7.8$, $Q\times f$ value ≈ 240,000 GHz, and $\tau_f \approx –67$ ppm/℃, sintered at 1450–1500 ℃) [2,24,25]. Nevertheless, the high sintering temperature and large τ_f value inhibit its application. To adjust τ_f value, both co-exited phase of $Mg_2SiO_4–Ca_{0.9}Sr_{0.1}TiO_3$ [26] and $Zn_2SiO_4–TiO_2$ [27] contributed to a near-zero τ_f value. Melting CuO could enhance the sintering procession of Zn_2SiO_4, and the quality factor reached 105,500 GHz when sintered at 1150 ℃ [28]. Zn-deficient formula was verified valid to suppress the formation of secondary phase in Zn_2SiO_4 ceramics, and $Zn_{1.8}SiO_{3.8}$ was estimated with properties of $\varepsilon_r \approx 6.451$, $Q\times f$ value ≈ 102,807 GHz, and $\tau_f \approx –32$ ppm/℃, sintered at 1300 ℃ [29].

After predicting the permittivity of $ZrO_2–SiO_2$, $HfO_2–SiO_2$, $La_2O_2–SiO_2$, and $Y_2O_3–SiO_2$, those systems were clarified as an alternative of dynamic random access memory capacitor dielectric materials [30]. The exploration of properties of Sm_2SiO_5 and Nd_2SiO_5 ceramics compensated the absence of study on microwave dielectric properties of $Re_2O_3–SiO_2$, where the microwave dielectric properties were listed as $\varepsilon_r \approx 8.44$, $Q\times f$ value ≈ 64,000 GHz, and $\tau_f \approx –37$ ppm/℃ and $\varepsilon_r \approx 7.94$, $Q\times f$ value ≈ 38,800 GHz, and $\tau_f \approx –53$ ppm/℃ with the molar ratio of Re_2O_3/SiO_2 = 1:1.05, respectively [31,32].

2.1.2 Ternary silicate and germanate ceramics

Clinopyroxene-type ABC_2O_6 (A = Ca; B = Co, Mg, Zn, Fe; C = Si, Ge) materials, akermanite-type $A_2BC_2O_7$ (A = Sr, Ca; B = Mg, Zn, Co, Mn; C = Si, Ge), and melilite-type $A_2BSi_2O_7$ (A = Sr, Ca, Ba; B = Mg, Zn, Co, Mn, Cu) occupied the primary family of ternary silicate ceramics. Increasing attention has been paid for $CaMgSi_2O_6$ owing to its low permittivity ≈ 7.5, which is suitable to be substrate [14,33–35]. Both the substitution of Zn^{2+}, Co^{2+}, Cu^{2+}, Mn^{2+} for Mg^{2+} and introduction of Sr^{2+} into Ca^{2+} of $CaMgSi_2O_6$ were benefit for reducing the dielectric loss. Microstructure with many pores of $CaMnSi_2O_6$ was observed by Chen *et al*. [36], and the effect of porosity on the properties was investigated by spherical-pore model. Akermanite-type $A_2BC_2O_7$ (A = Sr, Ca; B = Mg, Zn, Co, Mn; C = Si, Ge) systems belong to the structure group of $P\bar{4}21m$ (113) in tetragonal, while melilite-type $A_2BC_2O_7$ (A = Ba; B = Co, Zn, Cu, Mg; C = Si, Ge) and $AB_2C_2O_7$ (A = Ba; B = Co, Zn; C = Si, Ge) systems were clarified in monoclinic structure [37–44]. The literature about the effect of structure evolution and chemical bond parameters in $A_2BSi_2O_7$ and $AB_2Si_2O_7$ represented that

the Si–O bond played the significant role in structural stability and dielectric polarization.

The monoclinic $Ca_3SnSi_2O_9$ and $Ca_3MgSi_2O_8$ with space group $P2_1/c$ were investigated to supplement the compound of ternary silicate oxides. $Ca_3SnSi_2O_9$ ceramics were obtained in a wide sintering temperature region from 1400 to 1525 ℃, with non-stoichiometric composition (molar ratio of Ca:Sn:Si = 1:1.2:1) as raw materials [45]. Single phase $Ca_3MgSi_2O_8$ possessed near 99% of the theoretical density after sintered at 1375 ℃, with $\varepsilon_r \approx 13.8$, $Q\times f$ value ≈ 27,000 GHz, and $\tau_f \approx -62$ ppm/℃ [46]. Sintering behavior and phase composition of gillespite-structured $MCuSi_4O_{10}$ (M = $Ba_{1-x}Sr_x$, $Sr_{1-x}Ca_x$) ceramics were established by Song *et al*. [47], and $SrCuSi_4O_{10}$ possessed microwave dielectric properties of $\varepsilon_r \approx 5.59$, $Q\times f$ value ≈ 82,252 GHz, and $\tau_f \approx -41.34$ ppm/℃. The first-principles calculation was applied to determine where Ni^{2+} and Li^+ would occupy in $BaAl_2Si_2O_8$ ceramics, and the change of bond strength and bond valence were analyzed [48,49].

The unpresented ternary silicate and germanate phase in pseudo phase diagrams are summarized as well in this section. The rare earth-based ternary silicate oxides, such as apatite with general formula $A_{10}(MO_4)_6O_2$ (A = alkaline earth, rare earth, Pb; M = Si, Ge, P, V), have received much attention since the apatite structure allowed numbers of substitutions at all the three sites. The lattice parameters and the local charge compensation of apatite type compounds were determined in 1972 [50], and those ceramics were established as candidate of fluorescent lamp phosphors and laser technology. To improve the densification of lithium apatite $LiRe_9(SiO_4)_6O_2$ ceramics (Re = La, Pr, Nd, Sm, Eu, Gd, Er), relative density was higher than 90% for all samples after doping 1 wt% LiF [51]. The microwave dielectric properties of $SrRE_4Si_3O_{13}$ (RE = La, Pr, Nd, Sm, Eu, Gd, Tb, Dy, Er, Tm, Yb, and Y) were in the range of 9–16 for permittivity with the maximum of $Q\times f$ value ≈ 26,000 GHz [52], while the optimal microwave dielectric properties of $CaRE_4Si_3O_{13}$ (RE = La, Nd, Sm, and Er) were $\varepsilon_r \approx 13.37$, $Q\times f$ value ≈ 18,600 GHz, and $\tau_f \approx -17.8$ ppm/℃ at Re = Er [53].

To obtain new dielectric materials, some researchers pursued materials with the composition containing GeO_2 and Ga_2O_3 and reported microwave dielectric properties of those materials firstly. With inverse spinel structure, $LiGa_5O_8$ was verified as a cubic structure where Li^+ and Ga^{3+} distributed in the octahedral B site with 1:3 ordering [54]. The large deviation between ε_r and ε_{rth} in $Ba_2MGa_{11}O_{20}$ (M = Bi, La) was ascribed to the "rattling" effect of cations and the existence of lone pair ions of Bi^{3+} [55]. The different τ_f values of AGe_4O_9 (A = Ba, Sr) were ascribed to the distortion of [GeO_6] octahedron where τ_f values were –44.2 ppm/℃ for the former and –11.7 ppm/℃ for the later [56]. Normal garnet $A_3Y_2Ge_3O_{12}$ (A = Ca, Mg) ceramics possessed $\tau_f \approx 120.5$ ppm/℃ for A = Ca and –40.6 ppm/℃ for A = Mg [57]. As doped ions, $(Li_{0.5}Ga_{0.5})^{3+}$ in $Mg_2Al_4Si_5O_{18}$ would obtain the highest $Q\times f$ value of 50,560 GHz [58]. $Ca_3M_2Si_3O_{12}$ (M = Yb, Y) ceramics were consistent with the general formula of garnet structure, and those ceramics crystalized as silico-carnotite structure with high-energy ball milling method [59]. The microwave dielectric properties were recorded as $\varepsilon_r \approx 9.2$, $Q\times f$ value ≈ 56,400 GHz, and $\tau_f \approx -77.5$ ppm/℃ and $\varepsilon_r \approx 8.7$, $Q\times f$ value ≈ 29,094 GHz, and $\tau_f \approx -76.8$ ppm/℃ for $Ca_3Yb_2Si_3O_{12}$ and $Ca_3Y_2Si_3O_{12}$, respectively. A serial of $Ca_3MZrGe_3O_{12}$ (M = Co, Zn), $Ca_4ZrGe_3O_{12}$, and $Ca_3B_2Ge_3O_{12}$ (B = Al, Ga) ceramics were successfully prepared, and the quality factors were higher than that of $Ca_3M_2Si_3O_{12}$ [60–62]. Similarly, $Sr_3B_2Ge_3O_{12}$ (B = Yb, Ho) were investigated by Li *et al*. [63] using vibration spectroscopy, and the τ_f was tuned to near zero with $CaTiO_3$ ceramics. $0.8Y_3MgAl_3SiO_{12}$–$0.2TiO_2$ ceramic sintered at 1475 ℃ showed a $\tau_f \approx +5.2$ ppm/℃, where the co-existed phase contained $Y_2Ti_2O_7$ and TiO_2 along with $Y_3MgAl_3SiO_{12}$ phase [64]. Dense $Mg_3Ga_2GeO_8$ ceramics presented microwave dielectric properties of $\varepsilon_r \approx 9.41$, $Q\times f$ value ≈ 133,113 GHz, and $\tau_f \approx -63.54$ ppm/℃ [65]. Single phase $LiYSiO_4$ ceramics could be obtained in 1100–1140 ℃, and a near-zero τ_f of (+4.52)–(+8.03) ppm/℃ was observed [66].

Furthermore, phase transition from $A2/a$ to $P2_1/a$ was observed in new silicate in the formula of $CaSn_{1-x}Ti_xSiO_5$, where the variation of τ_f values was ascribed to the Sn/TiO_6 octahedral distortion [67]. Secondary phase of SnO_2 and $SrSiO_3$ appeared at $0.2 \leqslant x \leqslant 0.45$ in $Ca_{1-x}Sr_xSnSiO_5$ ceramics, which could adjust the positive τ_f of $CaSnSiO_5$ to –1.2 ppm/℃ [68]. $CaSiO_3$ and $CaSnSiO_5$ phases would improve the τ_f to –7.2 ppm/℃ in $Ca_2(Hf_{1-x}Sn_x)Si_4O_{12}$ when $x = 0.4$ [69].

2.2 Niobate and tantalate based on ZnO–Nb_2O_5–TiO_2

There is a large body of niobate and tantalate dielectric ceramics, and the relevant researches highlight the phase evolution, structure transformation, and chemical

bond characteristics. In order to elucidate the influence of undercoordinated sites on the dielectric properties, analysis according to P–V–L theory and vibration spectra is verified as valid approach to understand the relationship of the state of chemical bond with polarization and stability of lattice. Indeed, it seems that researchers could identify the contribution of each chemical bond to dielectric properties by P–V–L theory and infrared reflectivity spectrum. However, reaching general conclusions about the effect of a unique chemical bond or Wycoff site on different properties may be difficult, since the P–V–L theory is just predictable theoretically. The actual dielectric properties of ceramics are still evaluated based on experiments, and thorough, quantitative, and multi-perspective analysis is required. Figure 4 is the phase diagram of the mainly reported niobate and tantalate dielectric ceramics, where the rutile-type, ixiolite-type, and columbite-type structures were obtained after $(Zn_{1/3}Nb_{2/3})^{4+}$ was doped into TiO_2. The detailed phase division of $A_{0.5}B_{0.5}CO_4$ and the relevant investigations of this binary system are summarized in the following.

2.2.1 *Rutile–trirutile/ixiolite/wolframite–columbite type ceramics*

Rutile, brookite, and anatase are the three types of TiO_2 in nature. TiO_2 itself possesses a high permittivity ≈ 100, a low dielectric loss tangent (tanσ) value (6×10^{-5} at a frequency of 3 GHz), and a high τ_f value of 450 ppm/℃ [70]. It is valid that TiO_2 phase is used to target the aim of near zero τ_f value as a secondary phase in the system with a negative τ_f value. Meanwhile, long-term focus has been paid on the structure transformation and property optimization of TiO_2 with

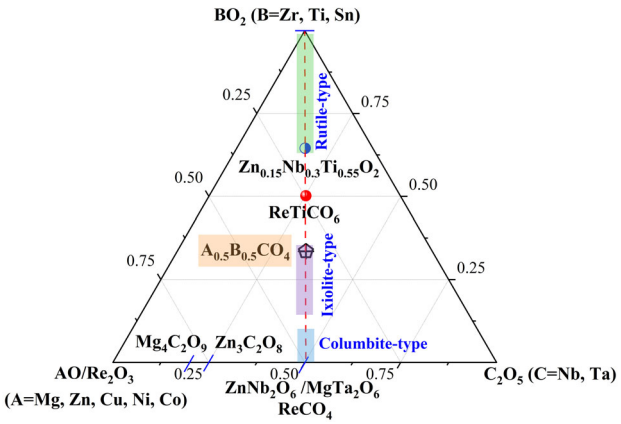

Fig. 4 Pseudo phase diagram of the niobate and tantalite.

substitution ions of different physicochemical properties. The cation substitution for Ti^{4+} can reduce the dielectric loss or tune the τ_f value, evolving monovalent, divalent, trivalent, tetravalent, or pentavalent cations, and their groups of two cations. Especially, the extensive elaboration of dependence of microwave dielectric properties on the crystal structure of $(Zn_{1/3}B^{5+}_{2/3})_xTi_{1-x}O_2$ (B^{5+} = Nb, Ta) ceramics was reported by Kim and Kang [71]. The phase relation of ternary system of ZnO–TiO_2–Nb_2O_5 was first discussed in 1992 [72]. It summarized that the solid solution of rutile phase appeared in the range of molar content of $(Zn_{1/3}Nb_{2/3})^{4+}$ lower than 58%, ixiolite $ZnTiNb_2O_8$ exited in the range of 69%–85%, while columbite solid solution of $ZnNb_2O_6$ formed when the content was higher than 93% [73], and the solid solution area of different types was marked with shadow in the pseudo phase diagram in Fig. 4.

Compared with the ongoing report of $ZnTiNb_2O_8$, the study of $Zn_{0.15}Nb_{0.3}Ti_{0.55}O_2$ is still rare. Generally, $Zn_{0.15}Nb_{0.3}Ti_{0.55}O_2$ appeared as the secondary phase which would control the dielectric properties of composite ceramics [74–76]. It possessed properties of $\varepsilon_r \approx 94.35$, $Q\times f$ value ≈ 10,889 GHz, and $\tau_f \approx 353.43$ ppm/℃, sintered at 1050 ℃ [71], which was potential to be τ_f compensator as TiO_2. Yang *et al*. [77] directly added the $Zn_{0.15}Nb_{0.3}Ti_{0.55}O_2$ into $Zn_{0.5}Ti_{0.5}NbO_4$ ceramics, and the structure evolution and chemical bond parameters have been calculated. Zr^{4+} with the larger radius than Ti^{4+} was used to dope into $Zn_{0.15}Nb_{0.3}(Ti_{1-x}Zr_x)_{0.55}O_2$ [78], where the expansion of bond length and cell volume renders the decline of covalency of all bonds. The decline of bond ionicity was obtained since the shrinking of cell volume and bond length in $Zn_{0.15}Nb_{0.3-x}Ta_xTiZr_{0.55}O_2$ [79].

The structure of formula $A_{0.5}B_{0.5}CO_4$ can be categorized into four types: wolframite-type $AZrB_2O_8$ (A = Mn, Zn, Mg, Co, Ni; B = Nb, Ta), rutile-type $A_{0.5}Ti_{0.5}NbO_4$ (A = Ni, Co, Cu), tetragonal trirutile-type $A_{0.5}Ti/Sn_{0.5}TaO_4$ structure (A = Co, Ni, Zn, Mg), and ixiolite-type $ZnTiNb_2O_8$. The schematic of those classifications is shown in Fig. 5, and the related investigations of each structure are illustrated in this section. The effects of different cations (Mn, Zn, Mg, Ni, and Co) at A-site of $AZrNb_2O_8$ illustrated that dielectric constant, quality factor, and τ_f values relied on the ionic polarizability, packing fraction, and B-site octahedral distortions, respectively [80–85]. Among them, $MgZrNb_2O_8$ shows the optimal quality factor

($\varepsilon_r \approx 26$, $Q\times f$ value ≈ 120,816 GHz, and $\tau_f \approx -50.2$ ppm/℃, at f = 6.85 GHz [86]). The microwave dielectric properties of wolframite-type $AZrB_2O_8$ (A = Mn, Zn, Mg, Co, Ni; B = Nb, Ta) and the structure-relationship were determined via combining the far-infrared and terahertz spectroscopy with P–V–L theory [87–91]. Partial replace of A-site (such as $Mg_{0.5}Zn_{0.5}ZrNb_2O_8$ [92], $Zn_{1-x}Co_xZrNb_2O_8$ [93–95]), Zr-site substitution of $Zn(Ti_{1-x}Zr_x)Ta_2O_8$ [96], $ZnZr_{1-x}Sn_xNb_2O_8$ [97,98], doped Nb-site of $MgZr(Nb_{1-x}Sb_x)_2O_8$ [99,100], $ZnZrNbTaO_8$ [101], $MgZrNb_{2-x}(Sn_{1/2}W_{1/2})_xO_8$ [102], and non-stoichiometric $MgZrNb_{2+x}O_{8+2.5x}$ [103] provided evidence that relative density, packing fraction, bond valence, and chemical bond characteristics majored the variation of microwave dielectric properties. To adjust the negative τ_f values, the study about the relationship of TiO_2 on $MgZrNb_2O_8$ [104] and $ZnZrNb_2O_8$ [105] presented that co-exited ceramics would reach near zero τ_f values. The microwave dielectric properties were $\varepsilon_r \approx 43$, $Q\times f$ value ≈ 46,110 GHz, and $\tau_f \approx -2.5$ ppm/℃ for $0.63MgZrNb_2O_8$–$0.37TiO_2$ ceramics; $\varepsilon_r \approx 44$, $Q\times f$ value ≈ 38,500 GHz, and $\tau_f \approx -2.4$ ppm/℃ for $0.3ZnZrNb_2O_8$–$0.7TiO_2$ ceramics. Additionally, literature demonstrated that H_3BO_3 or B_2O_3 addictive aids could contributed to densification and improvement of the sintering behavior for $ZnZrNb_2O_8$ and $MgZrNb_2O_8$ [106–108].

The dielectric properties of $A_{0.5}B_{0.5}NbO_4$ ceramics are much different. $Ni_{0.5}Ti_{0.5}NbO_4$ and $Cu_{0.5}Ti_{0.5}NbO_4$ crystalized in rutile structure presented with positive τ_f values of 79.1 and 49.2 ppm/℃, respectively [109,110]. The characteristic of rutile $Co_{0.5}Ti_{0.5}NbO_4$ was sought by solid state reaction and sol–gel method [111,112], where the microwave dielectric properties were $\varepsilon_r \approx 64$, $Q\times f$ value ≈ 65,300 GHz, $\tau_f \approx 223.2$ ppm/℃ and $\varepsilon_r \approx 64.19$, $Q\times f$ value ≈ 16,800 GHz, $\tau_f \approx 66.17$ ppm/℃, respectively. In the solid solution of $Ni_{0.5-x}Zn_xTi_{0.5}NbO_4$, the dielectric constant was enhanced from 56.8 to 62.54 [113]. Introduction of $CoNb_2O_6$ and $Zn_{1.01}Nb_2O_6$ into $CoTiNb_2O_8$ rendered the $Q\times f$ increasing considerably due to the enhanced densification and obtained the τ_f values of 0.5 and 0 ppm/℃, respectively [114,115]. Zhang *et al*. [116] and Li *et al*. [117] reported that τ_f value would shift from positive to negative after Zr substitution in $CoTi_{1-x}Zr_xNb_2O_8$, where the τ_f value was correlated with oxygen octahedral distortion and B-site bond valence. Superlattice diffraction peak which is relevant with cation ordering was observed in $Co_{0.5}Ti_{0.5}Nb_{1-x}Sb_xO_4$ ceramics, contributing to the augment of $Q\times f$ value [118].

The trirutile-type structure was observed in some tantalates, antimonates, and bismuthates. This crystal structure was built by ordering octahedral cations along *c*-axis, which possessed three times *c*-axis of rutile-type one [119,120]. Currently, $Co_{0.5}Ti_{0.5}TaO_4$ [121], $NiTiTa_2O_8$ [122], $Co_{0.5}Zr_{0.5}TaO_4$ [90], $NiSnTa_2O_8$ [123] were reported as trirutile-type structure. Among them, $NiSnTa_2O_8$ showed a near zero τ_f value ($\varepsilon_r \approx 21.04$, $Q\times f$ value ≈ 31,328 GHz, and $\tau_f \approx -2.63$ ppm/℃).

Ixiolite phase $ZnTiNb_2O_8$ is a fully disordered α-PbO_2 structure, where Zn/Ti/Nb ions statistically occupied the octahedral cation sites [124]. Up to now, numbers of substitution on $ZnTiNb_2O_8$ have been reported, such as Co [125], Mg [74], Ca [126], Sn [127], Zr [128], and Ta [129–131]. The crystal structure refinement and Raman spectrum study of $ZnTiNb_2O_8$, together with the mode assignment were completed by Liao and Li [132]. In the ZnO–Nb_2O_5–$xTiO_2$ ($1 \leqslant x \leqslant 2$) system, ceramics were composed of $Zn_{0.17}Nb_{0.33}Ti_{0.5}O_2$ and $ZnTiNb_2O_8$ when $x \geqslant 1.8$ [133]. Using the effective

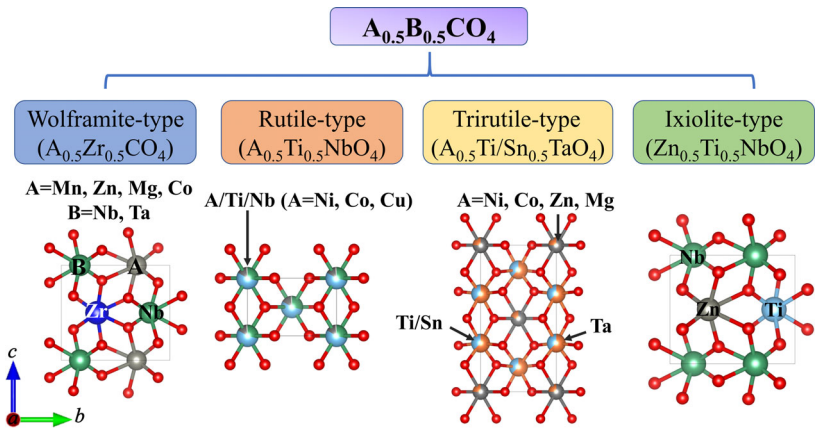

Fig. 5 Schematic of classification of $A_{0.5}B_{0.5}CO_4$.

route of sintering reaction for $ZnNb_2O_6$ and TiO_2 nano powders, a superior property of $ZnTiNb_2O_8$ was achieved compared with that prepared by solid-state method [134]. Dielectric constant and dielectric loss were evaluated in microwave and THz range in $Al_{0.5}Nb_{0.5}$ doped into $ZnTiNb_2O_8$, where the results indicated the negligible shift of dielectric constant in those frequencies, as shown in Fig. 6 [135]. Furthermore, ixiolite $MgTiNb_2O_8$ prepared by aqueous sol–gel process and then sintered at 1000 ℃ showed $\varepsilon_r \approx 33.8$, $Q\times f$ value ≈ 26,260 GHz, and $\tau_f \approx -19.2$ ppm/℃ [136].

In the family of AB_2O_6 (A = Ca, Mg, Mn, Co, Ni, Zn; B = Ta, Nb), the relationship of permittivity with electronegativity was presented by Lee *et al*. [137]. Two structure classifications have been identified in this system, namely rutile-type (trirutile) and α-PbO_2-type (tri-α-PbO_2, columbite) [138,139]. Comprehensive studies of columbite niobates concluded that the ε_r was in the range of 17–22, τ_f value varied from –45 to –76, and the $Q\times f$ value was over 95,000 GHz of $MgNb_2O_6$ [140,141]. The investigations about property optimization and preparation methods were concentrated on $MgNb_2O_6$, $ZnNb_2O_6$, and $ZnTa_2O_6$ due to their potential of application. For sintering behavior, the sintering temperature can be reduced to 1150 ℃ of $MgNb_2O_6$ by sol–gel method [142]. Doped ceramics of $(Zn_{1-x}Ni_x)Ta_2O_6$ [143], $Zn(Ta_{1-x}Nb_x)_2O_6$ [144], $Zn(Ta_{1-x}Sb_x)_2O_6$ [145], and composite ceramics composed of $ZnO–Nb_2O_5–1.75TiO_2$–5 mol% MgO, $(1–x)ZnTa_2O_6–xMgNb_2O_6$, $(1–x)ZrTi_2O_6–xZnNb_2O_6$, and $(1–x)ZnTa_2O_6–xNiNb_2O_6$ were designed successfully to reach near-zero τ_f value [146–149]. Liu and Deng [150] proposed that the grain size of $ZnNb_2O_6–(Zn_{0.7}Mg_{0.3})TiO_3$ ceramics became smaller with the $ZnNb_2O_6$ content increasing. The secondary ZnV_2O_6 was observed with higher than 1 wt% V_2O_5 into $ZnNb_2O_6$ [151]. The property comparison of $MgTa_2O_6$ was obtained by sol–gel procession and solid reaction sintering by Wu *et al*. [152]. Liu *et al*. [153] verified that the unpaired d-electrons contribution to the room temperature loss should be taken into consideration of $ZrTiO_4–ZnNb_2O_6$. It was interesting that the structure transformation was identified as tri-α-PbO_2, α-PbO_2, trirutile, and rutile in $(1–x)ZnTa_2O_6–xTiO_2$ along with the increase of x [154]. $ZnNb_2O_6$ ceramics prepared by microwave sintering exhibited relative density of 94.3%, and the quality factor was dominated by the distribution of grain size [155]. Recently, the intrinsic dielectric properties were investigated using chemical bond theory and lattice vibrational spectra, which indicated that B_{1u} mode at 168.87 cm^{-1} was highly related to the dielectric properties [156], and the fitted results of infrared-related spectrum are presented in Fig. 7.

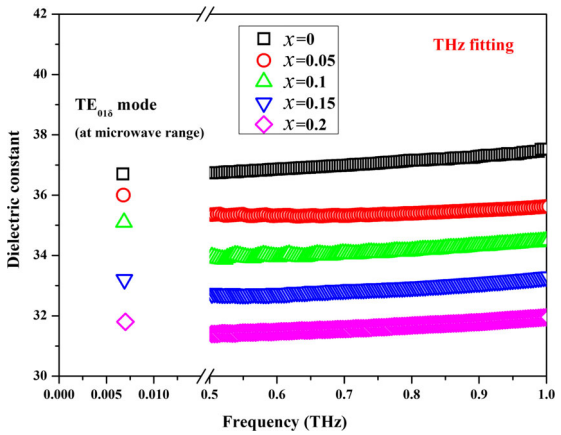

Fig. 6 Absorption coefficients of $ZnTi_{1-x}(Al_{0.5}Nb_{0.5})_xNb_2O_8$ ceramics at 0.6 and 0.9 THz. Reproduced with permission from Ref. [135], © The American Ceramic Society 2019.

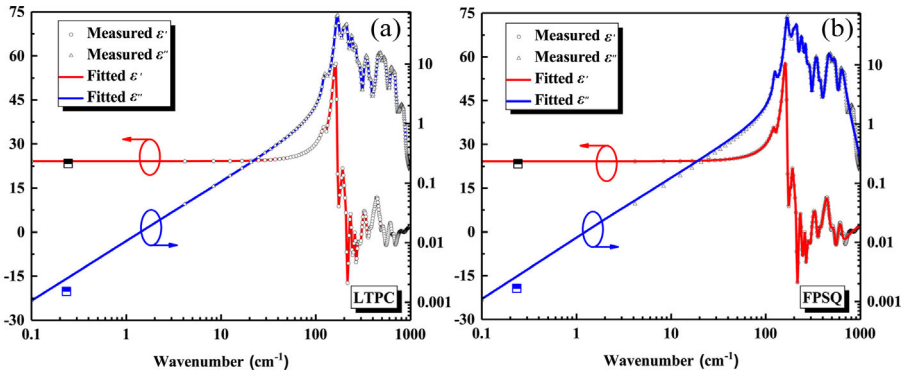

Fig. 7 Real $\varepsilon'(\omega)$ and imaginary $\varepsilon''(\omega)$ of relative permittivity after (a) LTPC and (b) FPSQ mode fit. LTPC, Lorentz three parameter semiquantum model; FPSQ, four parameter semiquantum model. Reproduced with permission from Ref. [156], © The American Ceramic Society 2019.

2.2.2 $ReTiCO_6$ ceramics

The crystal structure of double tantalates of rare-earth elements with titanium tantalite compounds based on $ReTiTaO_6$ is sorted into two parts: orthorhombic aeschynite symmetry with rare earth atomic number in the range of 55–66 and orthorhombic euxenite symmetry with that of 67–71 [157,158]. Generally, high ε_r and positive τ_f were obtained for the former, while relatively low ε_r and negative τ_f were observed for the latter. The effect of microstructure on properties of $RETiNbO_6$ (RE = La, Sm, and Y) ceramics was presented by Lei *et al*. [159]. The dielectric constant of $RETiNbO_6$ system (RE = Ce, Pr, Nd, Sm, Eu, Gd, Tb, Dy, Y, and Yb) and $RETiTaO_6$ (RE = La, Ce, Pr, Nd, Sm, Eu, Gd, Tb, Dy, Ho, Y, Er, Yb, Al, and In) increases with the RE ionic radius [157,158]. It was reported that $LaTiNbO_6$ usually stabilized as a monoclinic structure, and Zhang and Zuo [160] proposed that ceramics with coexistence of O and M phases could be achieved after prolonging the annealing time. And then, they [161–164] conducted out the substitutions for La and Nb sites, in which the structure evolution, octahedral distortion, and vibrational spectrum were elaborated in detail. More recently, dielectric and optical properties of $Ln_{0.8}Lu_{0.2}TiNbO_6$ (Ln = Ce, Pr, Nd, and Sm) were presented by John and Solomon [165], where the optimal microwave dielectric properties were shown for $Sm_{0.8}Lu_{0.2}TiNbO_6$: $\varepsilon_r \approx 35$, $Q\times f$ value ≈ 37,390 GHz, and $\tau_f \approx 15$ ppm/℃.

2.2.3 $ReCO_4/Mg_4C_2O_9/Zn_3C_2O_8$ ceramics

The ABO_4 composition material system of $RENbO_4$ (RE = lanthanoid atoms, being La to Lu as well as Y) was firstly investigated in light of their luminescence, damping, and phase transformation characteristics, and their microwave dielectric properties were firstly proposed in 2006 [166]. The satisfied properties of $LaNbO_4$, $NdNbO_4$, and $SmNbO_4$ attracted much attention recently. For $NdNbO_4$ ceramics, substitution for Nd site by single cations such as Sr, Ca, Mn, Co, Mg, Zn, Y, Al, Bi, Sm, La [167–175], and Nb site by Ta, Sb [176–179] were completed to adjust the microwave dielectric properties. In our recent reports, the groups of different isovalent cations of $(A_xB_{1-x})^{5+}$ (A = Mg, Al, Si, Zr; B = W, Mo) have been listed as valid substitution for Nb site to reduce dielectric loss [180–183]. The analysis of combination of P–V–L theory and vibration spectrum suggested that doping into Nb site was beneficial to improving quality factor. Meanwhile, $NdNbO_4$ prepared in sol–gel method or composite ceramics composed of $NdNbO_4$–$CaTiO_3$ [184], $NdNbO_4$–CaF_2 [185], and $NdNbO_4$–MgO [186] have also been reported to perfect the properties. Similarly, intrinsic dielectric properties of $EuNbO_4$ were studied by Liu *et al*. [187]. In the full range of La_2O_3–Nb_2O_5–V_2O_5 system, four typical phase regions were verified, including monoclinic fergusonite, tetragonal sheelite, B-site ordered sheelite, and composite of monoclinic $LaVO_4$ and tetragonal sheelite phases [188]. Likewise, MgO was designed as an addition for $LaNbO_4$ ceramics and the excellent properties were listed as $\varepsilon_r \approx 19.8$, $Q\times f$ value ≈ 94,440 GHz, and $\tau_f \approx 6.1$ ppm/℃ [189]. More recently, structure–property relationship of another $A^{3+}B^{5+}O_4$ binary oxide, zircon-type AVO_4 (A = Eu, Y) ceramics, was discussed by packing fraction and bond valence [190]. Ferroelastic phase transition from monoclinic fergusonite to tetragonal scheelite was observed by *in situ* Raman spectroscopy and X-ray diffraction of $La(Nb_{0.9}V_{0.1})O_4$, and the schematic of ε_r typical-ceramics versus temperature was shown by Zhou *et al*. [191]. NiO/CoO added into $LaNbO_4$ would distinctly optimize the quality factor since the larger and uniform grain was obtained [192]. Although the thermal properties [193–196] and the first-principles calculation of electronic structure and optic properties of $RETaO_4$ (RE = Y, La, Sm, Eu, Dy, Er) [197] have been investigated, the intrinsic dielectric loss has not been summarized in this system. Microwave dielectric properties of $ErNbO_4$ prepared by sol–gel method were reported by Devesa *et al*. [198], and the grain size varied from 31.27 to 86.65 μm and 40.96 to 78.23 μm by Rietveld refinement and Sherrer's formula, respectively. $ZrTiO_4$ followed the general formula of ABO_4, and the intrinsic dielectric loss of $Zr_{0.8}Sn_{0.2}TiO_4$ was investigated by THz time domain spectroscopy [199].

The structure of corundum-like phase of $Mg_4Nb_2O_9$ was verified by Kumada *et al*. [200], where the cations were ordered by the stack of two layers of a mixture of Mg and Nb and one layer of Mg along the *c*-axis. $Mg_4(Nb_{2-x}Ta_x)O_9$ solid solution was synthesized in the sintering temperature range of 1350–1400 ℃ [201], which possesses a comparable quality factor ($Q\times f$ value ≈ 350,000 GHz for $x = 2$) to that of Al_2O_3. To deal with the limitation of high sintering temperature, both $Mg_4Nb_2O_9$ and $Mg_4Ta_2O_9$ were generated by sol–gel method and the variation of property with

sintering temperature was analyzed [202–204]. An accompanying minor phase of $Mg_5Nb_4O_{15}$ gradually disappeared as the calcined temperature increased to 850 ℃. High frequency dielectric properties of $A_5B_4O_{15}$ microwave dielectric were evaluated by Kamba *et al*. [205] using far-infrared reflection, transmission spectroscopy, and time-resolved THz transmission spectroscopy. Considering the negative influence of second phase on properties and sintering behavior of $Mg_4Nb_2O_9$, excess MgO and $Mg(OH)_2$ were used to adjust the composition of $Mg_4Nb_2O_9$ [206,207], which presented that the appearance of $Mg_4Nb_2O_9$ pure phase was more easily with $Mg(OH)_2$ as raw materials. A dramatically improvement of quality factor was achieved by Ni and Ta co-doped into this system, and $(Mg_{0.95}Ni_{0.05})_4(Nb_{1-x}Ta_x)_2O_9$ shows satisfied properties of $\varepsilon_r \approx 12.76$, $Q\times f$ value ≈ 442,000 GHz, and $\tau_f \approx$ –54 ppm/℃, when $x = 1$ and sintered at 1375 ℃ [208]. $(B_xW_{1-x})^{5+}$ substitution at Nb^{5+} site (B = Li, Mg, Al, Ti) in $Mg_4Nb_2O_9$-based ceramics revealed that the τ_f depended on the distortion of the oxygen octahedra, while $(Ti_{1/2}W_{1/2})^{5+}$ substitution had the highest quality factor of 233,000 GHz [209]. The investigation of $y(Mg_{0.95}Co_{0.05})_4Ta_2O_9$–$(1-y)CaTiO_3$ ceramics provided a promising dielectric material for application with temperature stability, and the properties were shown as $\varepsilon_r \approx 25.78$, $Q\times f$ value ≈ 200,000 GHz, and $\tau_f \approx$ –4.69 ppm/℃ [210].

$Zn_3Nb_2O_8$ was another promising binary niobite compound, which could be successfully produced with 98% theoretical density sintered at 1100 ℃ [211]. A two-stage sintering method was proposed to optimize the microstructure of $Zn_3Nb_2O_8$ [212], where the sintering temperatures were 1150 and 1200 ℃ for the first time and the second sintering temperatures were 1050 and 1100 ℃, respectively. Sintered based on this approach, ceramics presented denser grain packing and less abnormal grain growth. Adding secondary phase into ceramics to compensate for τ_f value would introduce a large amount of second phase, which were ascribed to the large dielectric loss. Aiming to reduce the defects stemmed from the secondary phase, layer-cofired ceramic architectures were designed such as $Zn_{1.01}Nb_2O_6/TiO_2/Zn_{1.01}Nb_2O_6$ [3], $MgTiO_3/TiO_2/MgTiO_3$ [4], and $Zn_3Nb_2O_8/TiO_2/Zn_3Nb_2O_8$ [5]. High-Q value was remained and temperature-stable MWDCs were obtained for all the reported tri-layer co-fired ceramics.

2. 3 Rock-salt structure

Closely followed by the ever-growing explosion of global data volume and the rapid boost of millimeter-wave technology, the requirement of materials with low permittivity ($\varepsilon_r \leqslant 25$) and high $Q\times f$ value is increasingly urgent. In the exploration of new composition ceramics, many rock-salt Li-containing compounds emerge as focal points. The general formula of rock-salt ceramics is $A_aB_bO_{a+b}$ (A^+ = Li, Na; B^{4+} = Ti, Sn, Zr; B^{5+} = Nb and Ta). Li_2TiO_3 underwent an order–disorder phase transition at 1213 ℃, in which the structure consisted of ordered (Li,Ti) layer, with the property of $\varepsilon_r \approx 12.76$, $Q\times f$ value ≈ 44,200 GHz, and $\tau_f \approx$ –54 ppm/℃ [213]. The sintering behavior of excess Li for non-stoichiometry $Li_{2+x}TiO_3$ ceramics was investigated by Bian and Dong [214] and Hao *et al*. [215] after the determination of pseudo-binary of Li_2O–TiO_2 [216,217]. For co-doped substitution, $Zn_{1/3}Nb_{2/3}$, $Mg_{1/3}Nb_{2/3}$, and $Co_{1/3}Nb_{2/3}$ addition into Li_2TiO_3 could adjust the τ_f from positive to negative [218–220]. $Cu_{1/3}Nb_{2/3}$ doped ceramics with 3 wt% H_3BO_3 were designed as a patch antenna and a dielectric resonator antenna [221]. The solid solution of Li_2TiO_3–MgO [222], Li_2TiO_3–ZnO [223,224], and Li_2TiO_3–Li_3NbO_4 [225] attracted much interest of researcher owing to their high quality factor. The primarily reported ceramics of Li_2O–MgO/ZnO/CoO–Ti/Sn/ZrO_2 ternary system contain $Li_2Mg/NiTi/ZrO_4$, $Li_2Zn/Mg/CoTi_3O_8$, $Li_2Zn/Co/Mg_3Ti_4O_{12}$, $Li_2Mg/Ni_3Ti/SnO_6$, $Li_2ZnTi_5O_{12}$, $Li_2Mg_4TiO_7$, $Li_6Mg_7Ti_3O_{16}$, $Li_4MgSn_2O_7$, and Li_2NiZrO_4; while $LiZnNbO_4$, $Li_3Mg_2NbO_6$, and $Li_2Mg_3NbO_6$ occupied the dominated composition of Li_2O–MgO/ZnO/CoO–Nb/Ta/Sb_2O_5. The microwave dielectric properties of the mentioned pure phase ceramics are listed in Table 1 [224,226–246], and the phase diagram of rock-salt structure is plotted in Fig. 8, where the ordered–disordered range was summarized from Zhang *et al*. [246,247]. Simultaneously, Gu *et al*. [248] stated the two-phase and thermally stable ceramics of $0.8Li_3NbO_4$–$0.2Ca_{0.8}Sr_{0.2}TiO_3$, where the τ_f value was 5.2 ppm/℃.

2.3.1 Li_2O–MgO/ZnO/CoO–Ti/Sn/ZrO_2 ternary system

Secondary phases of Mg_2TiO_4 and $Li_2Mg_3Ti_4O_{12}$ were highly related to the properties when Yao *et al*. [249] prepared the Li_2MgTiO_4 after sintered higher than 1250 ℃. The variation of dielectric properties of $Li_2Mg_{0.95}A_{0.05}TiO_4$ (A = Ni, Co, Mn, Zn) indicated that the dielectric polarizability dominated the dielectric constant [250], and a near zero τ_f (–4.03 ppm/℃) was obtained for 0.1 mol Zn substitution for Mg [251].

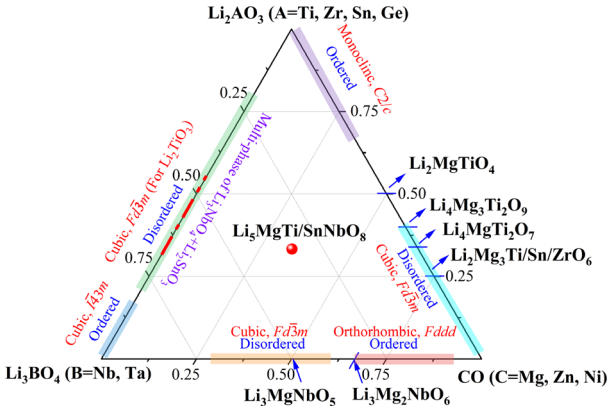

Fig. 8 Pseudo phase diagram of rock-salt structure.

Table 1 Microwave dielectric properties of pure phase with rock-salt structure

Formula	ε_r	$Q\times f$ (GHz)	τ_f (ppm/℃)	ST (℃)	Ref.
Li_2MgTiO_4	17.25	97,300	–27.2	1360	[226]
Li_2NiTiO_4	19.25	51,290	–20.1	1275	[230]
Li_2MgZrO_4	12.30	40,900	–12.31	1175	[234]
$Li_2MgTi_3O_8$	27.2	40,000	2.6	1000	[227]
$Li_2CoTi_3O_8$	28.9	52,600	7.4	1025	[228]
$Li_2ZnTi_3O_8$	25.6	90,000	–10.8	1000	[229]
$Li_2Co_3Ti_4O_{12}$	21.4	35,000	–22	1050	[233]
$Li_2Mg_3Ti_4O_{12}$	20.2	62,300	–27.1	1125	[232]
$Li_2Zn_3Ti_4O_{12}$	20.6	106,700	–48	1075	[231]
$Li_2Mg_3TiO_6$	15.2	152,000	–39	1280	[235]
$Li_2Ni_3TiO_6$	13.18	9800	–7.3	1275	[238]
$Li_2Mg_4TiO_7$	13.43	233,600	–7.24	1600	[239]
$Li_6Mg_7Ti_3O_{16}$	15.27	209,400	–11.31	1550	[240]
$Li_2ZnTi_5O_{12}$	38.4	54,300	82.9	1260	[237]
$Li_4MgSn_2O_7$	12.4	58,754	12.1	1180	[241]
Li_2NiZrO_4	12.3	20,000	–23.4	1300	[242]
$LiZnNbO_4$	15.6	85,310	–63.7	1070	[236]
$Li_3Mg_2NbO_6$	14.94	100,965	–21.96	1225	[243]
$Li_3Mg_2SbO_6$	10.5	84,600	–9.0	1300	[244]
$Li_2Mg_3NbO_6$	16.8	79,642	–22	1300	[224]
Li_3MgNbO_5	16.2	96,796	–24.8	1260	[245]

ST: sintering temperature (℃).

Both $Li_2Mg_4TiO_7$ and $Li_4Mg_3Ti_2O_9$ exhibited $LiFeO_2$-like cubic phase with space group $Fm\bar{3}m$. The optimal combination of microwave dielectric properties of $Li_2(Mg_{0.9}A_{0.1})_4TiO_7$ (A = Co, Ni, Mg, Zn, Ca) was observed for Zn doped ceramics ($\varepsilon_r \approx 14.77$, $Q\times f$ value ≈ 162,200 GHz, and $\tau_f \approx -4.30$ ppm/℃) and Ca ($\varepsilon_r \approx 15.79$, $Q\times f$ value ≈ 100,300 GHz, and $\tau_f \approx -1.43$ ppm/℃) [252]. Pure cubic $Li_4Mg_3Ti_2O_9$ phase was formed in the whole range of $0 \leqslant x \leqslant 0.4$ with $Mg_{1/3}Ta_{2/3}$ occupying Ti site [253].

Except for the sintering temperature, the heating rates and substation will directly influence the grain size, densification, and properties. Lu *et al*. [254] pointed out that the sintering rate increasing from 3 to 7 ℃/min would deteriorate the quality factor of $Li_2ZnTi_3O_8$ ceramics. If ball milling is applied for the raw materials at first for 4 h, then the sintering temperature of $Li_2ZnTi_3O_8$ ceramics could reduce from 1075 to 925 ℃, and those ceramics were chemically compatible with Ag [255]. Sintering the ceramics in a box type electric furnace and in a microwave furnace would obtain $Li_2ZnTi_3O_8$ ceramics with the grain size of 38 and 7 μm, respectively [256]. Mg, Co, and Zn substitution for Zn in $Li_2ZnTi_3O_8$ increased the quality factor because of the more compact microstructure [257–259]. Whereas, the secondary phases were recorded after the introduction of Sr^{2+} or (Sr_xCa_{1-x}) into $Li_2ZnTi_3O_8$ [260–262]. Phase evolution of $(1-x)Li_2ZnTi_3O_8$–$xTiO_2$ system indicated that pure $Li_2ZnTi_3O_8$ with cubic structure was observed when $x \leqslant 0.2$ (the lattice parameter is similar to $MgFe_2O_4$ with space group of $Fm\bar{3}m$ (227)), solid solution was exited in the range of $0.2 \leqslant x \leqslant 0.4$ with cubic structure (the lattice parameters is similar to $Zn_2Ti_3O_8$ with space group of $P4332$ (212)), and rutile TiO_2 phase appeared when $x \geqslant 0.6$ [263]. The τ_f value moves from –15 to 102.4 in $(1-x)Li_2ZnTi_3O_8$–$xTiO_2$ ($0 \leqslant x \leqslant 0.4$) [264]; meanwhile, near zero τ_f value was also achieved by Bari *et al*. [265] in this system. 4 wt% TiO_2 was added into $Li_2ZnTi_3O_8$ with different particle sizes, where the nanoparticles and micron particles all generated a more uniform microstructure and relative density reached to 98.5% [266]. Similar to TiO_2-doped $Li_2ZnTi_3O_8$ ceramics, phase composition and properties of $Li_2Mg(Ti_{1-x}Sn_x)_3O_8$ (x = 0.1–0.25) were concluded as with $0.10 \leqslant x \leqslant 0.15$, the spinel and rutile were co-exited; with $0.20 \leqslant x \leqslant 0.25$, the spinel, rutile, and ilmenite were obtained [267], and the optimal properties of $Li_2ZnTi_3O_8$–$0.2SnO_2$ composite ceramics exhibited: $\varepsilon_r \approx 20.9$, $Q\times f$ value ≈ 89,500 GHz, and $\tau_f \approx -24$ ppm/℃ [268]. The variation of dielectric properties with density of $(1-x)Li_2(Mg_{0.95}Zn_{0.05})_3Ti_3O_8$–$xLi_2TiO_3$ (x = 0.727, 0.778, 0.821, and 0.889) was discussed systematically by Zhang *et al*. [269]. The concentration of oxygen vacancy, relative density, and decrease in damping behavior would influence the $Q\times f$ value of $Li_2ZnTi_3O_8$–x wt% Nb_2O_5 [270]. To trace the dielectric response of lattice vibration, the response process of dielectric loss in $Li_2ZnTi_{3-x}M_xO_8$ (M = Al^{3+}, Nb^{5+}, $(Al_{0.5}Nb_{0.5})^{4+}$,

$(Zn_{1/3}Nb_{2/3})^{4+}$, and $(Li_{1/4}Nb_{3/4})^{4+}$) was discussed systematically containing the conduction loss and lattice vibration loss [271]. The conduction loss which acts at frequency lower than terahertz is neglectful by researchers concentrating on MWDCs, while AC impedance analysis was used to identify the effect of dopants and the mechanism of conduction loss in this system. Combining the fitting THz time domain spectrum and far infrared reflectivity spectrum, the dielectric response was illustrated in depth based on lattice loss and conduction loss.

Ultra-low loss microwave dielectric materials of $Li_2Mg_3TiO_6$-based ceramics are extensively studied via doping cations into Mg and Ti site. Bivalent cations [272] such as Ca^{2+}, Ni^{2+}, Zn^{2+}, and Mn^{2+} were verified effectively to adjust the microwave dielectric properties for Mg site, and co-doped of $Al_{1/2}Nb_{1/2}$ and $Zn_{1/3}Nb_{2/3}$ for Ti-site enhanced the $Q\times f$ values to 174,300 GHz [273] and 168,911 GHz [274], respectively. For MWDCs, compactness microstructure guarantees the satisfied microwave dielectric properties. However, porous microstructure caused by the loss of Li element under high temperature is a problem for all compounds containing Li. To cure the volatilization of lithium, Fang *et al*. [275–277] proposed a reliable method which provided the Li-rich sintering atmosphere, and they obtained serial MWDCs based on Li–Mg–Sn/Ti oxides with excellent properties. The schematic representation of the devices provided with the Li-rich atmosphere is shown in Fig. 9, and this similar method was gradually popularized to other systems with volatilization element to obtain the ceramics with dense microstructure. The negative τ_f values can be compensated by $Ca_{0.8}Sr_{0.2}TiO_3$, and the sample with $0.91Li_2Mg_3TiO_6$–$0.09Ca_{0.8}Sr_{0.2}TiO_3$ showed a τ_f value of –3.65 ppm/℃ [278].

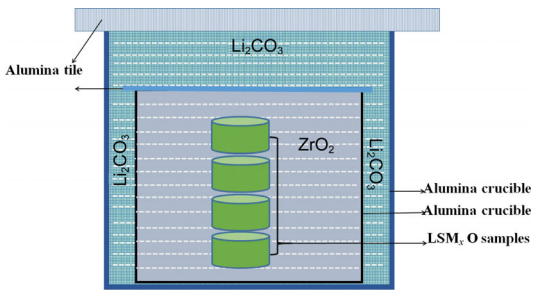

Fig. 9 Schematic representation of the $Li_{2/3(1-x)}Sn_{1/3(1-x)}Mg_xO$ (x = 0–4/7) placement for providing ZrO_2-burying protective atmosphere and Li-rich sintering atmosphere. Reproduced with permission from Ref. [277], © The American Ceramic Society 2017.

The phase evolution of Li_2O–3MgO–$m$$TiO_2$ ($1 \leqslant m \leqslant 6$) was summarized as the phase diagram shown in Fig. 10 [279], where the phase structures changed as ($Li_2Mg_3TiO_6$, m = 1)→($Li_2Mg_3Ti_4O_{12}$ and Mg_2TiO_4, m = 2, 3)→($Li_2Mg_3Ti_4O_{12}$, m = 4)→($Li_2Mg_3Ti_4O_{12}$, $MgTiO_3$, and $Li_2MgTi_3O_8$, m = 5)→($Li_2Mg_3Ti_4O_{12}$, $MgTiO_3$, $Li_2MgTi_3O_8$, and $MgTi_2O_5$, m = 6). The application of P–V–L theory to Li_2MgTiO_4 [280], $Li_4Mg_3Ti_2O_9$ [281], and $Li_2Mg_3TiO_6$ [282] revealed that the bond ionicity (f_i) descended as f_i(Ti–O) > f_i(Mg–O) > f_i(Li–O). As analogy with Li_2O–3MgO–$m$$TiO_2$ ceramics, Li_2ZrO_3–MgO ceramics were explored as well [234,283,284]. High quality factor could be obtained in $(Mg_{1/3}Sb_{2/3})^{4+}$ substitutions for $Li_2Mg_4ZrO_7$ ceramics, which reached 153,140 GHz [285]. Zirconium deficiency of $Li_2Mg_3Zr_{1-x}O_6$ ceramics was designed and remarkable dielectric properties were presented: $\varepsilon_r \approx 13.13$, $Q\times f$ value ≈ 116,400 GHz, and $\tau_f \approx -26.30$ ppm/℃ [286].

2.3.2 *Li_2O–MgO/ZnO/CoO–Nb/Ta_2O_5 ternary system*

An intermediate compound of $Li_3Mg_2NbO_6$ at x = 1/3 appeared in the investigation of structure evolution of $Li_{(3-3x)}M_{4x}Nb_{(1-x)}O_4$ (M = Mg, Zn), and the results indicated that solid solution could be formed in a wide range between Li_3NbO_4 and MgO [224]. Considering the existed compounds of Li_2TiO_3–MgO and Li_3NbO_4–MgO, Zhang *et al*. [246] supposed that a three-component solid solution would be formed in Li_2TiO_3–Li_3NbO_4–MgO, and the pseudo phase diagrams of those component were presented in Fig. 11. The most extensively studied ceramics in this system are Li_2Mg_3Nb/TaO_6 and $Li_3Mg_2NbO_6$. For instance, a large grain size (130 μm) was recorded after using reaction sintering process to generate $Li_3Mg_2NbO_6$ [287]. Single cation doped solid solution of $Li_3(Mg_{1-x}Co_x)_2NbO_6$ [288], $Li_3(Mg_{1-x}Mn_x)_2NbO_6$ [289], $Li_3Mg_2Nb_{1-x}Mo_xO_{6+x/2}$ [290],

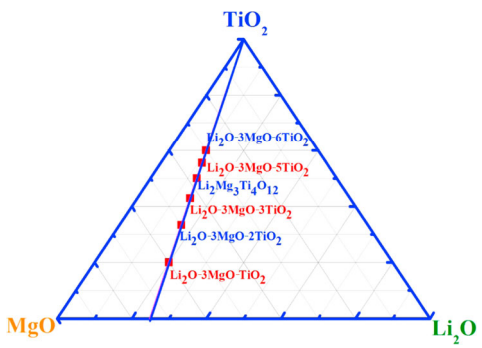

Fig. 10 Ternary phase diagram of Li_2O–3MgO–$m$$TiO_2$ systems. Reproduced with permission from Ref. [279], © Elsevier Ltd and Techna Group S.r.l. 2016.

$Li_3Mg_2Nb_{1-x}Ta_xO_6$ [291], $Li_3Mg_2Nb_{1-x}V_xO_6$ [292], $Li_3Mg_2Sb_{1-x}O_6$ [293], $Li_3Mg_{2-x}Zn_xSbO_6$ [294], $Li_3Mg_2(Nb_{1-x}W_x)O_{6+x/2}$ [295], $Li_3Mg_2Nb_{1-x}Ti_xO_{6-x/2}$ [296], $Li_{3+x}Mg_2Nb_{1-x}Ti_xO_6$ [297], and $Li_3Mg_2Nb_{0.96}(M_xW_{1-x})_{0.04}O_6$ ($M = Li^+$, Mg^{2+}, Al^{3+}, Ti^{4+}) [298] or non-stoichiometric $Li_3Mg_{2+x}SbO_6$ [299] have been probed and analyzed to explain the variation of dielectric properties through current theory including P–V–L theory, packing fraction, and C–M equations. It was interesting that the "dark hole" phenomenon of Li_2TiO_3 was cured by adding $Li_3Mg_2NbO_6$ and the τ_f value of $0.96Li_2TiO_3$–$0.04\ Li_3Mg_2NbO_6$ was 2.6 ppm/℃ [300]. Since yet there was no literature about the structure transformation of Li_2TiO_3–Li_3NbO_4–MgO to renew the understanding of rock-salt ceramics, Zhang *et al*. [247,301,302] gradually updated the reports about $Li_3Mg_2NbO_6$-based ceramics. The phase transitions among the orthorhombic, cubic, and monoclinic were verified by XRD (Fig. 12) and TEM analysis (Fig. 13). The systematical analysis of lattice evolution and ordering transformation indicated that the low dielectric loss of this system was mainly ascribed to the superlattice. The THz time-domain spectroscopy was firstly used in this system to evaluate the intrinsic dielectric loss associated with phonon oscillation. Meanwhile, the configurational entropy was calculated to explain the change of disordered and ordered crystal structures, where the disordering cubic phase generated much larger configurational entropy than the ordered orthorhombic and monoclinic phase (Fig. 14).

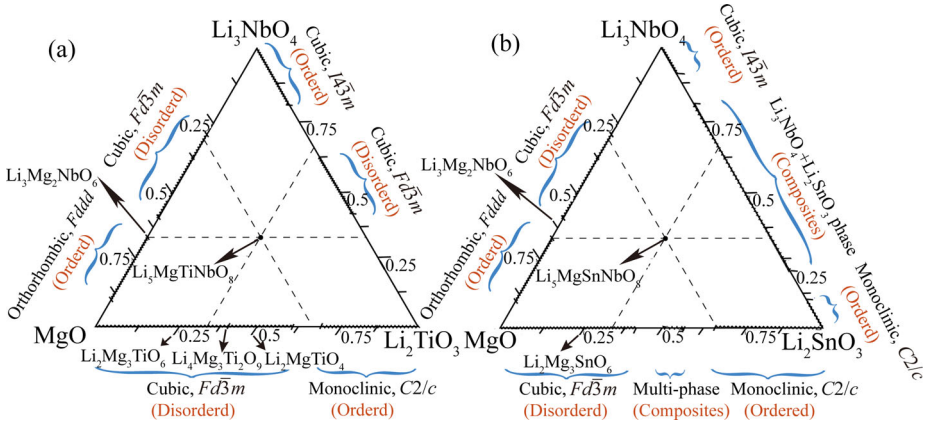

Fig. 11 Pseudo phase diagrams of (a) Li_2TiO_3–Li_3NbO_4–MgO and (b) Li_2SnO_3–Li_3NbO_4–MgO ternary systems. Reproduced with permission from Ref. [246], © Elsevier Ltd and Techna Group S.r.l. 2020.

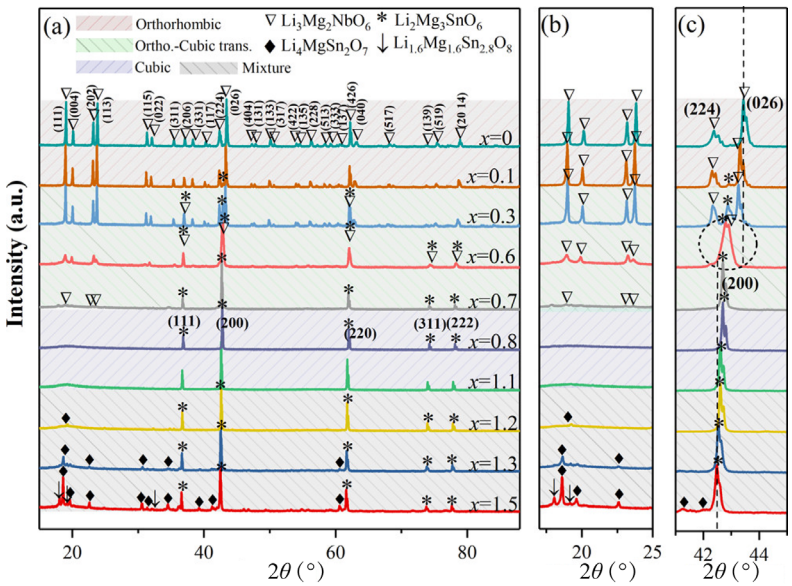

Fig. 12 (a) XRD patterns of $Li_3Mg_{2-x/3}Sn_xNb_{1-2x/3}O_6$ (x = 0–1.5) MWDCs sintered at 1290 ℃ for 4 h. (b) Amplified spectra of the XRD patterns from 17° to 25°. (c) Amplified spectra of the XRD patterns from 41° to 45°. Reproduced with permission from Ref. [302], © American Chemical Society 2020.

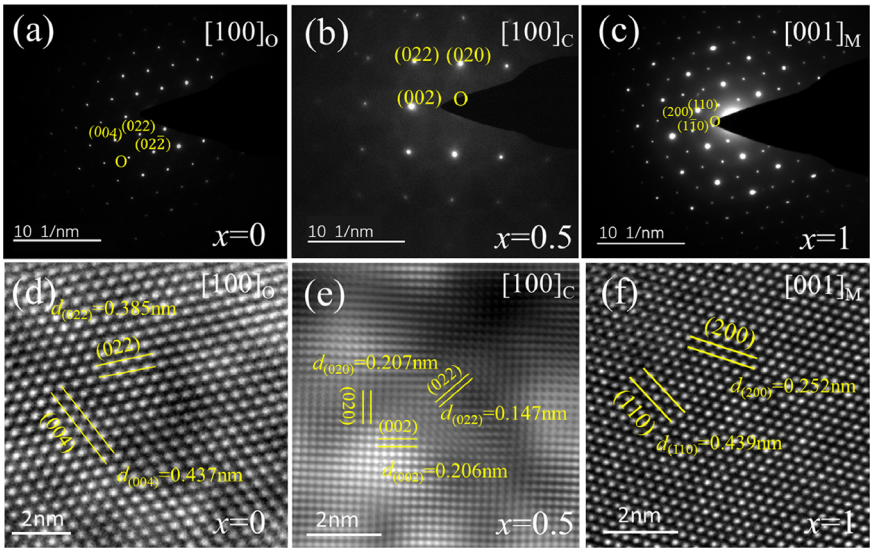

Fig. 13 Selected area electron diffraction (SAED) patterns of $Li_{3+x}Mg_{2-2x}Nb_{1-x}Ti_{2x}O_6$ ($0 \leqslant x \leqslant 1$) ceramics for (a) x = 0 sample taken along $[100]_O$ zone axis, (b) x = 0.5 sample along $[100]_C$ zone axis, and (c) x = 1 sample along $[001]_M$ zone axis. (d−f) Corresponding high resolution transmission electron microscopy (HRTEM) images of the selected areas of the above samples. Reproduced with permission from Ref. [247], © Elsevier Ltd and Techna Group S.r.l. 2020.

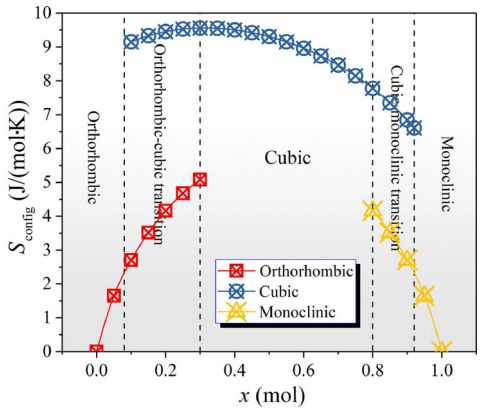

Fig. 14 Configurational entropy (S_{config}) of the cation substitutions for the three different types of phases in the $Li_{3+x}Mg_{2-2x}Nb_{1-x}Ti_{2x}O_6$ ($0 \leqslant x \leqslant 1$) system as a function of the substitution amount (x). Reproduced with permission from Ref. [247], © Acta Materialia Inc. 2021.

In contrast to the large scale studies of $Li_3Mg_2NbO_6$-based ceramics, only $Li_4MgSn_{(2-1.25x)}Nb_xO_7$ ($0 \leqslant x \leqslant 0.15$) was reported to evaluate the change of microstructure in $Li_4MgSn_2O_7$. The mean grain size of the doped ceramics ranged from 1.35 to 4.01 μm and the cracks appeared along with the occurrence of the secondary phase [303].

2. 4 Tungsten bronze structure and titanate based on $BaO–TiO_2$

Since 1970, the exploration of $BaO–TiO_2$ system has been continuous renewed. Among them, $BaO–4TiO_2$ and $2BaO–9TiO_2$ are the most extensively investigated ceramics as the representative ceramics with medium dielectric constant. The pseudo phase diagram of tungsten bronze structure and binary system based on $BaO–TiO_2$ system is shown in Fig. 15. In contrast to other sections in this review, the investigations about the compounds within this phase diagrams are relatively less, because the study of ceramics in $BaO–R_2O_3–TiO_2$ (R = La–Gd) has been almost accomplished and widely used in the industry.

2.4.1 $BaO–TiO_2/Nb_2O_5/Ta_2O_5$ system and Re_2TiO_5

The frequency dependence of $Q×f$ value was observed for $Ba_2Ti_9O_{20}$ ceramics, which was ascribed to the extrinsic dielectric loss [304]. After adding Sm_2O_3 into $BaTi_4O_9$, precursor of $BaTi_4O_9$ and $BaSm_2Ti_4O_{12}$ was

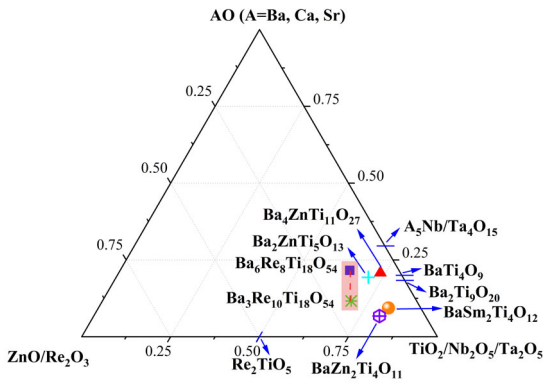

Fig. 15 Pseudo phase diagram of tungsten bronze structure and binary titanite.

modeled by a cool iso-static press and calcined at 1300 ℃, and a near-zero temperature coefficient of +2.2 ppm/℃ was achieved with 40 mol% Sm_2O_3 [305]. $(Zn_{1/3}Nb_{2/3})^{4+}$ substitution for Ti^{4+} in $Ba_2Ti_9O_{20}$ modified the τ_f value to +7 ppm/℃ [306]. Pseudobrookite-type $A_5B_4O_{15}$ (A = Ba, Sr, Mg, Ca; B = Nb, Ta) was firstly investigated by Jawahar *et al*. [307], which showed $\varepsilon_r \approx$ 11–51, $Q\times f$ value ≈ 2400–88,000 GHz, and $\tau_f \approx$ (–73)–232 ppm/℃. Based on sol–gel method, $Mg_5Nb_4O_{15}$ nano-powders were obtained at 600 ℃, and then the sintering temperature can be reduced to 1300 ℃ [204]. On the basis of P–V–L chemical bond theory, the relationship of chemical bond characteristic and microwave dielectric properties of Eu_2TiO_5 was discussed deeply [308]. Meanwhile, the electron localization function (ELF) based on the first-principles calculation was evaluated to provide the information of bond covalency [309], which provided a strategy to estimate the chemical bond characterization.

2.4.2 Tungsten bronze structure

The different compositions of tungstenbronze-type with $Ba_{6-3x}R_{8+2x}Ti_{18}O_{54}$ solid solution reported by Ohsato [310] in 2001, and the compounds were presented in Fig. 16. The relative permittivity of $BaO–R_2O_3–TiO_2$ (R = La–Gd) was higher than 80, and the solid solubility region became narrower as the ionic radius of rare earth increasing [311]. The doping effect and the determination of crystal structure of $Ba_{6-3x}R_{8+2x}Ti_{18}O_{54}$ were summarized in the review of dielectric materials for wireless communication [1]. After 2010, there are only a few studies focused on this system. Three distinct phases were formed using variable size TiO_2 reagents into $BaO–Nd_2O_3–TiO_2$ [312]. $Ba_{6-3x}R_{8+2x}Ti_{18}O_{54}$ (BRT, R = La, Pr, Nd, Sm) solid solution family was reported with high permittivity. When x = 2/3, $Ba_4Nd_{9.33}Ti_{18}O_{54}$ was regarded as the most investigated ceramics to lower its τ_f value and sintering temperature or improve its $Q\times f$ value. Yao *et al*. [313] and Chen *et al*. [314] proposed that with Al_2O_3 added $BaO–Nd_2O_3–TiO_3$ ceramics, the $Q\times f$ value would increase obviously. The temperature-stable ceramics could be obtained by Pb and Sr substitution for $Ba_{3.75}Nd_{9.5}Ti_{18}O_{54}$ [315]; $Ba_{4.5}Re_9Ti_{18}O_{54}$ (Re = La, Nd) [316]; solid solution of $Ba_{4.2}Nd_{9.2}Ti_{18-x}Sn_xO_{54}$ [317], $(Ba_{0.98}Sr_{0.02})_{3.75}Nd_{9.5}Ti_{18x}(Zn_{1/3}Nb_{2/3})_xO_{54}$ [318], $Ba_{6-3x}Nd_{8+2x}Ti_{18-y}(Cr_{1/2}Nb_{1/2})_yO_{54}$ [319], $Ba_4Nd_{9.33}(Al_{0.5}Nb_{0.5})_xTi_{18-x}O_{54}$ [320], $Ba_{3.75}Nd_{9.5}Ti_{18-z}(Al_{1/2}Nb_{1/2})O_{54}$ [321], and $Ba_xSr_{1-x}TiO_3$ [322]; $NdAlO_3$ [323] addition to $Ba_4Sm_{9.33}Ti_{18}O_{54}$; MgO, Al_2O_3, and MnO_2 substituted for Ti^{4+} [324] in $Ba_{4.2}Sm_{9.2}Ti_{18}O_{54}$, $Ba_4La_{3.73}Sm_{4.66}Bi_{0.93}Ti_{18}O_{54}$, $Ba_4(Pr_{0.4}Sm_{0.6})_{28/3}Ti_{18-y}Ga_{4y/3}O_{54}$ [325], and $Ba_4(Pr_{1-x}Sm_x)_{28/3}Al_{4y/3}O_{54}$ [326]. Among those reports, the analysis of Raman spectrum of $Ba_{3.75}Nd_{9.5}Ti_{18-z}(Al_{1/2}Nb_{1/2})O_{54}$ enriched the theoretical study of tungstenbronze-type.

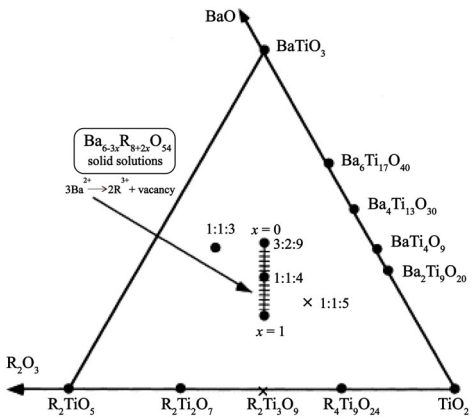

Fig. 16 $BaO–R_2O_3–TiO_2$ (R = rare earth) ternary system. Reproduced with permission from Ref. [310], © Elsevier Science Ltd. 2001.

2.4.3 BaO–ZnO–TiO₂ system

Ceramics based on the $BaO–ZnO–TiO_2$ system have been concluded as $Ba_4ZnTi_{11}O_{27}$, $BaZn_2Ti_4O_{11}$, $Ba_2ZnTi_5O_{13}$, and $Ba_xZn_xTi_{8-x}O_{16}$–hollandite [327]. The substitution of Cu for Zn dramatically increased the $Q\times f$ value because of the restrain of the formation of Ti^{3+} ions [328]. Considering the opposite τ_f values of $BaTi_4O_9$ and $BaZn_2Ti_4O_{11}$, the τ_f values of composite ceramic based on those two phases varied gradually from 12 to –13 ppm/℃ [329]. CuO also worked as flux former to enhance the densification in the $BaTi_4O_9$–$BaZn_2Ti_4O_{11}$ composite ceramics, and the $0.85BaTi_4O_9$–$0.15BaZn_2Ti_4O_{11}$–1 wt% CuO presented the properties as $\varepsilon_r \approx$ 36.4, $Q\times f$ value ≈ 62,600 GHz, and $\tau_f \approx$ +0.2 ppm/℃ [330]. Phase evolution of $BaZn_2Ti_4O_{11}$–$BaNd_2Ti_4O_{12}$ ceramics was determined by Yu *et al*. [331], where $0.8BaZn_2Ti_4O_{11}$–$0.2BaNd_2Ti_4O_{12}$ ceramics possessed properties as $\varepsilon_r \approx$ 39.1, $Q\times f$ value ≈ 37,850 GHz, and $\tau_f \approx$ –9 ppm/℃.

2. 5 Perovskite related structure

The ideal perovskite (written as ABO_3) is cubically symmetric with a space group of $Pm\bar{3}m$, and the represented material is $SrTiO_3$. Due to the flexibility of ABO_3 perovskite, variants of perovskite have been investigated, and the classification of perovskite-related structure with representative structure is summarized in Fig. 17. The perovskite-related structure

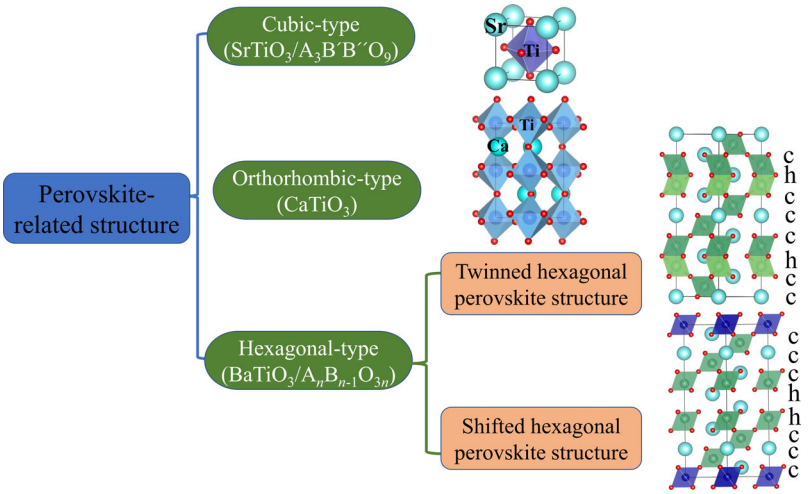

Fig. 17 Classification and the representative structure of perovskite-related structure.

contained cubic-type, orthorhombic-type, and hexagonal-type structures. For hexagonal-type structure, the twinned hexagonal structure means the closely packed AO_3 layers were stacked in the order of $(ccch)_2$, while the shifted hexagonal structure corresponds to ccchhccc order. The typical representative of twinned structure is $Ba_8CoTa_6O_{24}$ and the shifted structure is $Ba_8CoNb_6O_{24}$ with eight-layer hexagonal perovskite structure [332]. The pseudo phase diagram of ABO_3 and complex ABO_3 type is provided in Fig. 18. From cubic and orthorhombic to hexagonal perovskite structure, researchers have proposed that tolerance factor, distortion of octahedron, and temperature of phase transition determined the variation of τ_f value, and the ordered/disordered cations were primarily related to quality factor.

2.5.1 ABO_3 formula

This section contains the ceramics with a general formula of ABO_3 and their related structure or system. Perovskite family is entirely studied because of their pyro and piezo electricity, linear and non-linear electric–optic properties, and superconducting properties. A serials of investigation of $CaTiO_3$ with $MgTiO_3$-based [333–339], $LaAlO_3$-based [340–347], $LaGaO_3$ [348], $Re(Zn_{1/2}Ti_{1/2})O_3$ [349], $(Mg_{1-x}Zn_x)_{1.8}Ti_{1.1}O_4$ [350], $BiSbO_4$ [351], $Nd(Mg_{0.4}Zn_{0.1}Sn_{0.5})O_3$ [352], $Sm_{0.9}Nd_{0.1}AlO_3$ [353], $Ca(Mg_{1/3}Nb_{2/3})O_3$ [354], $(Li_{0.5}La_{0.5})TiO_3$ [355], $Li_{0.5}Nd_{0.5}TiO_3$ [356], $Li_{0.5}Sm_{0.5}TiO_3$ [357], $Mg_{0.95}Co_{0.05}TiO_3$ [335], $(Sm,Nd)AlO_3$ [358–364], Zn_2SnO_4 [365], Li_3NbO_4 [248], $Ca(Mg_{1/3}Nb_{2/3})O_3$ [366], $Sm_{0.9}Nd_{0.1}AlO_3$ [367], $Na_{0.5}Nd_{0.5}TiO_3$ [368], $Nd(Mg_{1/2}Ti_{1/2})O_3$ [369,370], $Bi_{0.5}Na_{0.5}TiO_3$ [371], $3CaO–Re_2O_3–2WO_3$ system [372], $Ba_{0.6}Sr_{0.4}La_4Ti_4O_{15}$ [373], La_2MgGeO_6 [374], $(Ca_{0.8}Sr_{0.2})(Sn_xTi_{1-x})O_3$ [375], $Ca_{0.7}Ti_{0.7}La_{0.3}(Al_{0.3-x}Ga_x)O_3$ [376], $Ca_{(1-x)}Nd_{2x/3}TiO_3$ [377], $Ca_{0.6}La_{0.2667}TiO_3$ [378], $Ca_{0.6}La_{0.267}Ti_{1-x}(Nb_{0.5}Ga_{0.5})_xO_3$ [379], $Ca_{0.6}Nd_{0.8/3}TiO_3–(Li_{0.5}Nd_{0.5})TiO_3$ [380], $Ca_{0.4-x}Mg_xSm_{0.4}TiO_3$ [381], $CaTi_{1-x}(Nb_{0.5}Ga_{0.5})_xO_3$ [382], $Ca_{0.66}Ti_{0.66}Sm_{0.34}Al_{0.34}O_3$ [383], $Ca_{0.66}Ti_{0.66}Nd_{0.34}Al_{0.34}O_3$ [384], $CaTi_{1-x}(Al_{0.5}Nb_{0.5})_xO_3$ [385,386], $Ca_{0.6}La_{0.8/3}(Sn_xTi_{1-x})O_3$ [387], $Ca_{(1-3x/2)}Ce_xTiO_3$ [388], $Ca_{0.35}Li_{0.25}Nd_{0.35}Ti_{1-x}(Zn_{1/3}Ta_{2/3})_xO_3$ [389], $Ca_{0.61}Nd_{0.26}Ti_{1-x}Cr_xO_3$ [390], $CaTi_{1-x}(Mg_{1/2}W_{1/2})_xO_3$ [391], and $Ca(Hf_xTi_{1-x})O_3$ [392] ceramics have been reported thoroughly. Different thermally treated methods to minimize the dielectric loss for $CaTiO_3$ were proposed by Hu *et al.* [393]. The dielectric constant values saturated at 7.7–8.5 of $Ca_{0.8}Sr_{0.2}SnO_3$ ceramics in the sintering temperature range of 1450–1540 ℃ [394]. $0.4Nd_{2.94/3}Ba_{0.03}(Mg_{0.5}Sn_{0.5})O_3–0.6Ca_{0.8}Sr_{0.2}TiO_3$ ceramics modified the τ_f value to –7 ppm/℃ when sintered at 1600 ℃ [395]. Although numbers of

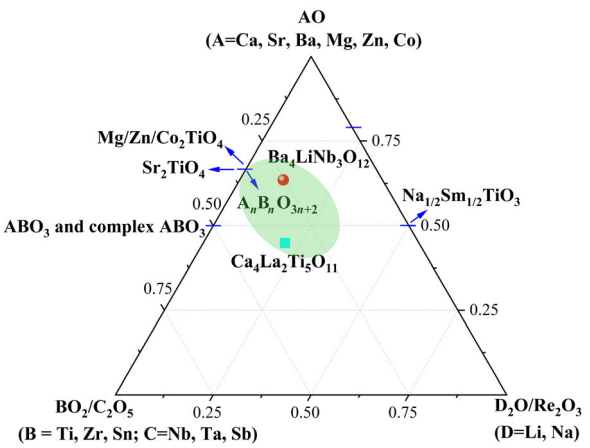

Fig. 18 Pseudo phase diagram of perovskite related structure.

investigations about optimizing the properties of $CaTiO_3$ ceramics have been reported, the vibrational characteristic of $CaTiO_3$ was verified by Shi *et al*. [396] in 2020.

For solid solution of $Ba[Ti_{0.4}Ga_{0.3}Nb_{0.3(1-x)}Sb_{0.3x}]O_3$, a near zero τ_f value of –1.1 ppm/℃ was obtained with x = 0.5 [397], while a τ_f value of 8.2 ppm/℃ was achieved for $(Sr_{0.2}Ga_{0.488}Nd_{0.208})Ti_{1-x}Ga_{4x/3}O_3$ with x = 0.5 [398]. A dramatical decrease of τ_f value from 1171 to –82 ppm/℃ was obtained for $Sr(Zr_xTi_{1-x})O_3$ [399]. In the chemical formula of $SrO(Sr_{1-x}Ba_xTiO_3)_n$ (x = 0, 0.5; n = 1–4), it is demonstrated that samples with n = 1, 2 had no dielectric non-linear behavior in the temperature range of (–165)–50 ℃, while the tunability increased with n increasing [400]. Two second phases containing $BaWO_4$ and $Ba_2Ti_5O_{12}$ were observed in $Ba_{0.5}Sr_{0.5}Ti1_{-3y/2}W_yO_3$ system with $y \geqslant 0.02$ [401], and $BaTiSiO_5$ phase was indexed in $Ba_{0.4}Sr_{0.6}Ti_{1-y}Si_yO_3$ [402]. The dielectric constant can be adjusted apparently in the $Ba_{0.4}Sr_{0.6}TiO_3$–$BaMoO_4$ and $Ba_{0.5}Sr_{0.5}TiO_3$–$AMoO_4$ (A = Ba, Sr) composite ceramics, where only cubic perovskite structure and scheelite structure were detected [403,404]. However, the $BaMoO_4$ was observed when $MgMoO_4$ added into $Ba_{0.5}Sr_{0.5}TiO_3$ [405]. Adding $Zr_{0.8}Sn_{0.2}TiO_4$ into $Ba_{0.4}Sr_{0.6}TiO_3$, the dielectric constant and dielectric loss increased with the increase of the content of $Zr_{0.8}Sn_{0.2}TiO_4$ [406]. Adding Fe power in $Ba_{0.4}Sr_{0.6}TiO_3$ ceramics indicated that the appearance of Fe^{2+} and Fe^{3+} would decrease the O vacancy concentrations and enhance the microwave dielectric properties [407]. In the ternary system of $Ba_{0.5}Sr_{0.5}TiO_3$–MgO–Mg_2TiO_4 [408], $Ba_{0.5}Sr_{0.5}TiO_3$–MgO–Mg_2SiO_4 [409], and $(1–x–y)BaTiO_3$–$xCr_2Ti_3O_9$–yBi_2O_3 [410], the dielectric constant reduced with more Mg_2TiO_4 and Mg_2SiO_4, while solid solution was observed with Cr^{3+} and Bi^{3+} into $BaTiO_3$. Co-doping ZnO, Al_2O_3, and MgO on the $Ba_{0.66}Sr_{0.4}TiO_3$ would generate $Mg(Zn)Al_2O_4$ as the secondary phase [411]. The lattice vibrations of $Ba_{0.4}Sr_{0.6}TiO_3$ ceramics were systematically investigated by Jiang *et al*. [412] after Mn substituted for Sr. Zr and Sn doped into $Ba_{0.1}Mg_{0.9}TiO_3$ ceramic would bring about $Ba_2Ti_9O_{20}$ and $BaTi_5O_{11}$ [413]. Similar to $CaTiO_3$, the effect of $LnAlO_3$ (Ln = Sm, Nd) on $BaTiO_3$-based ceramics was systematically studied by Liu *et al*. [414] and Xie *et al*. [415]. Solid solution of $Ba_xMg_{1-x}Ti_{0.95}Sn_{0.05}O_3$ [416] and local 1:1 ordering in B-site of $Sr(Ga_{0.5}Nb_{0.5})_{1-x}Ti_xO_3$ was verified by TEM and Raman spectroscopy, and the decline of quality factor stemmed from the anharmonicity by Ti substitution [417]. $0.2SrTiO_3$–$0.8Ca_{0.61}Nd_{0.26}Ti_{1-x}Al_{4x/3}O_3$ ceramics also reached a near zero τ_f value with x = 0.5 [418]. $(1–x)Mg(Ti_{0.95}Sn_{0.05})O_3$–$xBaTiO_3$ compounds experienced a phase transition of tetragonal-structure $BaTiO_3$, monoclinic-structure $Ba_4Ti_{11}O_{26}$, and triclinic-structure $Ba_2Ti_9O_{20}$ [419]. Likewise, $Sr_{(1-1.5x)}Ce_xTiO_3$ (x = 0.1–0.67) ceramics changed from cubic, tetragonal, to orthorhombic, and the dielectric behaviors were dominated by oxygen vacancies and defect dipoles [420]. Tian *et al*. [421,422] reported that $(Co_{0.5}W_{0.5})^{4+}$ and $(Zn_{0.5}W_{0.5})^{4+}$ occupying the Ti-site in $BaTiO_3$ would render the τ_f value change from positive to negative. $BaWO_4$ phase appeared in $Ba_{1-x}Sr_x(Mg_{0.5}W_{0.5})O_3$ ceramics and $Ba_2Mg_{0.95}Zn_{0.05}WO_6$, and the grain size distributed in a narrow range around 0.8 μm [423,424]. A τ_f value of –2.4 ppm/℃ was achieved for B-site deficient $Ba(Mg_{(1-x)/2}Y_{x/3}\square_{x/6}W_{1/2})O_3$ [425]. In the non-stoichiometric system of $(Sr_{0.4}Ce_{0.4})_{1-x}Nd_xTi_{0.8}Mg_{0.2}O_3$, solid solution was obtained when $x \leqslant 0.2$, while the satisfied properties were $\varepsilon_r \approx 53$, $Q{\times}f$ value ≈ 26,700 GHz, and $\tau_f \approx +2.8$ ppm/℃ with x = 0.4 [426]. Meanwhile, compositional dependence of microwave dielectric properties of doped $SrTiO_3$ sintered in air is presented as Fig. 19. It was demonstrated that $SrTiO_3$ added into $ZnAl_2O_4$–$3Zn_2SiO_4$–$2SiO_2$ could reduce the sintering temperature from 1320 to 1180–1200 ℃ [427].

With the same general formula of ABO_3, the investigations of $NdGaO_3$, $NdNbO_3$, and $AgTa/NbO_3$ are listed adjacently to $CaTiO_3$ and $SrTiO_3$. Phase composition was identified for $NdGaO_3$–$Bi_{0.5}Na_{0.5}TiO_3$ system, and new temperature-stable ceramics with $0.4NdGaO_3$–$0.6Bi_{0.5}Na_{0.5}TiO_3$ was obtained [428]. Order–disorder transformation of A-site-deficient perovskites plays a significant role in conductivity of materials. The investigation of crystal structure and dielectric properties of the $Nd_{(1-x)/3}M_xNbO_3$ (M = Li, Ag; $0 \leqslant x \leqslant 0.2$) suggested that the dielectric loss majored by the lithium or silver ionic conduction at low frequencies [429]. Solid solution of $AgNb/TaO_3$-based ceramics was then studied extensively [430,431]. Temperature-stable MWDCs with the formula of $(La,Nd)_{2/3}TiO_3$ were studied by Saleem *et al*. [432].

$MgTiO_3$ also belongs to the general formula of ABO_3. The substitution for $MgTiO_3$ such as Ni, Zn, Co, and Mn for Mg has been investigated systematically [433–436], where $(Mg_{1-x}Co_x)TiO_3$ ceramics were crystalized as ilmenite structure when $x \leqslant 0.5$, and the

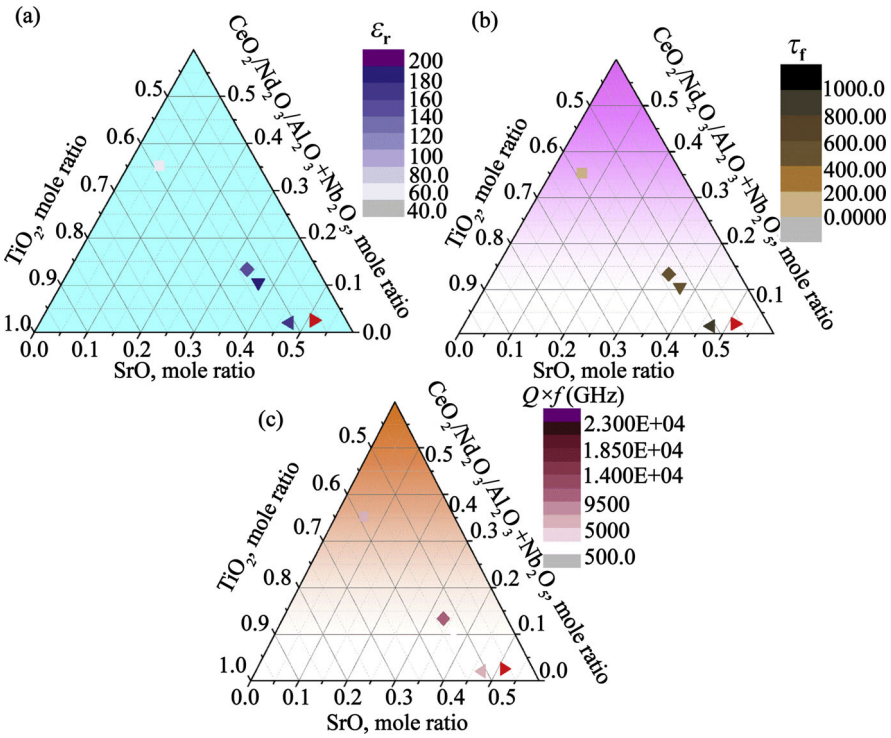

Fig. 19 Compositional dependence of microwave dielectric characteristics of Nd_2O_3, CeO_2, Al_2O_3, and Nb_2O_3 doped $SrTiO_3$ compound sintered in air, closed pipe, and nitrogen atmosphere with (a) relative permittivity (ε_r), (b) TCF (τ_f), and (c) $Q\times f$ value, respectively. Reproduced with permission from Ref. [426], © The Chinese Ceramic Society 2020.

secondary phase was detected with more doping cations [437]. $(Zn_{1-x}Mg_x)TiO_3$ was prepared and demonstrated that the dielectric constant and loss decreased with Mg increase [438]. For Sn doped into Ti site in $MgTiO_3$, in the range of x = 0.05–0.07, the ceramics exhibited excellent microwave dielectric properties of $\varepsilon_r \approx$ 16.8–17.1, $Q\times f$ value ≈ 298,000–312,000 GHz, and $\tau_f \approx$ (–53)–(–50) ppm/℃ [439]. $Mg_{0.95}Co_{0.05}TiO_3$ ceramics possessed properties as $\varepsilon_r \approx$ 17.03, $Q\times f$ value ≈ 170 THz, and $\tau_f \approx$ –40 ppm/℃ when prepared by Semi Alkoxide precursor method [440]. Gong *et al*. [441] obtained $Mg(Sn_{0.05}Ti_{0.95})O_3$ ceramics with microwave dielectric properties $\varepsilon_r \approx$17.6, $Q\times f$ value ≈ 328,543 GHz, and $\tau_f \approx$ –42 ppm/℃, and Jia *et al*. [442] proposed that $Mg(Ti_{1-x}Nb_x)O_3$ showed microwave dielectric properties: $\varepsilon_r \approx$ 18.12, $Q\times f$ value ≈ 163,618 GHz, and $\tau_f \approx$ –40.1 ppm/℃. Through sol–gel process, the quality factor of geikielite-type $MgTiO_3$ saturated when the ceramics sintered at 1200 ℃ [443]. After adding B_2O_3 into $MgTiO_3$, the composite ceramics could be densified at 1100 ℃ [444]. Investigation of introduction $SrTiO_3$ into $Mg(Zr_{0.05}Ti_{0.95})O_3$ ceramics suggested that a close zero τ_f value could achieve at $0.96Mg(Zr_{0.05}Ti_{0.95})O_3$–$0.04SrTiO_3$ [445,446]. In the study of a designed composition of $MgTiO_3$ (Mg/Ti = 1, 1.02, 1.04, 1.05, 1.07), the generation of $MgTi_2O_5$ which derived from Mg/Ti = 1 was restrained, and then pure phase of $MgTiO_3$ was obtained when Mg/Ti = 1.02 [447]. $(Co_{1-x}Zn_x)TiO_3$ sintered at 1350 ℃ possessed $\varepsilon_r \approx$ 20, $Q\times f$ value ≈ 107,000GHz, and $\tau_f \approx$ –60 ppm/℃ with x = 0.05 [448]. The choice of raw material of MgO and $Mg(OH)_2$ had a major influence on the phase formation and dielectric loss for $0.97MgTiO_3$–$0.03SrTiO_3$ [449]. In the system of $(1-x)MgTiO_{3-x}Mg_{2.05}SiO_{4.05}$–$0.06CaTiO_3$, $\tau_f \approx$ 1.45 ppm/℃ was obtained with x = 0.2 [450]. $ZnTiO_3$-type phase, Zn_2TiO_4-type, and TiO_2 phase were co-existed in $(Zn_{0.3}Co_{0.7})Ti_{1-x}Sn_xO_3$, and the satisfied microwave dielectric properties were $\varepsilon_r \approx$ 24, $Q\times f$ value ≈ 66,700GHz, and $\tau_f \approx$ –5.43 ppm/℃ with x = 0.02 [451]. It was interesting that $MgTiO_3$ and Mg_2TiO_4 were the main phases in $Mg_{n+1}Ti_nO_{3n+1}$ (n = 2, 3, 4, 5, 6, and 7), and the Mg_2TiO_4 was effectively inhibited with n increasing [452]. New cofired tri-layer ceramic architecture of $MgTiO_3/TiO_2/MgTiO_3$ was designed to realize the temperature-stable and ultrahigh-Q ceramics, where the property comparison of MgO–TiO_2 system (Fig. 20) indicated that this new strategy was effective for developing high-performance dielectric resonators [4]. 2 wt% B_2O_3 as an addictive could effectively reduce the sintering temperature from

1275 to 1175 ℃ in $0.9625MgTiO_3$–$0.0375Ca_{0.5}Sr_{0.5}TiO_3$ [453]. Mg_2TiO_4-related and $Mg_6Ti_5O_{16}$-based ceramics in MgO–TiO_2 system were also reported. $Mg_6Ti_5O_{16}$-based MWDCs were systematically investigated by Yu *et al*. [454], where the τ_f value could be adjusted to –3 ppm/℃ by Ca^{2+} substitution. To explore the application for mobile communication, Nb^{5+} ion was added into Mg_2SnO_4 to improve the quality factor [455]. By mechanical synthesis method, the value of quality factor was sensitive to the initial particle size and microstructure of Mg_2TiO_4 [456]. Meanwhile, the oxygen vacancies and average sizes were highly influenced on the dielectric loss of adding La_2O_3, V_2O_5, and CeO_2 into Mg_2TiO_4 [457,458]. A maximum quality factor value of 210,700 GHz was obtained in $(Mg_{1-x}Zn_x)_{1.8}Ti_{1.1}O_4$ with x = 0.06 [459]. $[(Mg_{0.5}Zn_{0.5})_{0.95}Co_{0.05}]_2TiO_4$ was demonstrated as the optimal composition in the solid solution of (Mg, Zn)$_2TiO_4$–Co_2TiO_4 with $Q\times f$ value ≈ 2100,000 GHz [460]. The average particle size of pure Mg_2TiO_4 nano-powders was reduced to 163 nm via high energy ball milling method, and the excellent properties were ε_r ≈ 13.9, $Q\times f$ value ≈ 98,600 GHz, and τ_f ≈ –50.9 ppm/℃ [461]. Similarly to the formula of Mg_2TiO_4, spinel-based $CoZnTiO_4$ ceramics were obtained after sintered at 1200 ℃, and the properties were majored by the relative density and grain size [462]. Solid solution of $Mg_2(Ti_{1-x}Sn_x)O_4$ [463] and $ZnNiTiO_4$/$ZnNiTi_{1-x}Sn_xO_4$ [464,465] was also reported. Until now, the intrinsic dielectric behavior of Mg_2TiO_4 based on P–V–L theory and infrared spectra was presented by Li *et al*. [466], where the Ti(1)–O bond plays a primary role in dielectric loss. Meanwhile, $Mg_2Ti_{1-x}Ga_{4x/3}O_4$ would reach a $Q\times f$ value ≈ 205,416 GHz [467].

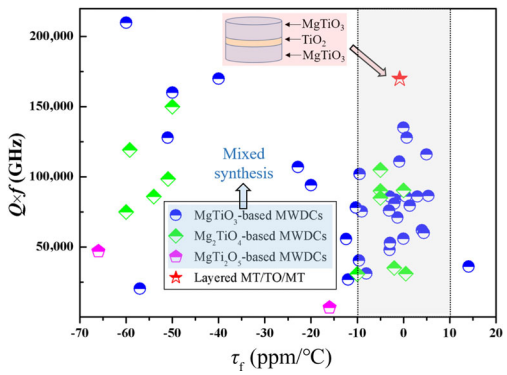

Fig. 20 Summary of $Q\times f$ value versus τ_f plot for MgO–TiO_2 system MWDCs. Reproduced with permission from Ref. [4], © Elsevier Ltd and Techna Group S.r.l. 2018.

Furthermore, there are some compounds in the formula of $Na_{0.5}Ln_{0.5}TiO_3$ (Ln = Sm, Nd). Fang *et al*. [468] and Zhou *et al*. [469] reported a serials of substitution, such as $Na_{0.5}Nd_{0.2}Sm_{0.3}Ti_{1-x}Sn_xO_3$, $Na_{0.5}Nd_{0.5}Ti_{1-x}Sn_xO_3$, $Na_{0.5}Nd_{0.2}Sm_{0.3}Ti_{1-x}Zr_xO_3$ [470], and $Na_{1/2}Sm_{1/2}Ti_{1-x}(Cr_{1/2}Nb_{1/2})_xO_3$ [471]. Near zero τ_f value appeared in $Li_{0.5}Sm_{0.5}TiO_3$–$Na_{0.5}Sm_{0.5}TiO_3$ [472].

2.5.2 $A_2B'B''O_6$ formula

Due to the flexibility and adjustability of the crystal structure of perovskite, the investigation of complex perovskite with various cations occupying Ti site gradually emerged. The structural studies of $A_2B'B''O_6$ (A = Ba, Sr, Ca; B′ = lanthanide, Mg, Cr, Bi; B″ = Nb, Ta, Sb, W) indicated that phase transitions were ascribed to the tilting of $B'O_6$/$B''O_6$. In the $Ba_{2-2x}Sr_{2x}SmSbO_6$ system, phase transitions of $Fm\bar{3}m$, $I2/m$, and $P2_1/n$ were observed and the τ_f value shifted from +25 to –50 ppm/℃ [473]. Effect of non-stoichiometry $Ba_{1+x}(MgW)_{1/2}O_3$, $Ba(Mg_{1+y}W)_{1/2}O_3$, and $Ba(MgW_{1+z})_{1/2}O_3$ and the sintering temperature on microwave dielectric properties was systematically investigated by Wu and Bian [474] and Chen *et al*. [475], respectively. A zero τ_f value ceramic was obtained in $Ba_2Mg_{1-x}Ca_xWO_6$ system with x = 0.1 [474]. First-principles calculation of assignment for vibrational spectra of $Ba(Mg_{1/2}W_{1/2})O_3$ MWDCs is shown in Fig. 21 [476], which proposed that $F_{1u}(2)$ modes originated from Mg–O_6 vibrations had the largest contribution to the dielectric properties. The investigation of microwave dielectric properties of giant permittivity ceramics with a $A_2B'B''O_6$ formula ($Ba(Fe_{1/2}Nb_{1/2})O_3$ and $Sr(Fe_{1/2}Nb_{1/2})O_3$) indicated that the permittivity was independent of frequency [477].

$Ln(B_{0.5}C_{0.5})O_3$ (Ln = La, Sm, Nd; B = Mg, Zn; C = Ti, Sn) ceramics belonging to the general formula of $A_2B'B''O_6$ have been reported as low dielectric loss materials with an adjustable temperature coefficient of resonant frequency. Among them, minor amount of low-melt point oxide of Bi_2O_3 and B_2O_3 was usually used to enhance the sintering densification of $Sm(Mg_{0.5}Ti_{0.5})O_3$ [478,479], CuO was added into $La_{2.98/3}Sr_{0.01}(Mg_{0.5}Sn_{0.5})O_3$ to enhance the densification [480], and V_2O_5 was valid for reducing the sintering temperature of $Nd(Zn_{1/2}Ti_{1/2})O_3$ [481]. Solid solution of $Nd_{(1-x)}Sm_x(Mg_{0.5}Sn_{0.5})O_3$ [482], $Nd(Mg_{0.5-x}Co_xSn_{0.5})O_3$ [483], $Nd_{(1-2x/3)}Ca_x(Mg_{0.5}Sn_{0.5})O_3$ [484], $Nd_{(1-2x/3)}Sr_x(Mg_{0.5}Sn_{0.5})O_3$ [485], $Nd_{(1-2x/3)}Ba_x(Mg_{0.5}Sn_{0.5})O_3$ [486],

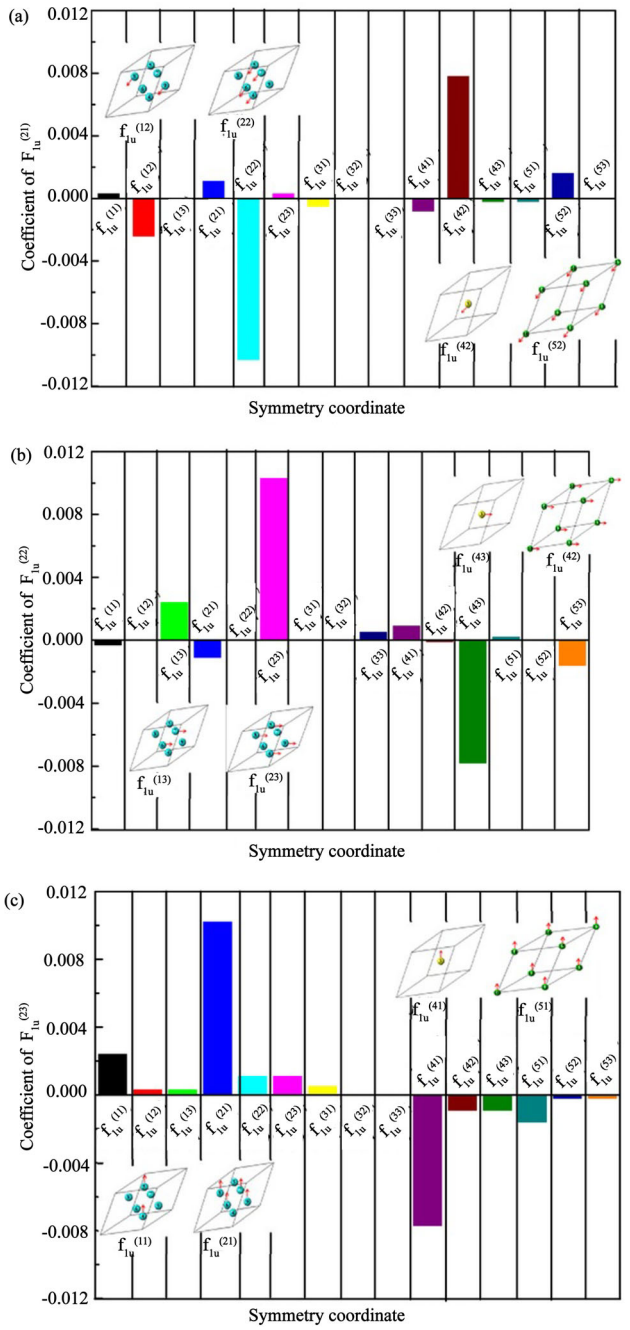

Fig. 21 Combinations of the symmetry coordinates (normalized) for IR-active $F_{1u}(2)$ modes. Reproduced with permission from Ref. [476], © The American Ceramic Society 2013.

$Nd(Mg_{0.5-x}Ni_xSn_{0.5})O_3$ [487], $Nd(Mg_{0.5-x}Zn_xSn_{0.5})O_3$ [488], $Nd(Mg_{0.5}Sn_{0.5-x}Ti_x)O_3$ [489], $Nd(Mg_{0.5-x}Ca_xSn_{0.5})O_3$ [490], $Nd[(Zn_{1-x}Co_x)_{0.5}Ti_{0.5}]O_3$ [491], $Nd(Zn_{0.5+x}Ti_{0.5})O_3$ [492], $Nd_{(1+x)}(Mg_{1/2}Sn_{1/2})O_3$ [493], $Nd(Mg_{0.5}Sn_{0.5(1+x)})O_3$ [494], $La_{1-x}B_x(Mg_{0.5}Sn_{0.5})O_3$ [495], $La_{(1-x)}Sm_x(Mg_{0.5}Sn_{0.5})O_3$ [495], $La_{0.97}Sm_{0.03}(Mg_{0.5}Sn_{0.5})O_3$–$Ca_{0.8}Sr_{0.2}TiO_3$ [395], $La_{1-x}Yb_x(Mg_{0.5}Sn_{0.5})O_3$ [496], $La(Mg_{0.5-x}Ba_xSn_{0.5})O_3$ [497], $Pr_{0.22}Y_{0.78}TiTaO_6$ [498], $La(Mg_{0.4}Sr_{0.1}Sn_{0.5})O_3$–$Nd(Co_{0.5}Ti_{0.5})O_3$–$Ca_{0.8}Sr_{0.2}TiO_3$ [499,500], $La(Mg_{0.5-x}Sr_xSn_{0.5})O_3$ [501], $Ca_{0.6}La_{0.267}TiO_3$–$Ca(Sm_{0.5}Nb_{0.5})O_3$ [502], and $La[Al_{1-x}(Mg_{0.5}Ti_{0.5})_x]O_3$ [503] was investigated based on sintering behavior and microstructure. Not only the investigations reported the microwave dielectric properties, but also the structure–property relationship containing intrinsic loss, vibrational modes, and chemical bond characteristics of Y_2MgTiO_6 was studied in detail, and the schematic representation of vibrational modes of Y site was presented in Fig. 22 [504].

2.5.3 *$A(B'_{1/3}B''_{2/3})O_3$ formula*

$A(B'_{1/3}B''_{2/3})O_3$ (A = Ba, Ca; B′ = Mg, Zn; B″ = Nb, Ta) ceramics have been commercially used due to their excellent $Q\times f$ value, and the near-zero τ_f value. The order structures of $Ca_{1-0.3x}La_{0.2x}[(Mg_{1/3}Ta_{2/3})_{1-x}Ti_x]O_3$-based, $Ba(Mg_{1/3}Nb_{2/3})O_3$-based, $Ba(Zn_{1/3}Ta_{2/3})O_3$-based and $Ba_3CaNb_2O_9$ ceramics were investigated by TEM and the vibrational spectra to explain the cation ordering [505–525]. Meanwhile, superstructure reflections were obviously recorded in this system, such as $Ba(Zn_{1/3}Ta_{2/3})O_3$ doped with Nb_2O_5, MnO_2, and V_2O_3 [526,527]. The wavelength of 1:2 ordered superlattice modulation was about 0.71 nm, while that of disordered superlattice modulation was 0.41 nm of $Ba((Co_{0.6-x/2}Zn_{0.4-x/2}Mg_x)_{1/3}Nb_{2/3})O_3$, shown as Fig. 23 [511]. Adding MnO_2 into $Ba(Co_{1/3}Nb_{2/3})O_3$ would enhance the grain growth and restrain the evaporation of CoO [527]. Meanwhile, the influence of B″-site non-stoichiometry of $Ba(Co_{0.56}Y_{0.04}Zn_{0.35})_{1/3}Nb_{2/3+x}$ on properties was reported by Tang *et al*. [528], where $Ba_5Nb_4O_{15}$ as a secondary phase was recorded. Simulation is carried out for $Ba(Zn_{1/3}Ta_{2/3})O_3$ for the design of linear metal taper [529]. Peng *et al*. [530] reported that addition of La_2O_3 into $Ba(Mg_{1/3}Ta_{2/3})O_3$, $Ba_{1-x}Ca_x(Mg_{1/3}Ta_{2/3})O_3$, and $Ba[Mg_{1-x}Zn_x]_{1/3}Ta_{2/3}O_3$ led to the appearance of $Ba_{0.5}TaO_3$, and τ_f value reached to near zero [531,532]. The optimal properties of $Ba[Mg_{(1-x)/3}Sn_xTa_{2(1-x)/3}]O_3$ exhibited as $\varepsilon_r \approx 24.1$, $Q\times f$ value ≈ 138,500 GHz, and $\tau_f \approx +0.2$ ppm/℃ [533]. The variation of τ_f values for 1:1 and 1:2 complex perovskites was clarified to be mainly relevant with tolerance factors, which are summarized in Fig. 24 [524]. It has been verified that samples with non-stoichiometric Mg^{2+} and Ta^{5+} in $Ba(Mg_{1/3}Ta_{2/3})O_3$ exhibited a wide temperature stability [525,534], and the correlations between $Q\times f$ versus ε_r and τ_f versus ε_r of high-Q (≥ 100,000 GHz) MWDCs are presented in Fig. 25.

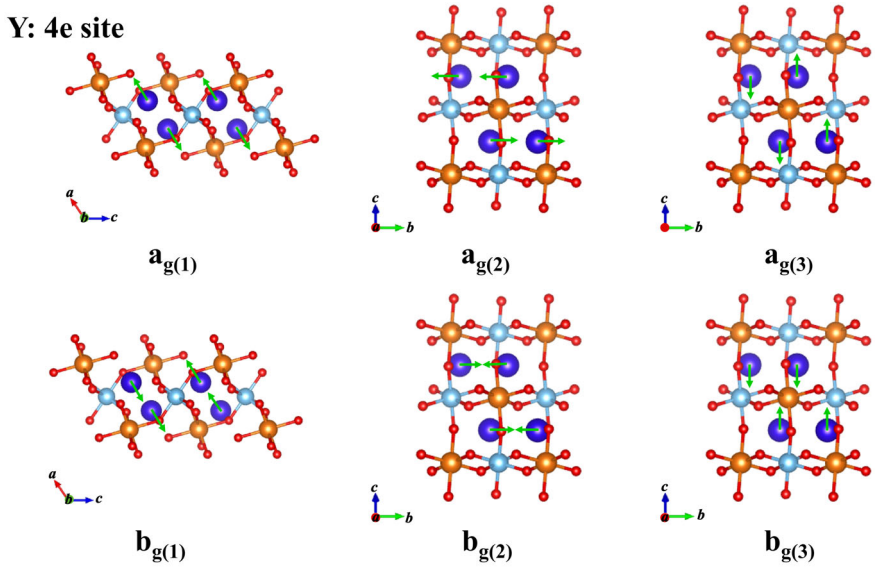

Fig. 22 Schematic representations of the vibrational modes of Y_2MgTiO_6 system (Y at 4e site). Reproduced with permission from Ref. [504], © The American Ceramic Society 2019.

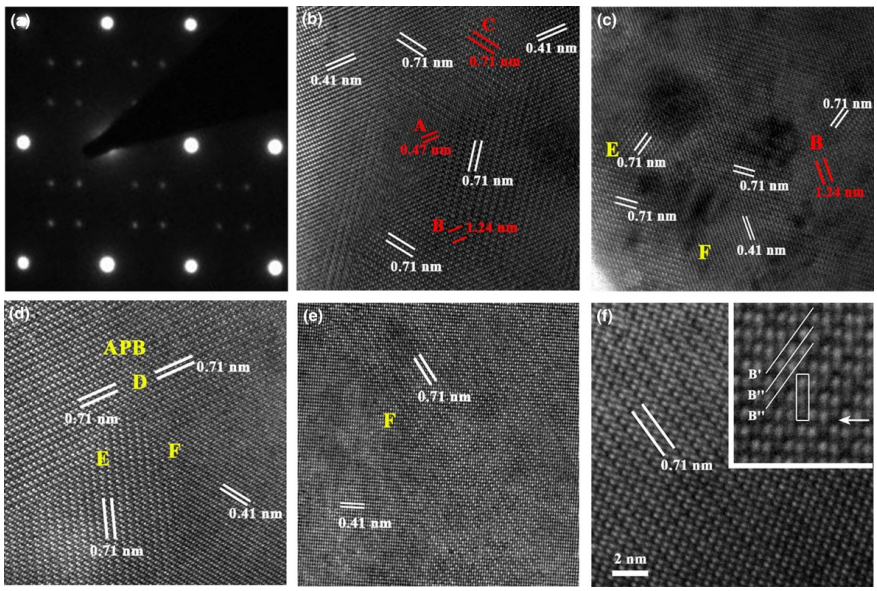

Fig. 23 SAED pattern with zone axis $[1\bar{1}0]_c$ and the corresponding HRTEM images for $Ba((Co_{0.6-x/2}Zn_{0.4-x/2}Mg_x)_{1/3}Nb_{2/3})O_3$ ceramics: (a) $x = 0.1$; (b) $x = 0$; (c) $x = 0.1$; (d) $x = 0.2$; (e) $x = 0.3$; (f) HRTEM image of an ordered area in high magnification. Reproduced with permission from Ref. [511], © The American Ceramic Society 2013.

2.5.4 $A_nB_nO_{3n+2}$ formula

Perovskite-related oxides of series $A_nB_nO_{3n+2} = ABO_x$ ($x = 3+2/n$) (A = Ca, Sr, or La and B = Ti or Nb) with $n = 4$, 4.33, 4.5, 5, 6, and 7 have been a focus owing to their electronic and dielectric properties. The crystal type and the physical properties rely on the value of n, which descripts the number of octahedral layers in the slabs [535]. Besides $Ca_5Nb_5O_{17}$, the $A_nB_nO_{3n+2}$ phases appeared in the binary system of $La_2Ti_2O_7$–$CaTiO_3$, $Nd_2Ti_2O_7$–$CaTiO_3$, and $Ca_2Nb_2O_7$–$CaTiO_3$. Joseph *et al.* [536] reported the microwave dielectric properties of $Ca_5A_4TiO_{17}$ (A = Nb, Ta) as $\varepsilon_r \approx 44.9$, $Q\times f$ value ≈ 17,600 GHz, and $\tau_f \approx -112.9$ ppm/℃ for $Ca_5Nb_4TiO_{17}$; $\varepsilon_r \approx 40.1$, $Q\times f$ value ≈ 16,500 GHz, and $\tau_f \approx -53.6$ ppm/℃ for $Ca_5Ta_4TiO_{17}$. The solid solution of $SrLa_{4-x}Sm_xTi_5O_{17}$ ($0 \leqslant x \leqslant 4$) and $Sr_{1-x}Ca_xLa_{4-x}Ti_5O_{17}$ ($0 \leqslant x \leqslant 1$) would lower the τ_f to zero with a dielectric constant of near 53 [537,538], while τ_f declined to +70 ppm/℃ by Zr substituted for Ti of

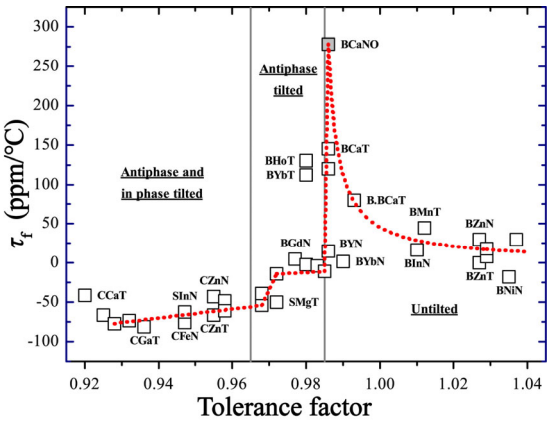

Fig. 24 Temperature coefficient of resonant frequency (τ_f) versus tolerance factor (t) for A(B′,B″)O_3 (A = Ca, Sr, Ba; B′ = Mg, Ca, Mn, Fe, Ni, Zn, Ga, In, Y, Gd, Tb, Dy, Ho, Er, Yb; B″ = Nb, Ta) 1:1 and 1:2 complex perovskites. Reproduced with permission from Ref. [524], © Elsevier Ltd and Techna Group S.r.l. 2016.

$SrLa_4Ti_5O_{17}$ [539]. The intermediate of two end member phases of $CaLa_4Ti_5O_{17}$ and $Ca_5Nb_4TiO_{17}$ showed that the ε_r varied from 45 to 52, $Q\times f$ was in the range of 9870–5680 GHz, and τ_f value ranged between –38 and –126.4 ppm/℃ [540]. $La_3Ti_2TaO_{11}$ is an member of n = 3 in this series, and the textured $La_3Ti_2TaO_{11}$ was fabricated by spark plasma sintering, showing that grain-orientation control was an effective way to tailor the properties of this ceramic [541]. $SrCa_4Nb_4TiO_{17}$ and $Ca_5Nb_4TiO_{17}$ sintered at their optimal temperature presented an elongated and plate-like grain [542]. From 0 to 4, the τ_f value shifted from –117 to 415 in $NaCa_{4-x}Sr_xNb_5O_{17}$ [543], while the τ_f value changed in the range of (–117)–473 ppm/℃ for $Na_{1-x}K_xCa_4Nb_5O_{17}$ [544].

2.5.5 $Ca_4La_2Ti_5O_{17}$

The dielectric properties of $Ca_4La_2Ti_5O_{17}$ were firstly reported by Rejini *et al*. [545], which were crystalized as perovskite structure and the XRD results were matched well based on the formula of $Ca_{0.706}La_{0.353}Ti_{0.882}O_3$. There are rare studies about this system, which just concentrated on the modification of τ_f value. For example, the dielectric constant declined from 71.86 to 35.23 in the solid solution of $Ca_4La_2Ti_{5-x}(Mg_{1/3}Nb_{2/3})_xO_{17}$ ($0 \leqslant x \leqslant 4$), and a near-zero τ_f value (1.62 ppm/℃) was achieved at x = 3 [546]. Meanwhile, a near-zero τ_f value was measured for $0.4Ca_4La_2Ti_5O_{17}$–$0.6NdAlO_3$ ceramics [547] and $Mg_4La_2Ti_5O_{17}$ ceramics [548].

2.5.6 $A_nB_{n-1}O_{3n}$ formula

A series of $A_4B_3O_{12}$-type cation-deficient perovskite ceramics were consistent with the formula of $Sr_{4-m}La_mTi_{m-1}Ta_{4-m}O_{12}$ (m = 1, 2, 3). $Sr_3LaNb_3O_{12}$ and $SrLa_3Ti_2NbO_{12}$ were firstly characterized by Fang *et al*. [549,550]. B-site deficient twinned perovskites such as $Ba_8Ti_3Nb_4O_{24}$, $Ba_8MTa_6O_{24}$ (M = Mg, Zn, Ni, Co, Cu), and $Ba_8Ga_{4-x}Ta_{4+0.6x}O_{24}$ are classified as $A_nB_{n-1}O_{3n}$

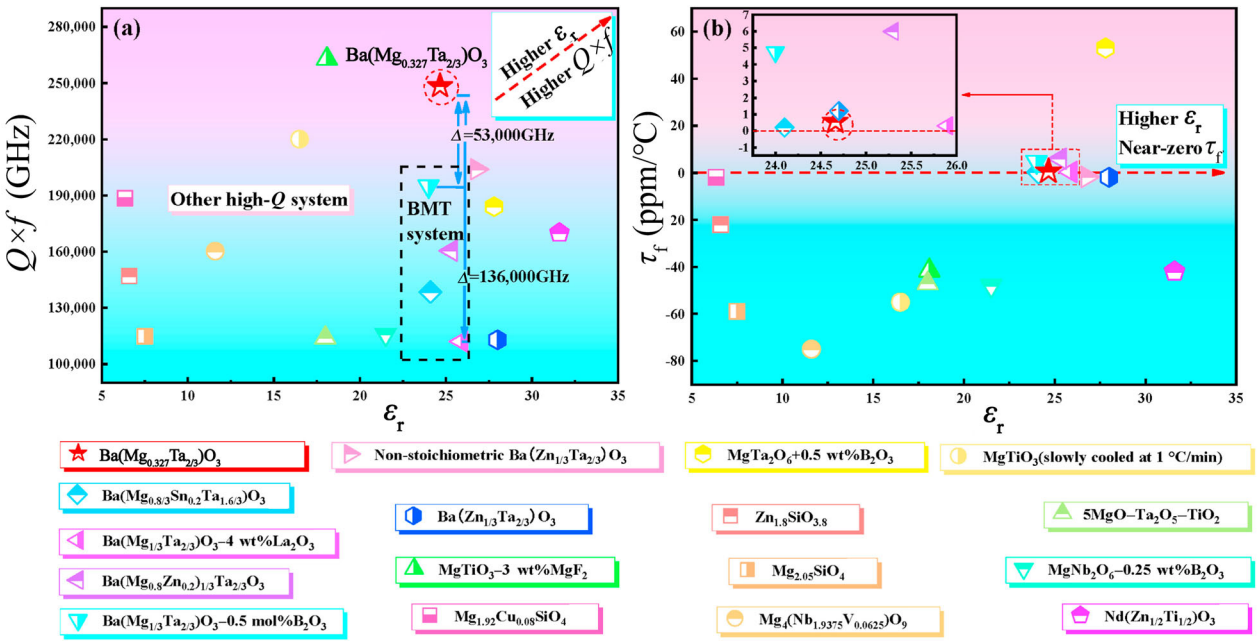

Fig. 25 Correlation between microwave dielectric properties of high-Q ($Q \times f \geqslant$ 100,000GHz) MWDCs: (a) $Q\times f$ versus ε_r; (b) τ_f versus ε_r. Reproduced with permission from Ref. [534], © Elsevier Ltd and Techna Group S.r.l. 2020.

hexagonal perovskites. $Ba_8ZnTa_6O_{24}$ is a secondary phase of $Ba(Zn_{1/3}Ta_{2/3})O_3$-based systems, and the dielectric properties in the range of 5 Hz–50 MHz of Sb substitution for Nb-site have been systematically studied by Suresh *et al*. [551,552] through spectroscopic methods. In the microwave frequency region, the $Q\times f$ value and τ_f values of $Ba_8(Mg_{1-x}Zn_x)Ta_6O_{24}$ ceramics decreased with the augment of x [553]. Similarly, a single phase with hexagonal 8H perovskite structure of $Ba_8Ti_3Nb_{4-x}Sb_xO_{24}$ ceramics was prepared, and τ_f value declined from 110 to 2 ppm/℃ [554]. $BaWO_4$ was used to adjust the large τ_f value of 8H hexagonal perovskite $Ba_4LiNb_3O_{12}$, and the properties of $\varepsilon_r \approx 16.9$, $Q\times f$ value ≈ 75,500 GHz, and $\tau_f \approx +8.7$ ppm/℃ were obtained [555]. Phase transformation in the sequence of hexagonal, hexagonal along with cubic, and cubic was observed in $Ba_4LiNb_{3-x}Sb_xO_{12}$ and $Ba_4LiTa_{3-x}Sb_xO_{12}$ system. Especially, the optimal microwave dielectric properties were achieved for $Ba_4LiNb_2SbO_{12}$ with a zero τ_f [556,557]. τ_f value dropped from positive to negative in $Ba_3LiTa_{3-x}Sb_xTi_5O_{21}$ [558], and $Ba_3LiNb_{3-x}Sb_xTi_5O_{21}$ [559], while the τ_f value just reduced from 205 to 70 ppm/℃ for $Ba_3LiNb_{3-x}Ta_xTi_5O_{21}$ [560]. A-site deficient perovskite structure was well matched for $LiSmTa_4O_{12}$ ceramics with tetragonal perovskite structure (A-site deficient perovskite structure), and the optimal microwave dielectric properties were $\varepsilon_r \approx 59.60$, $Q\times f$ value ≈ 7760 GHz, and $\tau_f \approx +41.8$ ppm/℃ [561].

2.5.7 $Sr_{n+1}Ti_nO_{3n+1}$ (n = 1, 2, 3 4, ∞) formula

Researchers paid their attention to Ruddlesden–Popper (R–P) structure until the dielectric properties of $CaReAlO_4$ (Re = Nd, Sm, Y) were reported. The general formula of R–P compounds was written as $(A,A')_{n+1}B_nO_{3n+1}$, where the structure was built by corner-sharing (BO_6) octahedral and interlayer of ((A,A′)O). $MLnAlO_4$ and $SrLn_2Al_2O_7$ (M = Ca, Sr; R = Y, Sm, Nd, La) belong to the R–P series with n = 1 and 2, respectively. The crystal structures of $SrLaAlO_4$ and $SrLa_2Al_2O_7$ are presented in Fig. 26. Single crystals of $ABCO_4$ layered compounds with K_2NiF_4 structure were used as substrates for high-temperature superconductive thin films, while dielectric properties in this system were mainly investigated by Chen and his co-workers [562–574]. They contributed to analyze the relation between the intrinsic dielectric properties and crystal structure of $MRAlO_4$ (M = Ca, Sr; and R = Y, Sm, Nd, La). Combining the compression/dilation effects of different cation–oxygen bonds and the stability of crystal structure with vibrational spectrum, they emphasized that the drop of the quality factor was ascribed to the abnormal variations of axial bonds and the theoretical dielectric loss was obtained after fitted the infrared reflectivity spectra. With $(Zn_{0.5}Ti_{0.5})^{3+}$ substituted for Al^{3+} of $SrLaAlO_4$, the best combination of microwave dielectric properties was $\varepsilon_r \approx 23.5$, $Q\times f$ value ≈ 102,000 GHz, and $\tau_f \approx -3.4$ ppm/℃ [572]. In the $SrLaAlO_4$–Sr_2TiO_4 system, some diffraction peaks shifted toward higher angles along with the variation of x, while some of them shifted toward lower angles, as shown in Fig. 27 [569]. This phenomenon was explained by the opposite change of a-axis and c-axis, where the octahedron elongated in the ab plane with the shrinkage in the c direction. The tolerance factor (t) of perovskite layer was used to evaluate the stability of those compounds, and the relation of t and $r(M^{2+})/r(Ln^{3+})$ was plotted in Fig. 28 [573]. $Sr_{0.6}Ca_{0.4}LaAlO_4$ with 10 wt% TiO_2 presented a near zero $\tau_f \approx -2.5$ ppm/℃ [575].

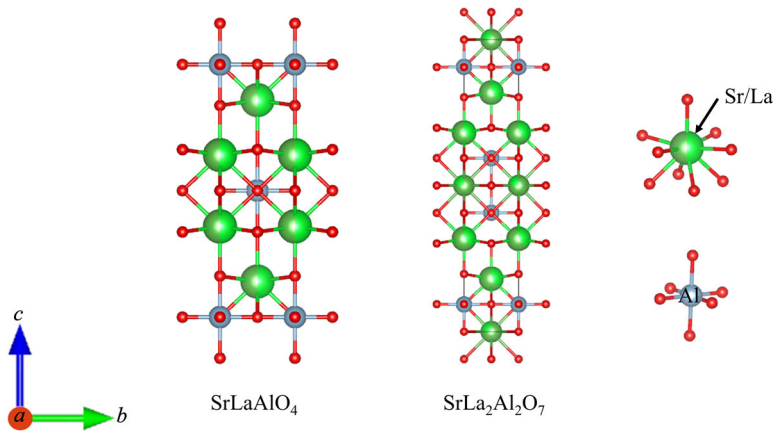

Fig. 26 Crystal structures of $SrLaAlO_4$ and $SrLa_2Al_2O_7$.

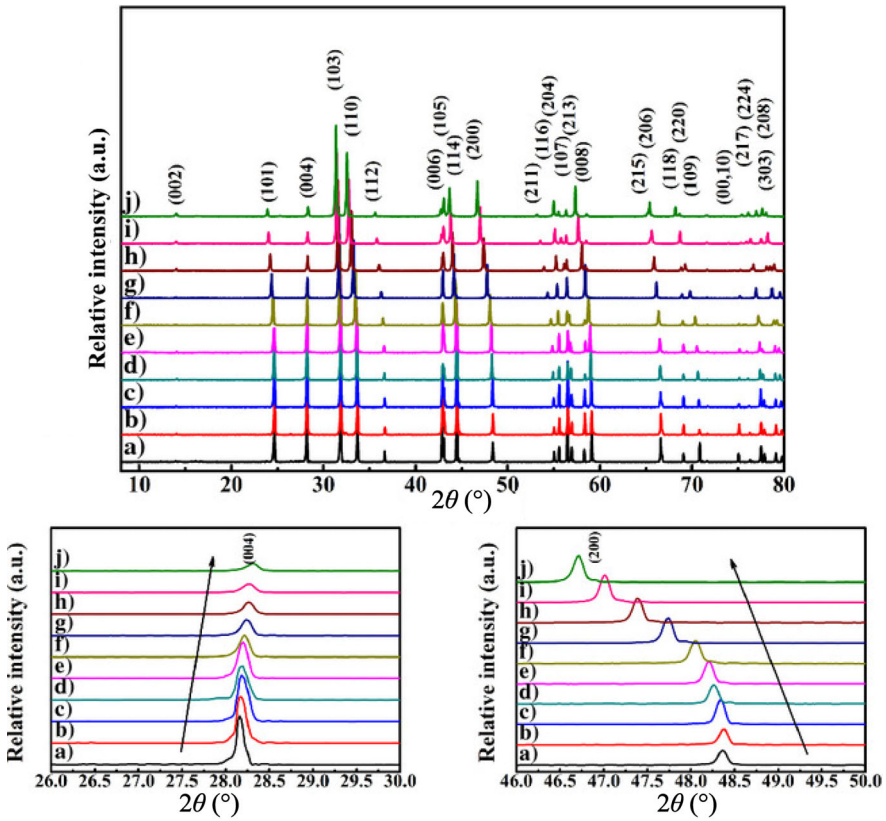

Fig. 27 XRD powder diffraction patterns of ceramics in $(1-x)SrLaAlO_4$–xSr_2TiO_4 system with enlarged (004) and (200) diffraction peaks: (a) x = 0, (b) x = 0.025, (c) x = 0.05, (d) x = 0.10, (e) x = 0.15, (f) x = 0.2, (g) x = 0.4, (h) x = 0.6, (i) x = 0.8, and (j) x = 1. Reproduced with permission from Ref. [569], © The American Ceramic Society 2011.

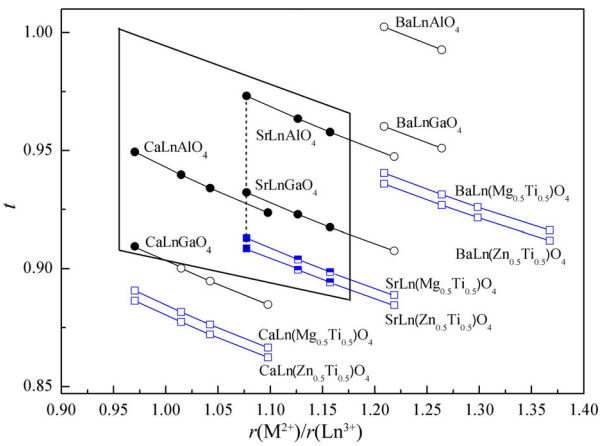

Fig. 28 Stability of K_2NiF_4 structure in $MLnBO_4$ (M = Ca, Sr, Ba; Ln = Y, Sm, Nd, La; B = Al, Ga, $(Mg_{0.5}Ti_{0.5})$, $(Zn_{0.5}Ti_{0.5})$) compounds in relation to t and $r(M^{2+})/r(Ln^{3+})$. Reproduced with permission from Ref. [573], © The American Ceramic Society 2017.

On the other hand, the R–P structure such as $Sr_{n+1}Ti_nO_{3n+1}$ (n = 1, 2) [576], $SrLn_2Al_2O_7$ (Ln = La, Nd, Sm) [577–581], was also established as K_2NiF_4 structure. The interlayer polarization was verified to influence the microstructure and internal stress, and the complete structure information of $SrLn_2Al_2O_7$ ceramics was obtained by TEM. Solid solution of $(Sr_{1-x}Ca_x)_2TiO_4$ [582], $Sr_2Ti_{1-x}Sn_xO_4$ [583], $Sr_2[Ti_{1-x}(Al_{0.5}Nb_{0.5})_x]O_4$ [584], and $(Sr_{1-3x/2}La_x)_2Ti_{1-y}Ce_yO_4$ [585] was prepared to reduce the large τ_f value of Sr_2TiO_4. Moreover, Sr_2CeO_4 was obtained by Dai and Zuo [586], and the substitution of Ti^{4+} for Ce^{4+} in Sr_2CeO_4 generated a ceramic with excellent properties of $\varepsilon_r \approx 20.7$, $Q\times f$ value ≈ 115,550 GHz, and $\tau_f \approx -1.8$ ppm/℃.

2. 6 Other system and machine learning in MWDCs

Although the pseudo phase diagrams contain various primary systems, some ceramics such as CeO_2, $MgAl_2O_4$, $Ca_3Ln_2W_2O_{12}$, and Ln_2MoO_6 (Ln = La, Y) do not classify. It is difficult to arrange those ceramics to any phase diagram and the relevant reports are relatively less, and thus, the investigations about the mentioned ceramics are listed in this section. $Ce_{0.75}Y_{0.25}O_{1.875}$ ceramic was indexed as CeO_2 phase, and the grain size changed from 0.64 to 1.23 μm contributing to a higher $Q\times f$ value [587]. The τ_f value

of $(1-x)Bi_2(Li_{0.5}Ta_{1.5})O_7$–$xTiO_2$ was tuned to –1.45 ppm/℃ with x = 0.04 [588]. $0.875CeO_2$–$0.125TiO_2$ composition possessed properties of $\varepsilon_r \approx 27.38$, $Q\times f$ value ≈ 12,950 GHz, and $\tau_f \approx -2.49$ ppm/℃, which could meet the criterion of practical application [589]. $MgAl_2O_4$ transparent ceramic was designed and optimal microwave dielectric properties were obtained: $\varepsilon_r \approx 8.2$, $Q\times f$ value ≈ 110,510 GHz, and $\tau_f \approx -74.1$ ppm/℃ [590]. The $(Mg_{0.5}Ti_{0.4})^{3+}$ for Al^{3+} in $MgAl_2O_4$ could reduce the sintering temperature approximately 200 ℃ due to the less concentration of the Al–O bond [591]. Vibrational spectroscopy and microwave dielectric properties of $Ca_3Ln_2W_2O_{12}$ (Ln = La, Sm) were analyzed by Liu and Song [592], and the ε_r of those two phases were 18.7 and 19.5. Ln_2MoO_6 (Ln = La, Y) ceramics possessed a relative permittivity of 14.1–17.1, and the quality factor was 67,090 GHz for La_2MoO_6 and 27,760 GHz for Y_2MoO_6, respectively [593].

In the wake of the update of computer science, date-driven approaches including data mining and machine learning have been applied in many disciplines for obtaining the obscure quantitative relationships. For material science, machine learning was used to realize the property prediction, composition optimization, and experimental design [594–600]. Qin *et al*. [601] employed five commonly-used algorithms with 32 intrinsic chemical, structural, and thermodynamic features for modeling to predict low permittivity materials, where a database of 3300 materials has not been reported and the distribution of permittivity in virtual space of materials was shown in Fig. 29. Quantitative prediction of the $Q\times f$ value of gillespite-type $ACuSi_4O_{10}$ (A = Ca, Sr, Ba) ceramics was obtained by machine learning, and the results of $(Ca_xSr_{1-x})CuSi_4O_{10}$ and $(Ba_ySr_{1-y})CuSi_4O_{10}$ ceramics matched well with the experimental $Q\times f$ value, as shown in Fig. 30 [602].

3 Conclusions and further outlook

MWDCs with a suitable permittivity, low dielectric loss, and temperature stability are a perpetual pursuit for researchers. Those ceramics offer technoeconomic advantages including integration, lightweight, and reliability. With the continuous exploration, significant progress is presently being made in designing new compounds, analyzing the polarization mechanism

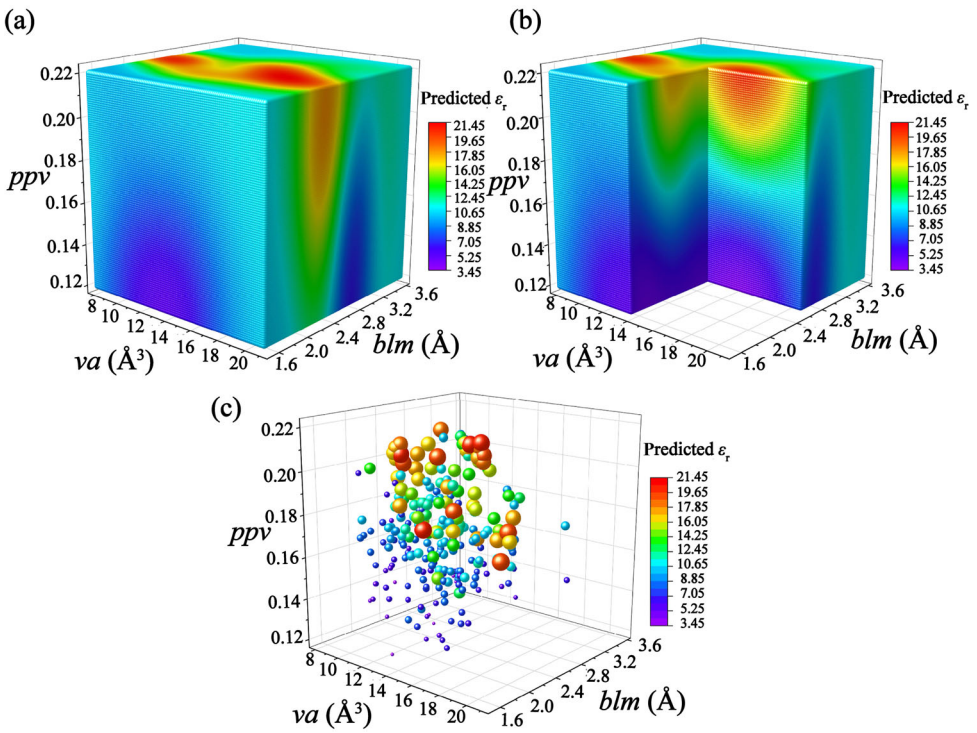

Fig. 29 Distributions of (a) model predicted relative permittivity in virtual space of materials, (b) cross-section of (a) for a clear view of low permittivity zone, and (c) measured permittivity. The notations of *va*, *blm*, and *ppv* are average cell volume per atom, average bond length, and polarizability per unit volume, respectively. Reproduced with permission from Ref. [601], © The Chinese Ceramic Society 2021.

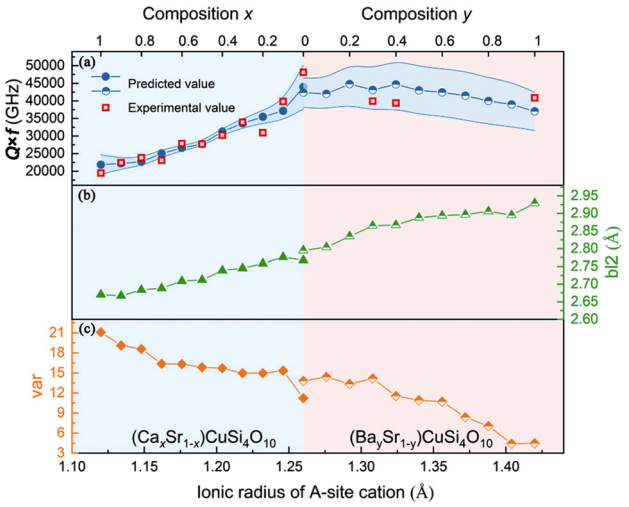

Fig. 30 Machine learning prediction results. (a) Experimental and predicted $Q\times f$ values, (b) feature of bl2 (bond length of A–O_2 bond), and (c) feature of var (variance in bond lengths of A–O bond) of $(Ca_xSr_{1-x})CuSi_4O_{10}$ and $(Ba_ySr_{1-y})CuSi_4O_{10}$ ceramics. The shadow area in (a) represents the standard error of 100 trials. Reproduced with permission from Ref. [602], © American Chemical Society 2021.

along with the origin of dielectric loss, and predicting the microwave dielectric properties by theoretical model of machine learning. The relevant computational and experimental methods currently used to probe, predict, and understand intrinsic mechanisms are covered in this review. Because target ceramic system and their associated investigations are so diverse, we provide a brief classification on the composition of ceramics using pseudo phase diagram. The exploration of substitution of the given ceramics or new compounds is listed briefly following the pseudo phase diagram. Experimentally, it appears that substitution and composite ceramics are the most common used methods to optimize the microwave dielectric properties for a given system (reduce dielectric loss or adjust the τ_f value to near zero). The previous doping researches are concentrated on single ion substitution, while more development of the co-doping (group of two aliovalent cations with a certain mole ratio) appears recently. For the probe of new dielectric materials, the new system usually belongs to germanate and gallate, besides the familiar system of silicate, titanate, niobate, and tantalate. Comparing with conventional solid state reaction method, fabrication techniques containing solution-processed sol–gel method, high energy ball milling method, spark plasma sintering, and microwave sintering have been demonstrated as the promising approaches to improve the properties or sintering behaviors so far. Providing the atmosphere with the volatile element in the sintering procession is a valid method to reduce the pores. Multi-layer ceramic architecture has been verified as a design for temperature-stable ceramics, and the wide application for more system or in the industry is waiting for the exploration.

The influence factor of microwave dielectric properties evolves extrinsic and intrinsic parts. The defects such as porosity, microstructure, and secondary phase are related to the relative density and grain size, which are extrinsic factors. Those results of a unique ceramics can be easily obtained by XRD and SEM, while the investigation of dielectric responded mechanism of intrinsic part is difficult due to the restrain of characterization techniques and the lack of general theory. Theoretically, from Clausius–Mossotti equation, packing fraction, cation valence, distortion of octahedron to the combination of P–V–L theory, lattice dynamics, and THz time-domain spectroscopy with the first-principles calculation, the intrinsic mechanism for MWDCs is gradually created. Recent efforts to employ P–V–L theory and infrared reflectivity spectra to understanding the intrinsic mechanism seem to be an easy and potential approach to draw conclusions for prediction the microwave dielectric properties. However, the development of "try and error" situation in experiments is a long-term procession. Toward this state end, greater fundamental understanding of dielectric response mechanism and increased practical performance metrics are required. The experimental trials and theoretical calculation serve as a database of MWDCs, and then, the machine learning is applied to predict new materials and their microwave dielectric properties. There has been an emerging trend about machine learning to provide new insight to draw a general conclusion to verify the effect of each factor on the variation of microwave dielectric properties. Challenges remain in the reconciliation of conclusion between existing theoretical approaches, the evaluation of P–V–L theory on microwave dielectric properties, and the advancement of first-principles calculation for describing the state of bond. Based on the theoretical analysis of MWDCs and the careful control of extrinsic influence, more comprehensive application-specific analyses to justify their adoption in electronic market may be able to complete.

While there is always a need for fundamental research,

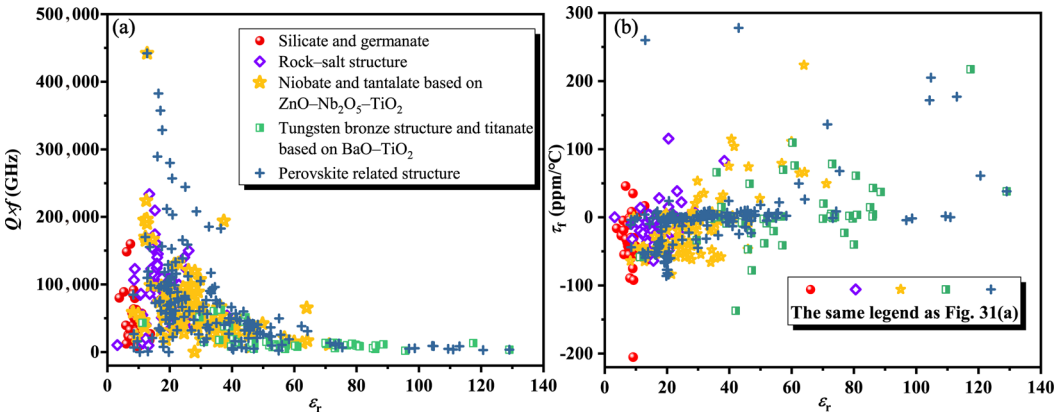

Fig. 31 Microwave dielectric properties of listed references: (a) ε_r versus $Q\times f$ values and (b) ε_r versus τ_f values.

the acceleration of the commercial application of new materials and property optimized ceramics is another persistent target for researchers. This includes ending the limitation of currently available system and exploration materials with stable and excellent properties for electronic market. For example, alternative materials with satisfied microwave dielectric properties equal to perovskite ceramics are required in the industry. With the development of 5G and 6G, there is an urgent need for ceramics with ultra-low dielectric constant (< 5), low dielectric loss, and excellent temperature-stability in high frequencies. The compounds of borate, aluminate, silicate, and fluoride with low polarization should take into consideration as promising candidate. It may be a direction for discovering composite materials consisted of ceramics and organics. Meanwhile, reducing the sintering temperature of ceramics for meeting the need of LTCC is a highly challenging issue owing to its advantages in fabrication of electronic devices. On the other hand, the repeatability of microwave dielectric properties and the normalized evaluation method should be emphasized. The advancement of preparation method with simplified procedures should be taken into consideration as well. The investigation combining the discussion of the performance of a simulated and fabricated device with the analysis of fundamental mechanism of structure–property relationship should be more popularized to provide an entire and systematical exploration. As a summary, the microwave dielectric properties listed in the references are presented in Figs. 31(a) and 31(b).

Lastly, we hope this brief progress report helps to understand the recent experimental methods and suggests an insight to take a new research direction for MWDCs.

Acknowledgements

This work is supported by the National Natural Science Foundation of China (Grant No. 51872037).

References

[1] Sebastian M T. *Dielectric Materials for Wireless Communication*. London, UK: Elsevier, 2008.

[2] Ohsato H, Tsunooka T, Sugiyama T, *et al*. Forsterite ceramics for millimeterwave dielectrics. *J Electroceramics* 2006, **17**: 445–450.

[3] Zhang J, Luo Y, Yue ZX, *et al*. High-*Q* and temperature-stable microwave dielectrics in layer cofired $Zn_{1.01}Nb_2O_6$/TiO_2/$Zn_{1.01}Nb_2O_6$ ceramic architectures. *J Am Ceram Soc* 2019, **102**: 342–350.

[4] Zhang J, Yue ZX, Luo Y, *et al*. $MgTiO_3$/TiO_2/$MgTiO_3$: An ultrahigh-*Q* and temperature-stable microwave dielectric ceramic through cofired trilayer architecture. *Ceram Int* 2018, **44**: 21000–21003.

[5] Luo WJ, Li LX, Zhang BW, *et al*. The mechanism of microwave response in layer-cofired $Zn_3Nb_2O_8$–TiO_2–$Zn_3Nb_2O_8$ ceramic architecture. *J Alloys Compd* 2020, **824**: 153978.

[6] Levine BF. Bond susceptibilities and ionicities in complex crystal structures. *J Chem Phys* 1973, **59**: 1463–1486.

[7] Sebastian MT, Jantunen H. Low loss dielectric materials for LTCC applications: A review. *Int Mater Rev* 2008, **53**: 57–90.

[8] Sebastian MT, Wang H, Jantunen H. Low temperature co-fired ceramics with ultra-low sintering temperature: A review. *Curr Opin Solid State Mater Sci* 2016, **20**: 151–170.

[9] Zhou D, Pang LX, Wang DW, *et al*. $BiVO_4$ based high *k* microwave dielectric materials: A review. *J Mater Chem C* 2018, **6**: 9290–9313.

[10] Fang Y, Li L, Xiao Q, *et al*. Preparation and microwave dielectric properties of cristobalite ceramics. *Ceram Int* 2012, **38**: 4511–4515.

[11] Li F, Liu P, Ruan P, *et al*. Microwave dielectric properties of $(1-x)SiO_2-xTiO_2$ ceramics. *Ceram Int* 2015, **41**: S582–S587.

[12] Sreekanth Chakradhar RP, Nagabhushana BM, Chandrappa GT, *et al*. Solution combustion derived nanocrystalline macroporous wollastonite ceramics. *Mater Chem Phys* 2006, **95**: 169–175.

[13] Wang HP, Zhang QL, Yang H, *et al*. Synthesis and microwave dielectric properties of $CaSiO_3$ nanopowder by the sol–gel process. *Ceram Int* 2008, **34**: 1405–1408.

[14] Sun HP, Zhang QL, Yang H, *et al*. $(Ca_{1-x}Mg_x)SiO_3$: A low-permittivity microwave dielectric ceramic system. *Mater Sci Eng*: *B* 2007, **138**: 46–50.

[15] Wang HP, Chen JM, Yang WY, *et al*. Effects of Al_2O_3 addition on the sintering behavior and microwave dielectric properties of $CaSiO_3$ ceramics. *J Eur Ceram Soc* 2012, **32**: 541–545.

[16] Hu W, Liu HX, Hao H, *et al*. Influence of Al_2O_3 addition on the microstructure and microwave dielectric properties of α-$CaSiO_3$ ceramics. *J Mater Sci*: *Mater Electron* 2015, **26**: 211–216.

[17] Hu W, Liu HX, Hao H, *et al*. Phase transition, microstructure and microwave dielectric properties of α-$CaSiO_3$ ceramics with SiO_2 addition. *J Mater Sci*: *Mater Electron* 2015, **26**: 1977–1981.

[18] Hu W, Liu HX, Hao H, *et al*. Influence of TiO_2 additive on the microwave dielectric properties of α-$CaSiO_3$–Al_2O_3 ceramics. *Ceram Int* 2015, **41**: S510–S514.

[19] Ma Q, Wu SP, Jiang C, *et al*. Microwave dielectric properties of SnO_2-doped $CaSiO_3$ ceramics. *Ceram Int* 2013, **39**: 2223–2229.

[20] Joseph T, Sebastian MT. Microwave dielectric properties of alkaline earth orthosilicates M_2SiO_4 (M=Ba,Sr,Ca). *Mater Lett* 2011, **65**: 891–893.

[21] Li LX, Wang YC, Xia WS, *et al*. Effects of Zn/Mg ratio on the microstructure and microwave dielectric properties of$(Zn_{1-x}Mg_x)_2SiO_4$ ceramics. *J Electron Mater* 2012, **41**: 684–688.

[22] Ullah A, Liu HX, Hao H, *et al*. Phase and microstructure evaluation and microwave dielectric properties of $Mg_{1-x}Ni_xSiO_3$ ceramics. *J Electron Mater* 2016, **45**: 5133–5139.

[23] Fu ZF, Ma JL, Liu P, *et al*. Crystal structure and microwave dielectric properties of middle-temperature-sintered $Mg_2Si_{1-x}V_xO_4$ ceramics. *J Electroceramics* 2016, **36**: 82–86.

[24] Tsunooka T, Androu M, Higashida Y, *et al*. Effects of TiO_2 on sinterability and dielectric properties of high-*Q* forsterite ceramics. *J Eur Ceram Soc* 2003, **23**: 2573–2578.

[25] Song KX, Chen XM, Fan XC. Effects of Mg/Si ratio on microwave dielectric characteristics of forsterite ceramics. *J Am Ceram Soc* 2007, **90**: 1808–1811.

[26] Liu L, Feng YB, Qiu T, *et al*. Microstructures and microwave dielectric properties of Mg_2SiO_4–$Ca_{0.9}Sr_{0.1}TiO_3$ ceramics. *J Mater Sci*: *Mater Electron* 2015, **26**: 1316–1321.

[27] Weng ZZ, Song CX, Xiong ZX, *et al*. Microstructure and broadband dielectric properties of Zn_2SiO_4 ceramics with nano-sized TiO_2 addition. *Ceram Int* 2019, **45**: 13251–13256.

[28] Lai YM, Zeng YM, Han J, *et al*. Structure dependence of microwave dielectric properties in $Zn_{2-x}SiO_{4-x}$–*x*CuO ceramics. *J Eur Ceram Soc* 2021, **41**: 2602–2609.

[29] Liang Z, Han XN, Wang G, *et al*. Microwave dielectric properties and sintering behaviors of $Zn_{1.8}SiO_{3.8}$ ceramics. *J Mater Sci*: *Mater Electron* 2021, **32**: 517–523.

[30] Kingon AI, Maria JP, Streiffer SK. Alternative dielectrics to silicon dioxide for memory and logic devices. *Nature* 2000, **406**: 1032–1038.

[31] Wu SP, Jiang C, Mei YX, *et al*. Synthesis and microwave dielectric properties of Sm_2SiO_5 ceramics. *J Am Ceram Soc* 2012, **95**: 37–40.

[32] Jiang C, Wu SP, Ma Q, *et al*. Synthesis and microwave dielectric properties of Nd_2SiO_5 ceramics. *J Alloys Compd* 2012, **544**: 141–144.

[33] Lai YM, Su H, Wang G, *et al*. Improved microwave dielectric properties of $CaMgSi_2O_6$ ceramics through CuO doping. *J Alloys Compd* 2019, **772**: 40–48.

[34] Xiao M, Wei YS, Zhang P. The effect of sintering temperature on the crystal structure and microwave dielectric properties of $CaCoSi_2O_6$ ceramic. *Mater Chem Phys* 2019, **225**: 99–104.

[35] Cai CY, Chen XQ, Li H, *et al*. Microwave dielectric properties of $Ca_{1-x}Sr_xMgSi_2O_6$ ceramics. *Ceram Int* 2020, **46**: 27679–27685.

[36] Chen XQ, Li H, Zhang PC, *et al*. Phase composition, microstructure, and microwave dielectric properties of $CaMnSi_2O_6$ ceramics. *Ceram Int* 2021, **47**: 4083–4089.

[37] Li CC, Yin CZ, Chen JQ, *et al*. Crystal structure and dielectric properties of germanate melilites $Ba_2MGe_2O_7$ (M = Mg and Zn) with low permittivity. *J Eur Ceram Soc* 2018, **38**: 5246–5251.

[38] Manu KM, Karthik C, Ubic R, *et al*. Effect of Ca^{2+} substitution on the structure, microstructure, and microwave dielectric properties of $Sr_2Al_2SiO_7$ ceramic. *J Am Ceram Soc* 2013, **96**: 3842–3848.

[39] Manu KM, Joseph T, Sebastian MT. Temperature compensated $Sr_2Al_2SiO_7$ ceramic for microwave applications. *Mater Chem Phys* 2012, **133**: 21–23.

[40] Xiao M, Wei YS, Sun HR, *et al*. Crystal structure and microwave dielectric properties of low-permittivity $Sr_2MgSi_2O_7$ ceramic. *J Mater Sci*: *Mater Electron* 2018, **29**: 20339–20346.

[41] Xiao M, Wei YS, Zhang P. The correlations between complex chemical bond theory and microwave dielectric properties of $Ca_2MgSi_2O_7$ ceramics. *J Electron Mater* 2019, **48**: 1652–1659.

[42] Song XQ, Lei W, Xie MQ, *et al*. Sintering behaviour, lattice energy and microwave dielectric properties of

melilite-type $BaCo_2Si_2O_7$ ceramics. *Mater Res Express* 2020, **6**: 126322.

[43] Song XQ, Lu WZ, Lou YH, *et al*. Synthesis, lattice energy and microwave dielectric properties of $BaCu_{2-x}Co_xSi_2O_7$ ceramics. *J Eur Ceram Soc* 2020, **40**: 3035–3041.

[44] Song XQ, Zou ZY, Lu WZ, *et al*. Crystal structure, lattice energy and microwave dielectric properties of melilite-type $Ba_{1-x}Sr_xCu_2Si_2O_7$ solid solutions. *J Alloys Compd* 2020, **835**: 155340.

[45] Wu SP, Chen DF, Mei YX, *et al*. Synthesis and microwave dielectric properties of $Ca_3SnSi_2O_9$ ceramics. *J Alloys Compd* 2012, **521**: 8–11.

[46] Bafrooei HB, Liu B, Su WT, *et al*. $Ca_3MgSi_2O_8$: Novel low-permittivity microwave dielectric ceramics for 5G application. *Mater Lett* 2020, **263**: 127248.

[47] Song XQ, Lei W, Wang F, *et al*. Phase evolution, crystal structure, and microwave dielectric properties of gillespite-type ceramics. *J Am Ceram Soc* 2021, **104**: 1740–1749.

[48] Li C, Ding SH, Zhang Y, *et al*. Effects of Ni^{2+} substitution on the crystal structure, bond valence, and microwave dielectric properties of $BaAl_{2-2x}Ni_{2x}Si_2O_{8-x}$ ceramics. *J Eur Ceram Soc* 2021, **41**: 2610–2616.

[49] Li C, Ding SH, Song TX, *et al*. Structure and microwave dielectric properties of $BaAl_{2-2x}Li_{2x}Si_2O_{8-2x}$ ceramics. *Ceram Int* 2021, **47**: 4895–4904.

[50] Felsche J. Rare earth silicates with the apatite structure. *J Solid State Chem* 1972, **5**: 266–275.

[51] Manu KM, Karthik C, Leu LC, *et al*. Crystal structure and microwave dielectric properties of $LiRE_9(SiO_4)_6O_2$ ceramics (RE = La, Pr, Nd, Sm, Eu, Gd, and Er). *J Am Ceram Soc* 2013, **96**: 1504–1511.

[52] Thomas S, Sebastian MT. Microwave dielectric properties of $SrRE_4Si_3O_{13}$ (La, Pr, Nd, Sm, Eu, Gd, Tb, Dy, Er, Tm, Yb, and Y) ceramics. *J Am Ceram Soc* 2009, **92**: 2975–2981.

[53] Du K, Zou ZY, Song XQ, *et al*. Correlation between crystal structure and microwave dielectric properties of $CaRE_4Si_3O_{13}$ (RE = La, Nd, Sm, and Er). *J Mater Sci: Mater Electron* 2020, **31**: 3274–3280.

[54] Ao LY, Tang Y, Li J, *et al*. Structure characterization and microwave dielectric properties of $LiGa_5O_8$ ceramic with low-ε_r and low loss. *J Eur Ceram Soc* 2020, **40**: 5498–5503.

[55] Ao LY, Li J, Tang Y, *et al*. Structure, far-infrared reflectance spectra, and microwave dielectric properties of $Ba_2MGa_{11}O_{20}$ (M = Bi, La) ceramics. *Ceram Int* 2021, **47**: 11899–11905.

[56] Li FH, Tang Y, Li J, *et al*. Effect of A-site cation on crystal structure and microwave dielectric properties of AGe_4O_9 (A = Ba, Sr) ceramics. *J Eur Ceram Soc* 2021, **41**: 4153–4159.

[57] Tang Y, Zhang ZW, Li J, *et al*. $A_3Y_2Ge_3O_{12}$ (A = Ca, Mg): Two novel microwave dielectric ceramics with contrasting τ_f and $Q\times f$. *J Eur Ceram Soc* 2020, **40**: 3989–3995.

[58] Lou WC, Song KX, Hussain F, *et al*. Bond characteristics and microwave dielectric properties of $(Li_{0.5}Ga_{0.5})^{2+}$ doped $Mg_2Al_4Si_5O_{18}$ ceramics. *Ceram Int* 2020, **46**: 28631–28638.

[59] Wang Y, Tang Y, Li J, *et al*. Microwave dielectric properties of silico-carnotite $Ca_3M_2Si_3O_{12}$ (M=Yb,Y) ceramics synthesized via high energy ball milling. *Ceram Int* 2021, **47**: 4831–4837.

[60] Su CX, Fang L, Ao LY, *et al*. Structure, Raman spectra and microwave dielectric properties of novel garnet-type $Ca_3MZrGe_3O_{12}$ (M = Co, Zn) ceramics. *J Asian Ceram Soc* 2021, **9**: 424–432.

[61] Zhai YF, Tang Y, Li J, *et al*. Structure, Raman spectra and properties of two low-ε microwave dielectric ceramics $Ca_3B_2Ge_3O_{12}$ (B = Al, Ga). *Ceram Int* 2020, **46**: 28710–28715.

[62] Su CX, Ao LY, Zhai YF, *et al*. Novel low-permittivity microwave dielectric ceramics in garnet-type $Ca_4ZrGe_3O_{12}$. *Mater Lett* 2020, **275**: 128149.

[63] Li J, Tang Y, Zhang ZW, *et al*. Two novel garnet $Sr_3B_2Ge_3O_{12}$ (B = Yb, Ho) microwave dielectric ceramics with low permittivity and high Q. *J Eur Ceram Soc* 2021, **41**: 1317–1323.

[64] Tan ZY, Song KX, Bafrooei HB, *et al*. The effects of TiO_2 addition on microwave dielectric properties of $Y_3MgAl_3SiO_{12}$ ceramic for 5G application. *Ceram Int* 2020, **46**: 15665–15669.

[65] Yang AH, Tang Y, Li J, *et al*. Structure and infrared reflectivity spectra of novel $Mg_3Ga_2GeO_8$ microwave dielectric ceramic with high Q. *Ceram Int* 2021, **47**: 2450–2455.

[66] Su CX, Ao LY, Zhang ZW, *et al*. Crystal structure, Raman spectra and microwave dielectric properties of novel temperature-stable $LiYbSiO_4$ ceramics. *Ceram Int* 2020, **46**: 19996–20003.

[67] Du K, Wang F, Song XQ, *et al*. Correlation between crystal structure and dielectric characteristics of Ti^{4+} substituted $CaSnSiO_5$ ceramics. *J Eur Ceram Soc* 2021, **41**: 2568–2578.

[68] Du K, Fan J, Zou ZY, *et al*. Crystal structure, phase compositions, and microwave dielectric properties of malayaite-type $Ca_{1-x}Sr_xSnSiO_5$ ceramics. *J Am Ceram Soc* 2020, **103**: 6369–6377.

[69] Du K, Song XQ, Zou ZY, *et al*. Improved microwave dielectric properties of novel low-permittivity Sn-doped $Ca_2HfSi_4O_{12}$ ceramics. *Mater Res Bull* 2020, **129**: 110887.

[70] Templeton A, Wang XR, Penn SJ, *et al*. Microwave dielectric loss of titanium oxide. *J Am Ceram Soc* 2000, **83**: 95–100.

[71] Kim ES, Kang DH. Relationships between crystal structure and microwave dielectric properties of $(Zn_{1/3}B_{2/3}^{5+})_xTi{-}xO_2$ (B^{5+} = Nb, Ta) ceramics. *Ceram Int* 2008, **34**: 883–888.

[72] Baumgarte A, Blachnik R. Phase relations in the system titaniumdioxide-diniobium-zinc-hexoxide. *Mater Res Bull* 1992, **27**: 1287–1294.

[73] Yang HY, Zhang SR, Yang HC, *et al*. Usage of P–V–L bond theory in studying the structural/property regulation of microwave dielectric ceramics: A review. *Inorg Chem Front* 2020, **7**: 4711–4753.

[74] Liao QW, Li LX, Ding X, *et al*. A new temperature stable microwave dielectric material $Mg_{0.5}Zn_{0.5}TiNb_2O_8$. *J Am Ceram Soc* 2012, **95**: 1501–1503.

[75] Yang HY, Li EZ, Duan SX, *et al*. Structure, microwave properties and low temperature sintering of Ta_2O_5 and Co_2O_3 codoped $Zn_{0.5}Ti_{0.5}NbO_4$ ceramics. *Mater Chem Phys* 2017, **199**: 43–53.

[76] Li LX, Cai HC, Yu XX, *et al*. Structure analysis and microwave dielectric properties of $Ca_xZn_{1-x}Sn_{0.08}Ti_{1.92}Nb_2O_{10}$ ceramics. *J Alloys Compd* 2014, **584**: 315–321.

[77] Yang HY, Zhang SR, Yang HC, *et al*. Structural evolution and microwave dielectric properties of $xZn_{0.5}Ti_{0.5}NbO_4$–$(1–x)Zn_{0.15}Nb_{0.3}Ti_{0.55}O_2$ ceramics. *Inorg Chem* 2018, **57**: 8264–8275.

[78] Yang HY, Zhang SR, Yang HC, *et al*. Effects of ZrO_2 substitution on crystal structure and microwave dielectric properties of $Zn_{0.15}Nb_{0.3}(Ti_{1-x}Zr_x)_{0.55}O_2$ ceramics. *Ceram Int* 2018, **44**: 22710–22717.

[79] Chen YW, Zhang SR, Yang HY, *et al*. Bond ionicity, lattice energy and structural evolution of Ta substituted $0.15ZnO–0.15Nb_2O_5–0.55TiO_2$ dielectric ceramics. *Ceram Int* 2019, **45**: 8832–8839.

[80] Ramarao SD, Murthy VRK. Crystal structure refinement and microwave dielectric properties of new low dielectric loss $AZrNb_2O_8$ (A: Mn, Zn, Mg and Co) ceramics. *Scripta Mater* 2013, **69**: 274–277.

[81] Jiang XS, Pan HL, Feng ZB, *et al*. Characterization of microwave dielectric materials $NiZrNb_2O_8$ based on the chemical bond theory. *J Mater Sci*: *Mater Electron* 2016, **27**: 10963–10969.

[82] Pan HL, Feng ZB, Bi JX, *et al*. Preparation, characterization, and dielectric properties of wolframite-structure $MnZrNb_2O_8$ ceramics at microwave frequency. *J Alloys Compd* 2015, **651**: 440–444.

[83] Xia WS, Yang FY, Zhang GY, *et al*. New low-dielectric-loss $NiZrNb_2O_8$ ceramics for microwave application. *J Alloys Compd* 2016, **656**: 470–475.

[84] Wu HT, Bi JX, Wang HJ, *et al*. Sintering characteristics and microwave dielectric properties of low loss $ZnZrNb_2O_8$ ceramics achieved by reaction sintering process. *J Mater Sci*: *Mater Electron* 2016, **27**: 5670–5675.

[85] Wu HT, Feng ZB, Mei QJ, *et al*. Correlations of crystal structure, bond energy and microwave dielectric properties of $AZrNb_2O_8$ (A = Zn, Co, Mg, Mn) ceramics. *J Alloys Compd* 2015, **648**: 368–373.

[86] Cheng Y, Zuo RZ, Lv Y. Preparation and microwave dielectric properties of low-loss $MgZrNb_2O_8$ ceramics. *Ceram Int* 2013, **39**: 8681–8685.

[87] Yang HY, Zhang SR, Li YP, *et al*. Investigations of dielectric properties of wolframite $A_{0.5}Zr_{0.5}NbO_4$ ceramics by bond theory and far-infrared spectroscopy. *Ceram Int* 2020, **46**: 3688–3694.

[88] Wu HT, Kim ES. Characterization of crystal structure and microwave dielectric properties of $AZrNb_2O_8$ (A=Zn,Co, Mg,Mn) ceramics based on complex bond theory. *Ceram Int* 2016, **42**: 5785–5791.

[89] Zhang Y, Ding SH, Li C, *et al*. Bond analysis of novel $MnZrTa_2O_8$ microwave dielectric ceramics with monoclinic structure. *J Mater Sci* 2020, **55**: 8491–8501.

[90] Yang HY, Zhang SR, Yang HC, *et al*. Structure, phase composition, Raman spectra, and microwave dielectric properties of novel $Co_{0.5}Zr_{0.5}TaO_4$ ceramics. *Ceram Int* 2019, **45**: 15445–15450.

[91] Xia WS, Zhang LY, Wang Y, *et al*. Extrinsic effects on microwave dielectric properties of high-Q $MgZrTa_2O_8$ ceramics. *J Mater Sci*: *Mater Electron* 2016, **27**: 11325–11330.

[92] Cai HC, Li LX, Sun H, *et al*. A microwave dielectric material $Mg_{0.5}Zn_{0.5}ZrNb_2O_8$. *Mater Lett* 2015, **144**: 78–81.

[93] Ye J, Li LX, Sun H, *et al*. Microstructure and microwave dielectric characteristics of $(Zn_{1-x}Co_x)ZrNb_2O_8$ ceramics. *J Mater Sci*: *Mater Electron* 2015, **26**: 8954–8959.

[94] Yang ZL, Pan HL, Jiang XS, *et al*. Characterization of low loss microwave dielectric materials $Zn_{0.92}Co_{0.08}ZrNb_2O_8$ based on the complex chemical bond theory. *J Mater Sci*: *Mater Electron* 2017, **28**: 1597–1604.

[95] Pan HL, Liu QQ, Zhang YH, *et al*. Crystal structure and microwave dielectric characteristics of Co-substituted $Zn_{1-x}Co_xZrNb_2O_8$ ($0 \leqslant x \leqslant 0.1$) ceramics. *RSC Adv* 2016, **6**: 86889–86903.

[96] Wang SY, Xiao BY, Li JY, *et al*. Structural evolution, Raman spectra, and microwave dielectric properties of Zr-substituted $ZnTiTa_2O_8$ ceramics. *J Mater Sci*: *Mater Electron* 2020, **31**: 10298–10305.

[97] Li LX, Zhang S, Ye J, *et al*. Crystal structure and microwave dielectric properties of the low dielectric loss $ZnZr_{1-x}Sn_xNb_2O_8$ ceramics. *Ceram Int* 2016, **42**: 9157–9161.

[98] Ye J, Li LX, Li S, *et al*. A new microwave dielectric material $ZnZr_{0.8}Sn_{0.2}Nb_2O_8$. *J Mater Sci*: *Mater Electron* 2016, **27**: 97–102.

[99] Xiao M, He SS, Lou J, *et al*. Structure and microwave dielectric properties of $MgZr(Nb_{1-x}Sb_x)_2O_8$ ($0 \leq x \leq 0.1$) ceramics. *J Alloys Compd* 2019, **777**: 350–357.

[100] Zhao YG, Zhang P. A novel low loss microwave dielectric ceramic $ZnZrNb_{1.84}Sb_{0.16}O_8$ with wolframite structure. *J Mater Sci*: *Mater Electron* 2016, **27**: 2933–2937.

[101] Li LX, Sun H, Lv X, *et al*. A new microwave dielectric material $ZnZrNbTaO_8$. *Mater Lett* 2015, **160**: 363–365.

[102] Xiao M, He SS, Meng J, *et al*. Dependence of microwave dielectric properties on the substitution of isovalent composite ion for Nb-site of $MgZrNb_{2-x}(Sn_{1/2}W_{1/2})_xO_8$ ($0 \leqslant x \leqslant 0.15$) ceramics. *J Mater Sci*: *Mater Electron* 2019, **30**: 18280–18286.

[103] Xiao M, He SS, Meng J, *et al*. Bond ionicity, lattice energy,

bond energy and the microwave dielectric properties of non-stoichiometric $MgZrNb_{2+x}O_{8+2.5x}$ ceramics. *Mater Chem Phys* 2020, **242**: 122412.

[104] Zhang J, Zuo RZ, Cheng Y. Relationship of the structural phase transition and microwave dielectric properties in $MgZrNb_2O_8$–TiO_2 ceramics. *Ceram Int* 2016, **42**: 7681–7689.

[105] Lyu XS, Li LX, Zhang S, *et al*. Crystal structure and microwave dielectric properties of novel $(1-x)ZnZrNb_2O_8$–$xTiO_2$ ceramics. *Mater Lett* 2016, **171**: 129–132.

[106] Wu HT, Guo JD, Bi JX, *et al*. Effect of H_3BO_3 addition on the sintering behavior and microwave dielectric properties of wolframite-type $MgZrNb_2O_8$ ceramics. *J Alloys Compd* 2016, **661**: 535–540.

[107] Wu HT, Mei QJ, Xing CF, *et al*. Effects of B_2O_3 addition on sintering behavior and microwave dielectric properties of ixiolite-structure $ZnTiNb_2O_8$ ceramics. *J Alloys Compd* 2016, **679**: 26–31.

[108] Bi JX, Xing CF, Jiang XS, *et al*. Effect of H_3BO_3 on sintering behavior and microwave dielectric properties of monoclinal structure $ZnZrNb_2O_8$ ceramics. *J Mater Sci*: *Mater Electron* 2016, **27**: 8055–8061.

[109] Liao QW, Li LX, Ren X, *et al*. A new microwave dielectric material $Ni_{0.5}Ti_{0.5}NbO_4$. *Mater Lett* 2012, **89**: 351–353.

[110] Tseng CF. Microwave dielectric properties of a new $Cu_{0.5}Ti_{0.5}NbO_4$ ceramics. *J Eur Ceram Soc* 2015, **35**: 383–387.

[111] Tseng CF. Microwave dielectric properties of low loss microwave dielectric ceramics: $A_{0.5}Ti_{0.5}NbO_4$ (A = Zn, Co). *J Eur Ceram Soc* 2014, **34**: 3641–3648.

[112] Zhang Y, Zhang YC. Microwave dielectric properties of sol–gel derived $CoTiNb_2O_8$ ceramics. *J Alloys Compd* 2016, **683**: 86–91.

[113] Chen TK, Ma WB, Sun QC, *et al*. The microwave dielectric properties of $(Ni,Zn)_{0.5}Ti_{0.5}NbO_4$ solid solution. *Mater Lett* 2013, **113**: 111–113.

[114] Zhang Y, Zhang YC, Xiang MQ. Microwave dielectric properties of temperature stable $CoTiNb_2O_8$–$CoNb_2O_6$ composite ceramics. *Mater Lett* 2016, **178**: 175–177.

[115] Zhang Y, Ding SH, You L, *et al*. Temperature stable microwave dielectric ceramic $CoTiNb_2O_8$–$Zn_{1.01}Nb_2O_6$ with ultra-low dielectric loss. *J Electron Mater* 2019, **48**: 867–872.

[116] Zhang Y, Zhang YC, Xiang MQ. Crystal structure and microwave dielectric characteristics of Zr-substituted $CoTiNb_2O_8$ ceramics. *J Eur Ceram Soc* 2016, **36**: 1945–1951.

[117] Li YY, Lu XC, Zhang Y, *et al*. Characterization of $Co_{0.5}(Ti_{1-x}Zr_x)_{0.5}NbO_4$ microwave dielectric ceramics based on structural refinement. *Ceram Int* 2017, **43**: 11516–11522.

[118] Wang J, Lu XC, Li YY, *et al*. Correlations between microwave dielectric properties and crystal structures of Sb-doped $Co_{0.5}Ti_{0.5}NbO_4$ ceramics. *Ceram Int* 2020, **46**: 3464–3470.

[119] Kremer RK, Greedan JE. Magnetic ordering in $CoTa_2O_6$ and $NiTa_2O_6$. *J Solid State Chem* 1988, **73**: 579–582.

[120] Reimers JN, Greedan JE, Stager CV, *et al*. Crystal structure and magnetism in $CoSb_2O_6$ and $CoTa_2O_6$. *J Solid State Chem* 1989, **83**: 20–30.

[121] Yang HY, Zhang SR, Chen YW, *et al*. Crystal chemistry, Raman spectra, and bond characteristics of trirutile-type $Co_{0.5}Ti_{0.5}TaO_4$ microwave dielectric ceramics. *Inorg Chem* 2019, **58**: 968–976.

[122] Kumada N, Koike N, Nakanome K, *et al*. Synthesis of rutile-type solid solution $Ni_{1-x}Co_xTi(Nb_{1-y}Ta_y)_2O_8$ ($0 \leqslant x \leqslant 1$, $0 \leqslant y \leqslant 1$) and its optical property. *J Asian Ceram Soc* 2017, **5**: 284–289.

[123] Li EZ, Wen QY, Yang HC, *et al*. Novel temperature stable $NiSnTa_2O_8$ microwave dielectric ceramics with trirutile structure. *Ceram Int* 2020, **46**: 6079–6084.

[124] Baumgarte A, Blachnik R. Isothermal sections in the systems ZnO–AO_2–Nb_2O_5 (A=Ti,Zr,Sn) at 1473 K. *J Alloys Compd* 1994, **210**: 75–81.

[125] Huan ZL, Sun QC, Ma WB, *et al*. Crystal structure and microwave dielectric properties of $(Zn_{1-x}Co_x)TiNb_2O_8$ ceramics. *J Alloys Compd* 2013, **551**: 630–635.

[126] Li LX, Sun H, Lv X, *et al*. Microstructure and microwave dielectric characteristics of the $Ca_xZn_{1-x}TiNb_2O_8$ temperature stable ceramics. *J Mater Sci*: *Mater Electron* 2016, **27**: 126–133.

[127] Liao QW, Li LX, Zhang P, *et al*. Correlation of crystal structure and microwave dielectric properties for $Zn(Ti_{1-x}Sn_x)Nb_2O_8$ ceramics. *Mater Sci Eng*: *B* 2011, **176**: 41–44.

[128] Liao QW, Li LX, Ding X. Phase constitution, structure analysis and microwave dielectric properties of $Zn_{0.5}Ti_{1-x}Zr_xNbO_4$ ceramics. *Solid State Sci* 2012, **14**: 1385–1391.

[129] Liao QW, Li LX, Zhang P, *et al*. Correlation of crystal structure and microwave dielectric properties for $ZnTi(Nb_{1-x}Ta_x)_2O_8$ ceramics. *Solid State Sci* 2011, **13**: 1201–1204.

[130] Liao QW, Li LX, Ren X, *et al*. New low-loss microwave dielectric material $ZnTiNbTaO_8$. *J Am Ceram Soc* 2011, **94**: 3237–3240.

[131] Park JH, Choi YJ, Nahm S, *et al*. Crystal structure and microwave dielectric properties of $ZnTi(Nb_{1-x}Ta_x)_2O_8$ ceramics. *J Alloys Compd* 2011, **509**: 6908–6912.

[132] Liao QW, Li LX. Structural dependence of microwave dielectric properties of ixiolite structured $ZnTiNb_2O_8$ materials: Crystal structure refinement and Raman spectra study. *Dalton Trans* 2012, **41**: 6963.

[133] Ruan P, Liu P, Guo BC, *et al*. Microwave dielectric properties of ZnO–Nb_2O_5–$xTiO_2$ ceramics prepared by reaction-sintering process. *J Mater Sci*: *Mater Electron* 2016, **27**: 4201–4205.

[134] Bafrooei HB, Feizpour M, Sayyadi-Shahraki A, *et al*. High-performance $ZnTiNb_2O_8$ microwave dielectric

ceramics produced from $ZnNb_2O_6$–TiO_2 nano powders. *J Alloys Compd* 2020, **834**: 155082.

[135] Luo WJ, Li LX, Yu SH, *et al*. Bond theory, terahertz spectra, and dielectric studies in donor-acceptor (Nb–Al) substituted $ZnTiNb_2O_8$ system. *J Am Ceram Soc* 2019, **102**: 4612–4620.

[136] Mei QJ, Li CY, Guo JD, *et al*. Synthesis, characterization, and microwave dielectric properties of ternary-phase ixiolite-structure $MgTiNb_2O_8$ ceramics. *Mater Lett* 2015, **145**: 7–10.

[137] Lee HJ, Kim IT, Hong KS. Dielectric properties of AB_2O_6 compounds at microwave frequencies (A = Ca, Mg, Mn, Co, Ni, Zn, and B = Nb, Ta). *Jpn J Appl Phys* 1997, **36**: L1318–L1320.

[138] Blasse G. Qualitative approach to the structural differences between some mixed metal oxides containing Sb^{5+}, Nb^{5+} and Ta^{5+}. *J Inorg Nucl Chem* 1964, **26**: 1191–1199.

[139] Lee HJ, Hong KS, Kim SJ, *et al*. Dielectric properties OF MNb_2O_6 compounds (where M = Ca, Mn, Co, Ni, or Zn). *Mater Res Bull* 1997, **32**: 847–855.

[140] Pullar RC, Breeze JD, Alford NM. Characterization and microwave dielectric properties of $M^{2+}Nb_2O_6$ ceramics. *J Am Ceram Soc* 2005, **88**: 2466–2471.

[141] Chen YC, Weng MZ, Chang KC. Effect of sintering temperature and time on microwave dielectric properties of $CaNb_2O_6$ ceramics. *J Mater Sci*: *Mater Electron* 2014, **25**: 844–851.

[142] Wu HT, Jiang YS, Wu WB, *et al*. Synthesis and microwave dielectric properties of columbite-structure $MgNb_2O_6$ ceramics by aqueous sol–gel technique. *J Electroceramics* 2012, **28**: 191–196.

[143] Xia WS, Li LX, Ji LJ, *et al*. Phase evolution, bond valence and microwave characterization of $(Zn_{1-x}Ni_x)Ta_2O_6$ ceramics. *Mater Lett* 2012, **66**: 296–298.

[144] Xia WS, Li LX, Ning PF, *et al*. Relationship between bond ionicity, lattice energy, and microwave dielectric properties of $Zn(Ta_{1-x}Nb_x)_2O_6$ ceramics. *J Am Ceram Soc* 2012, **95**: 2587–2592.

[145] Xia WS, Zhang GY, Shi LW, *et al*. Enhanced microwave dielectric properties of $ZnTa_2O_6$ ceramics with Sb^{5+} ion substitution. *Mater Lett* 2014, **124**: 64–66.

[146] Sp W, Jh L. Mg-substituted $ZnNb_2O_6$–TiO_2 composite ceramics for RF/microwaves ceramic capacitors. *J Alloys Compd* 2011, **509**: 8126–8129.

[147] Fu BJ, Zhang YC, Yue H. Microwave dielectric properties of $(1-x)ZnTa_2O_6$–$xMgNb_2O_6$ ceramics. *Ceram Int* 2013, **39**: 3789–3793.

[148] Zhang YC, You CY, Fu BJ, *et al*. Tailoring of microwave dielectric properties in $(1-x)ZnTa_2O_6$–$xNiNb_2O_6$ ceramics. *Ferroelectrics* 2013, **451**: 54–61.

[149] Yu SQ, Tang B, Zhang SR, *et al*. Phase structure and microwave dielectric properties of Mn-doped $(1-x)ZrTi_2O_6$–$xZnNb_2O_6$ (x = 0.13−0.53) ceramics. *J Mater Sci*: *Mater Electron* 2013, **24**: 418–422.

[150] Liu XC, Deng JP. Phase structure and dielectric property of the $ZnNb_2O_6$–$(Mg_{0.3}Zn_{0.7})TiO_3$ multiphase ceramics. *J Mater Sci*: *Mater Electron* 2012, **23**: 506–510.

[151] Yan Z, Huang JL, Gu YJ, *et al*. Effects of V_2O_5 addition on the microstructure and microwave dielectric properties of $ZnNb_2O_6$ ceramics. *Adv Mater Res* 2012, **476–478**: 940–943.

[152] Wu HT, Jiang YS, Yue YL. Low-temperature synthesis and microwave dielectric properties of trirutile-structure $MgTa_2O_6$ ceramics by aqueous sol–gel process. *Ceram Int* 2012, **38**: 5151–5156.

[153] Liu LT, Matusevich A, Garg C, *et al*. The dominance of paramagnetic loss in microwave dielectric ceramics at cryogenic temperatures. *Appl Phys Lett* 2012, **101**: 252901.

[154] Park JH, Nahm S, Park JG. Crystal structure and microwave dielectric properties of $(1-x)ZnTa_2O_6$–$xTiO_2$ ceramics. *J Alloys Compd* 2012, **537**: 221–226.

[155] Shahgholi N, Asadian K, Ebadzadeh T. Microstructural and microwave dielectric properties of $ZnNb_2O_6$ ceramics prepared through microwave sintering. *Ceram Int* 2014, **40**: 14335–14339.

[156] Yang HY, Zhang SR, Yang HC, *et al*. Intrinsic dielectric properties of columbite $ZnNb_2O_6$ ceramics studied by P–V–L bond theory and Infrared spectroscopy. *J Am Ceram Soc* 2019, **102**: 5365–5374.

[157] Sebastian MT, Solomon S, Ratheesh R, *et al*. Preparation, characterization, and microwave properties of $RETiNbO_6$ (RE = Ce, Pr, Nd, Sm, Eu, Gd, Tb, Dy, Y, and Yb) dielectric ceramics. *J Am Ceram Soc* 2001, **84**: 1487–1489.

[158] Surendran KP, Solomon S, Varma MR, *et al*. Microwave dielectric properties of $RETiTaO_6$ (RE = La, Ce, Pr, Nd, Sm, Eu, Gd, Tb, Dy, Ho, Y, Er, Yb, Al, and In) ceramics. *J Mater Res* 2002, **17**: 2561–2566.

[159] Lei Y, Reaney IM, Liu YC, *et al*. Microwave dielectric properties and microstructures of $RETiNbO_6$ (RE = La, Sm and Y). *Adv Mater Res* 2011, **197–198**: 285–289.

[160] Zhang J, Zuo RZ. A novel self-composite property-tunable $LaTiNbO_6$ microwave dielectric ceramic. *Mater Res Bull* 2016, **83**: 568–572.

[161] Zhang J, Zuo RZ. Sintering behavior, structural phase transition, and microwave dielectric properties of $La_{1-x}Zn_xTiNbO_{6-x/2}$ ceramics. *J Am Ceram Soc* 2017, **100**: 4362–4368.

[162] Zhang J, Zuo RZ. Phase structural transition and microwave dielectric properties in isovalently substituted $La_{1-x}Ln_xTiNbO_6$ (Ln = Ce, Sm) ceramics. *Ceram Int* 2017, **43**: 7065–7072.

[163] Zhang J, Zuo RZ. Octahedral distortion, phase structural stability, and microwave dielectric properties in equivalently substituted $LaTiNbO_6$ ceramics. *J Am Ceram Soc* 2017, **100**: 5249–5258.

[164] Zhang J, Zuo RZ. Raman scattering and infrared reflectivity study of orthorhombic/monoclinic $LaTiNbO_6$ microwave dielectric ceramics by A/B-site substitution.

Ceram Int 2018, **44**: 16191–16198.

[165] John F, Solomon S. Dielectric and optical properties of $Ln_{0.8}Lu_{0.2}TiNbO_6$ (Ln = Ce, Pr, Nd & Sm) ceramics. *Phys Lett A* 2020, **384**: 126731.

[166] Kim DW, Kwon DK, Yoon SH, *et al*. Microwave dielectric properties of rare-earth ortho-niobates with ferroelasticity. *J Am Ceram Soc* 2006, **89**: 3861–3864.

[167] Zhang P, Song ZK, Wang Y, *et al*. Effect of ion substitution for Nd^{3+} based on structural characteristic on the microwave dielectric properties of $NdNbO_4$ ceramic system. *J Am Ceram Soc* 2014, **97**: 976–981.

[168] Song ZK, Zhang P, Wang Y, *et al*. Improved quality factor of $NdNbO_4$ microwave dielectric ceramic by Mn^{2+} substitution. *J Alloys Compd* 2014, **583**: 546–549.

[169] Chen YH, Wang H, Pang LX, *et al*. Effect of Zn^{2+} substitution on sintering behavior and dielectric properties of $NdNbO_4$ ceramics. *Ferroelectrics* 2010, **407**: 61–68.

[170] Xiao M, Gu QQ, Zhou ZQ, *et al*. Study of the microwave dielectric properties of $(La_{1-x}Sm_x)NbO_4$ (x = 0–0.10) ceramics via bond valence and packing fraction. *J Am Ceram Soc* 2017, **100**: 3952–3960.

[171] Zhang P, Zhao YG. Influence of Sm^{3+} substitutions for Nd^{3+} on the microwave dielectric properties of $(Nd_{1-x}Sm_x)NbO_4$ (x = 0.02–0.15) ceramics. *J Alloys Compd* 2016, **654**: 240–245.

[172] Zhao YG, Zhang P. Complex chemical bond theory, Raman spectra and microwave dielectric properties of low loss ceramics $NdNbO_4$–xAl_2O_3. *J Mater Sci*: *Mater Electron* 2016, **27**: 2511–2522.

[173] Zhang P, Zhao YG. New temperature stable $(Nd_{1-x}La_x)_{1.02}Nb_{0.988}O_4$ microwave dielectric ceramics. *Mater Lett* 2015, **161**: 620–623.

[174] Zhang P, Zhao YG, Li LX. The correlations among bond ionicity, lattice energy and microwave dielectric properties of $(Nd_{1-x}La_x)NbO_4$ ceramics. *Phys Chem Chem Phys* 2015, **17**: 16692–16698.

[175] Pang LX, Zhou D. Modification of $NdNbO_4$ microwave dielectric ceramic by Bi substitutions. *J Am Ceram Soc* 2019, **102**: 2278–2282.

[176] Zhang P, Zhao Y, Liu J, *et al*. Correlation of crystal structure and microwave dielectric properties of $Nd_{1.02}(Nb_{1-x}Ta_x)_{0.988}O_4$ ceramic. *Dalton Trans* 2015, **44**: 5053–5057.

[177] Zhang P, Zhao YG, Liu J, *et al*. Enhanced microwave dielectric properties of $NdNbO_4$ ceramic by Ta^{5+} substitution. *J Alloys Compd* 2015, **640**: 90–94.

[178] Zhang P, Zhao YG, Wang XY. The relationship between bond ionicity, lattice energy, coefficient of thermal expansion and microwave dielectric properties of $Nd(Nb_{1-x}Sb_x)O_4$ ceramics. *Dalton Trans* 2015, **44**: 10932–10938.

[179] Zhang P, Zhao YG, Wang XY. The correlations between electronic polarizability, packing fraction, bond energy and microwave dielectric properties of $Nd(Nb_{1-x}Sb_x)O_4$ ceramics. *J Alloys Compd* 2015, **644**: 621–625.

[180] Yang HC, Zhang SR, Yang HY, *et al*. Influence of $(Al_{1/3}W_{2/3})^{5+}$ co-substitution for Nb^{5+} in $NdNbO_4$ and the impact on the crystal structure and microwave dielectric properties. *Dalton Trans* 2018, **47**: 15808–15815.

[181] Yang HC, Zhang SR, Yang HY, *et al*. Structure stability, bond characteristics and microwave dielectric properties of co-substituted $NdNbO_4$ ceramics. *Ceram Int* 2019, **45**: 3620–3626.

[182] Yang HC, Zhang SR, Yang HY, *et al*. $NdNb_{1-x}(Mg_{1/4}W_{3/4})_xO_4$ ($0.02 \leqslant x \leqslant 0.06$) solid solution characterized by infrared spectrum and complex chemical theory. *J Alloys Compd* 2019, **787**: 358–366.

[183] Yang HC, Zhang SR, Yang HY, *et al*. Bond characteristics, vibrational spectrum and optimized microwave dielectric properties of chemically substituted $NdNbO_4$. *Ceram Int* 2019, **45**: 16940–16947.

[184] Zhang P, Song ZK, Wang Y, *et al*. Effect of $CaTiO_3$ addition on microwave dielectric properties of $NdNbO_4$ ceramics as multi-function material. *J Alloys Compd* 2013, **581**: 741–746.

[185] Zhang P, Wang T, Xia WS, *et al*. Microwave dielectric properties of a new ceramic system $NdNbO_4$ with CaF_2 addition. *J Alloys Compd* 2012, **535**: 1–4.

[186] Peng Y, Xia WS, Yi CJ, *et al*. Effects of MgO additive on microwave dielectric properties of $NdNbO_4$ ceramics. *J Mater Sci*: *Mater Electron* 2020, **31**: 785–790.

[187] Liu LT, Chen YG, Feng ZB, *et al*. Crystal structure, infrared spectra, and microwave dielectric properties of the $EuNbO_4$ ceramic. *Ceram Int* 2021, **47**: 4321–4326.

[188] Guo D, Zhou D, Li WB, *et al*. Phase evolution, crystal structure, and microwave dielectric properties of water-insoluble $(1-x)LaNbO_4$–$xLaVO_4$ ($0 \leqslant x \leqslant 0.9$) ceramics. *Inorg Chem* 2017, **56**: 9321–9329.

[189] Tang TL, Xia WS, Zhang B, *et al*. Optimization on quality factor of $LaNbO_4$ microwave dielectric ceramics. *J Mater Sci*: *Mater Electron* 2019, **30**: 15293–15298.

[190] Chen JW, Fang L, Li J, *et al*. Packing fraction, bond valence and crystal structure of AVO_4 (A = Eu, Y) microwave dielectric ceramics with low permittivity. *J Mater Sci*: *Mater Electron* 2020, **31**: 19180–19187.

[191] Zhou D, Guo HH, Fu MS, *et al*. Anomalous dielectric behaviour during the monoclinic to tetragonal phase transition in $La(Nb_{0.9}V_{0.1})O_4$. *Inorg Chem Front* 2021, **8**: 156–163.

[192] Deng JY, Xia WS, Zhang WH, *et al*. Optimization of sintering behavior and microwave dielectric properties of $LaNbO_4$ ceramics with NiO/CoO additive. *J Alloys Compd* 2021, **859**: 158378.

[193] Chen L, Hu MY, Wu P, *et al*. Thermal expansion performance and intrinsic lattice thermal conductivity of ferroelastic $RETaO_4$ ceramics. *J Am Ceram Soc* 2019, **102**: 4809–4821.

[194] Wu P, Hu MY, Chen L, *et al*. The effect of ZrO_2 alloying on the microstructures and thermal properties of $DyTaO_4$ for high-temperature application. *J Am Ceram Soc* 2019,

102: 889–895.

[195] Wu P, Hu MY, Chen L, *et al*. Investigation on microstructures and thermo-physical properties of ferroelastic $(Y_{1-x}Dy_x)TaO_4$ ceramics. *Materialia* 2018, **4**: 478–486.

[196] Wu P, Chong XY, Feng J. Effect of Al^{3+} doping on mechanical and thermal properties of $DyTaO_4$ as promising thermal barrier coating application. *J Am Ceram Soc* 2018, **101**: 1818–1823.

[197] Ma Z, Zheng J, Wang S, *et al.* First-principle calculations of crystal structures, electronic structures, and optical properties of $RETaO_4$ (RE = Y, La, Sm, Eu, Dy, Er). *Opt Eng* 2018, **57**: 017107.

[198] Devesa S, Teixeira SS, Rooney AP, *et al*. Structural, morphological and dielectric properties of $ErNbO_4$ prepared by the sol–gel method. *J Phys Chem Solids* 2020, **146**: 109619.

[199] Nedelcu L, Geambasu CD, Enculescu M, *et al*. Intrinsic dielectric loss in $Zr_{0.8}Sn_{0.2}TiO_4$ ceramics investigated by terahertz time domain spectroscopy. *Materials* 2021, **14**: 216.

[200] Kumada N, Taki K, Kinomura N. Single crystal structure refinement of a magnesium niobium oxide: $Mg_4Nb_2O_9$. *Mater Res Bull* 2000, **35**: 1017–1021.

[201] Ogawa H, Kan A, Ishihara S, *et al*. Crystal structure of corundum type $Mg_4(Nb_{2-x}Ta_x)O_9$ microwave dielectric ceramics with low dielectric loss. *J Eur Ceram Soc* 2003, **23**: 2485–2488.

[202] Wu HT, Li LX, Zou Q, *et al*. Synthesis, characterization, and microwave dielectric properties of $Mg_4Nb_2O_9$ ceramics produced through the aqueous sol–gel process. *J Alloys Compd* 2011, **509**: 2232–2237.

[203] Mei QJ, Li CY, Guo JD, *et al*. Influence of sintering temperature on dielectric properties and crystal structure of corundum-structured $Mg_4Ta_2O_9$ ceramics at microwave frequencies. *Ceram Int* 2013, **39**: 9145–9149.

[204] Wu HT, Wu WB, Yue YL, *et al*. Synthesis and microwave dielectric properties of pseudobrookite-type structure $Mg_5Nb_4O_{15}$ ceramics by aqueous sol–gel technique. *Ceram Int* 2012, **38**: 4271–4276.

[205] Kamba S, Petzelt J, Buixaderas E, *et al*. High frequency dielectric properties of $A_5B_4O_{15}$ microwave ceramics. *J Appl Phys* 2001, **89**: 3900–3906.

[206] Guo JD, Li CY, Mei QJ, *et al*. Effect of MgO excess on structure and microwave dielectric properties of $Mg_4Nb_2O_9$ ceramics. *Mater Technol* 2015, **30**: 134–137.

[207] Yang T, Han ZX, Liu P, *et al*. Microwave dielectric properties of $Mg_4Nb_2O_9$ ceramics with excess $Mg(OH)_2$ produced by a reaction-sintering process. *Ceram Int* 2015, **41**: S572–S575.

[208] Li BJ, Wang SY, Lin SH, *et al*. Dielectric properties and crystal structure of $(Mg_{0.95}Ni_{0.05})_4(Nb_{1-x}Ta_x)_2O_9$ ceramics. *J Ceram Soc Japan* 2016, **124**: 140–144.

[209] Kim JH, Kim ES. Microwave dielectric properties of $Mg_4Nb_2O_9$-based ceramics with $(B_xW_{1-x})^{5+}$ substitutions at Nb^{5+} sites (B = Li, Mg, Al, Ti). *Ceram Int* 2017, **43**: S339–S342.

[210] Li BJ, Wang SY, Chiu CY, *et al*. Dielectric properties and mixture behavior of $y(Mg_{0.95}Co_{0.05})_4Ta_2O_9$–$(1-y)CaTiO_3$ ceramic system at microwave frequency. *J Alloys Compd* 2016, **661**: 357–362.

[211] Pakawanit P, Ananta S. Influence of sintering temperature on densification and microstructure of $Zn_3Nb_2O_8$ ceramics derived from nanopowders. *Adv Mater Res* 2011, **194–196**: 656–659.

[212] Amonpattaratkit P, Ngamjarurojana A, Ananta S. Microstructure and dielectric properties of $Zn_3Nb_2O_8$ ceramics prepared by a two-stage sintering method. *Ceram Int* 2013, **39**: S331–S334.

[213] Bian JJ, Wang L, Yuan LL. Microwave dielectric properties of $Li_{2+x}Ti_{1-4x}Nb_{3x}O_3$ ($0 \leqslant x \leqslant 0.1$). *Mater Sci Eng*: *B* 2009, **164**: 96–100.

[214] Bian JJ, Dong YF. Sintering behavior, microstructure and microwave dielectric properties of $Li_{2+x}TiO_3$ ($0 \leqslant x \leqslant 0.2$). *Mater Sci Eng*: *B* 2011, **176**: 147–151.

[215] Hao YZ, Zhang QL, Zhang J, *et al*. Enhanced sintering characteristics and microwave dielectric properties of Li_2TiO_3 due to nano-size and nonstoichiometry effect. *J Mater Chem* 2012, **22**: 23885.

[216] Izquierdo G, West AR. Phase equilibria in the system Li_2O–TiO_2. *Mater Res Bull* 1980, **15**: 1655–1660.

[217] Mikkelsen JC. Pseudobinary phase relations of $Li_2Ti_3O_7$. *J Am Ceram Soc* 1980, **63**: 331–335.

[218] Chen GH, Xu HR, Yuan CL. Microstructure and microwave dielectric properties of $Li_2Ti_{1-x}(Zn_{1/3}Nb_{2/3})_xO_3$ ceramics. *Ceram Int* 2013, **39**: 4887–4892.

[219] Guo HH, Zhou D, Pang LX, *et al*. Influence of $(Mg_{1/3}Nb_{2/3})$ complex substitutions on crystal structures and microwave dielectric properties of Li_2TiO_3 ceramics with extreme low loss. *J Materiomics* 2018, **4**: 368–382.

[220] Chen WS, Hung ML, Hsu CH. Effects of $(Co_{1/3}Nb_{2/3})^{4+}$ substitution on microstructure and microwave dielectric properties of $Li_2Ti_{1-x}(Co_{1/3}Nb_{2/3})_xO_3$ ceramics for applications in ceramic antenna. *J Asian Ceram Soc* 2021, **9**: 433–442.

[221] Guo HH, Fu MS, Zhou D, *et al*. Design of a high-efficiency and -gain antenna using novel low-loss, temperature-stable $Li_2Ti_{1-x}(Cu_{1/3}Nb_{2/3})_xO_3$ microwave dielectric ceramics. *ACS Appl Mater Interfaces* 2021, **13**: 912–923.

[222] Bian JJ, Dong YF. New high *Q* microwave dielectric ceramics with rock salt structures: $(1-x)Li_2TiO_3$+*x*MgO system ($0 \leqslant x \leqslant 0.5$). *J Eur Ceram Soc* 2010, **30**: 325–330.

[223] Huang CL, Tseng YW, Chen JY. High-*Q* dielectrics using ZnO-modified Li_2TiO_3 ceramics for microwave applications. *J Eur Ceram Soc* 2012, **32**: 3287–3295.

[224] Bian JJ, Liang Z, Wang L. Structural evolution and microwave dielectric properties of $Li_{(3-3x)}M_{4x}Nb_{(1-x)}O_4$ (M = Mg, Zn; $0 \leqslant x \leqslant 0.9$). *J Am Ceram Soc* 2011, **94**:

1447–1453.

[225] Wu NX, Bian JJ. Microstructure and microwave dielectric properties of $(1-y)Li_3NbO_4+yLi_2TiO_3(Li_2SnO_3)$ ceramics. *Mater Sci Eng*: *B* 2012, **177**: 1793–1798.

[226] Tseng YW, Chen JY, Kuo YC, *et al*. Low-loss microwave dielectrics using rock salt oxide Li_2MgTiO_4. *J Alloys Compd* 2011, **509**: L308–L310.

[227] Chen XL, Zhou HF, Fang L, *et al*. Microwave dielectric properties and its compatibility with silver electrode of $Li_2MgTi_3O_8$ ceramics. *J Alloys Compd* 2011, **509**: 5829–5832.

[228] Fang L, Chu DJ, Zhou HF, *et al*. Microwave dielectric properties and low temperature sintering behavior of $Li_2CoTi_3O_8$ ceramic. *J Alloys Compd* 2011, **509**: 1880–1884.

[229] Taghipour Armaki H, Taheri-Nassaj E, Bari M. Phase analysis and improvement of quality factor of $Li_2ZnTi_3O_8$ ceramics by annealing treatment. *J Alloys Compd* 2013, **581**: 757–761.

[230] Lyu XS, Li LX, Cai HC, *et al*. A new microwave dielectric material $LiNi_{0.5}Ti_{0.5}O_2$. *Ceram Int* 2015, **41**: 9168–9171.

[231] Zhou HF, Liu XB, Chen XL, *et al*. $ZnLi_{2/3}Ti_{4/3}O_4$: A new low loss spinel microwave dielectric ceramic. *J Eur Ceram Soc* 2012, **32**: 261–265.

[232] Zhou HF, Liu XB, Chen XL, *et al*. Preparation, phase structure and microwave dielectric properties of a new low cost $MgLi_{2/3}Ti_{4/3}O_4$ compound. *Mater Chem Phys* 2012, **137**: 22–25.

[233] Zhou HF, Liu XB, Chen XL, *et al*. Preparation, phase structure and microwave dielectric properties of $CoLi_{2/3}Ti_{4/3}O_4$ ceramic. *Mater Res Bull* 2012, **47**: 1278–1280.

[234] Bi JX, Xing CF, Jiang XS, *et al*. Characterization and microwave dielectric properties of new low loss Li_2MgZrO_4 ceramics. *Mater Lett* 2016, **184**: 269–272.

[235] Fu ZF, Liu P, Ma JL, *et al*. New high *Q* low-fired $Li_2Mg_3TiO_6$ microwave dielectric ceramics with rock salt structure. *Mater Lett* 2016, **164**: 436–439.

[236] Zhou HF, Gong JZ, Fan GC, *et al*. Enhanced sintering ability and microwave dielectric properties of $LiZnNbO_4$ ceramics with pretreatment of raw materials. *J Alloys Compd* 2016, **665**: 113–118.

[237] Su CH, Huang CL. Investigation of the microwave dielectric properties of $Li_2ZnTi_5O_{12}$ ceramics. *J Alloys Compd* 2016, **678**: 102–108.

[238] Liu QQ, Pan HL, Tao WH, *et al*. New rock salt structure dielectric material $Li_2Ni_3TiO_6$ at microwave frequency. *J Mater Sci*: *Mater Electron* 2017, **28**: 9893–9899.

[239] Bi JX, Li CC, Zhang YH, *et al*. Crystal structure, infrared spectra and microwave dielectric properties of ultra low-loss $Li_2Mg_4TiO_7$ ceramics. *Mater Lett* 2017, **196**: 128–131.

[240] Pan HL, Wu HT. Crystal structure, infrared spectra and microwave dielectric properties of new ultra low-loss $Li_6Mg_7Ti_3O_{16}$ ceramics. *Ceram Int* 2017, **43**: 14484–14487.

[241] Zuo RZ, Qi H, Qin F, *et al*. A new Li-based ceramic of $Li_4MgSn_2O_7$: Synthesis, phase evolution and microwave dielectric properties. *J Eur Ceram Soc* 2018, **38**: 5442–5447.

[242] Jiang PB, Hu YD, Bao SX, *et al*. A novel microwave dielectric ceramic Li_2NiZrO_4 with rock salt structure. *RSC Adv* 2019, **9**: 32936–32939.

[243] Wu HT, Kim ES. Characterization of low loss microwave dielectric materials $Li_3Mg_2NbO_6$ based on the chemical bond theory. *J Alloys Compd* 2016, **669**: 134–140.

[244] Pei CJ, Hou CD, Li Y, *et al*. A low ε_r and temperature-stable $Li_3Mg_2SbO_6$ microwave dielectric ceramics. *J Alloys Compd* 2019, **792**: 46–49.

[245] Li J, Zhang ZW, Tian YF, *et al*. Crystal structure and microwave dielectric properties of a novel rock-salt type Li_3MgNbO_5 ceramic. *J Mater Sci* 2020, **55**: 15643–15652.

[246] Zhang X, Jiang ZH, Tang B, *et al*. A new series of low-loss multicomponent oxide microwave dielectrics with a rock salt structure: Li_5MgABO_8 (A = Ti, Sn; B = Nb, Ta). *Ceram Int* 2020, **46**: 10332–10340.

[247] Zhang X, Fang ZX, Yang HY, *et al*. Lattice evolution, ordering transformation and microwave dielectric properties of rock-salt $Li_{3+x}Mg_{2-2x}Nb_{1-x}Ti_{2x}O_6$ solid-solution system: A newly developed pseudo ternary phase diagram. *Acta Mater* 2021, **206**: 116636.

[248] Gu FF, Chen GH, Li XQ, *et al*. Structural and microwave dielectric properties of the $(1-x)Li_3NbO_4-xCa_{0.8}Sr_{0.2}TiO_3$ thermally stable ceramics. *Mater Chem Phys* 2015, **167**: 354–359.

[249] Yao GG, Hu XS, Tian XL, *et al*. Synthesis and microwave dielectric properties of Li_2MgTiO_4 ceramics. *Ceram Int* 2015, **41**: S563–S566.

[250] Du H, Li CC, Liu FL, *et al*. Influence of ionic substitution on the microwave dielectric properties of $Li_2Mg_{0.95}A_{0.05}TiO_4$ (A = Ni, Co, Mn, Zn) ceramics. *J Mater Sci*: *Mater Electron* 2017, **28**: 8304–8308.

[251] Wang P, Wang YR, Bi JX, *et al*. Effects of Zn^{2+} substitution on the crystal structure, Raman spectra, bond energy and microwave dielectric properties of Li_2MgTiO_4 ceramics. *J Alloys Compd* 2017, **721**: 143–148.

[252] Xing CF, Liu QQ, Wu HT. Sintering characteristics, crystal structure, and microwave dielectric properties of $Li_2(Mg_{0.9}A_{0.1})_4TiO_7$ ($A = Co^{2+}$, Ni^{2+}, Mg^{2+}, Zn^{2+}, Ca^{2+}). *J Mater Sci*: *Mater Electron* 2019, **30**: 302–307.

[253] Xing CF, Wu HT. Crystal structure and microwave dielectric properties of $Li_4Mg_3[Ti_{1-x}(Mg_{1/3}Ta_{2/3})_x]_2O_9$ ($x = 0$–0.4) ceramics. *Ceram Int* 2019, **45**: 4142–4145.

[254] Lu XP, Zheng Y, Huang Q, *et al*. Correlation of heating rates, crystal structures, and microwave dielectric properties of $Li_2ZnTi_3O_8$ ceramics. *J Electron Mater* 2015, **44**: 4243–4249.

[255] Zhou HF, Wang N, Gong JZ, *et al*. Processing of low-fired glass-free $Li_2MgTi_3O_8$ microwave dielectric ceramics. *J Alloys Compd* 2016, **688**: 8–13.

[256] Tajik Z, Sayyadi-Shahraki A, Taheri-Nassaj E, *et al*. Effect of synthesis and sintering technique on the long-range 1:3 cation ordering and microwave dielectric loss of $Li_2ZnTi_3O_8$ ceramics. *Ceram Int* 2020, **46**: 20905–20913.

[257] Huang CL, Su CH, Chang CM. High *Q* microwave dielectric ceramics in the $Li_2(Zn_{1-x}A_x)Ti_3O_8$ (A = Mg, Co; x = 0.02–0.1) system. *J Am Ceram Soc* 2011, **94**: 4146–4149.

[258] Fang L, Chu DJ, Zhou HF, *et al*. Microwave dielectric properties of temperature stable $Li_2Zn_xCo_{1-x}Ti_3O_8$ ceramics. *J Alloys Compd* 2011, **509**: 8840–8844.

[259] Wang LJ, Sun QC, Ma WB, *et al*. Microwave dielectric characteristics of $Li_2(Mg_{0.94}M_{0.06})Ti_3O_8$ (M = Zn, Co, and Mn) ceramics. *Ceram Int* 2013, **39**: 5185–5190.

[260] Ren HS, Wu ZL, He F, *et al*. Investigation on phase and microstructures of a temperature stable high-*Q* $Li_2Zn_{0.95}Sr_{0.05}Ti_3O_8$ microwave dielectric ceramic. *J Mater Sci*: *Mater Electron* 2019, **30**: 8154–8159.

[261] Ren HS, Xie TY, Wu ZL, *et al*. Crystal structure, phase evolution and dielectric properties in the $Li_2ZnTi_3O_8$–$SrTiO_3$ system as temperature stable high-*Q* material. *J Alloys Compd* 2019, **797**: 18–25.

[262] Tian S, Liao ZL, Wang H, *et al*. Influence of Ca_xSr_{1-x} ($0 \leqslant x \leqslant 1$) substitution for Zn on microwave dielectric properties of $Li_2ZnTi_3O_8$ ceramic as temperature stable materials. *J Wuhan Univ Technol Mater Sci Ed* 2020, **35**: 686–690.

[263] Liu XB, Zhou HF, Chen XL, *et al*. Phase structure and microwave dielectric properties of $(1-x)Li_2Zn_3Ti_4O_{12}$–$xTiO_2$ ceramics. *J Alloys Compd* 2012, **515**: 22–25.

[264] Wang W, Zhou HF, Chen XL, *et al*. Crystal structure and optimized microwave dielectric properties of $(1-x)LiZn_{0.5}Ti_{1.5}O_4$–$xTiO_2$ ceramics for application in dielectric resonator. *J Mater Sci*: *Mater Electron* 2013, **24**: 2641–2645.

[265] Bari M, Taheri-Nassaj E, Taghipour-Armaki H. Phase evolution, microstructure, and microwave dielectric properties of reaction-sintered $Li_2ZnTi_3O_8$ ceramic obtained using nanosized TiO_2 reagent. *J Electron Mater* 2015, **44**: 3670–3676.

[266] Bari M, Taheri-Nassaj E, Taghipour-Armaki H. Role of nano- and micron-sized particles of TiO_2 additive on microwave dielectric properties of $Li_2ZnTi_3O_8$–4 wt%TiO_2 ceramics. *J Am Ceram Soc* 2013, **96**: 3737–3741.

[267] Zhang P, Wang Y, Liu J, *et al*. A high improved quality factor of $Li_2MgTi_3O_8$ microwave dielectric ceramics system. *Mater Lett* 2014, **123**: 195–197.

[268] Zhang P, Zhao YG. High-*Q* microwave dielectric materials of $Li_2ZnTi_3O_8$ ceramics with SnO_2 additive. *Ceram Int* 2016, **42**: 2882–2886.

[269] Zhang YD, Han J, Liang R, *et al*. Novel temperature stable Li_2TiO_3-based microwave dielectric ceramics with low loss. *Mater Lett* 2015, **153**: 118–120.

[270] Li W, Li JH, Shen JX, *et al*. Crystal structure, Raman spectra, and microwave dielectric properties of high-*Q* $Li_2ZnTi_3O_8$ systems with Nb_2O_5 addition. *Ceram Int* 2021, **47**: 8601–8609.

[271] Zhang BW, Li LX, Luo WJ. Oxygen vacancy regulation and its high frequency response mechanism in microwave ceramics. *J Mater Chem C* 2018, **6**: 11023–11034.

[272] Zhang P, Xie H, Zhao YG, *et al*. Microwave dielectric properties of low loss $Li_2(Mg_{0.95}A_{0.05})_3TiO_6$(A = Ca^{2+}, Ni^{2+}, Zn^{2+}, Mn^{2+}) ceramics system. *J Alloys Compd* 2016, **689**: 246–249.

[273] Shi XL, Zhang HW, Zhang DN, *et al*. Structure and microwave dielectric properties of $Li_2Mg_3Ti_{1-x}(Al_{1/2}Nb_{1/2})_xO_6$ ceramics. *Ceram Int* 2020, **46**: 13737–13742.

[274] Zhan Y, Li LX. Low-permittivity and high-*Q* value $Li_2Mg_3Ti_{1-x}(Zn_{1/3}Nb_{2/3})_xO_6$ microwave dielectric ceramics for microstrip antenna applications in 5G millimeter wave. *J Alloys Compd* 2021, **857**: 157608.

[275] Fang ZX, Tang B, Si F, *et al*. Phase evolution, structure and microwave dielectric properties of $Li_{2+x}Mg_3SnO_6$ (x = 0.00–0.12) ceramics. *Ceram Int* 2017, **43**: 13645–13652.

[276] Fang ZX, Tang B, Si F, *et al*. Temperature stable and high-Q microwave dielectric ceramics in the $Li_2Mg_{3-x}Ca_xTiO_6$ system (x = 0.00–0.18). *Ceram Int* 2017, **43**: 1682–1687.

[277] Fang ZX, Tang B, Yuan Y, *et al*. Structure and microwave dielectric properties of the $Li_{2/3(1-x)}Sn_{1/3(1-x)}Mg_xO$ systems (x = 0–4/7). *J Am Ceram Soc* 2018, **101**: 252–264.

[278] Xie TY, Zhang LZ, Ren HS, *et al*. A novel temperature-stable and low-loss microwave dielectric using $Ca_{0.8}Sr_{0.2}TiO_3$-modified $Li_2Mg_3TiO_6$ ceramics. *J Mater Sci*: *Mater Electron* 2017, **28**: 13705–13709.

[279] Zhou HF, Tan XH, Huang J, *et al*. Sintering behavior, phase evolution and microwave dielectric properties of thermally stable Li_2O–3MgO–$mTiO_2$ ceramics ($1 \leqslant m \leqslant 6$). *Ceram Int* 2017, **43**: 3688–3692.

[280] Pan HL, Xing CF, Jiang XS, *et al*. Characterization on low loss dielectric Li_2MgTiO_4 ceramics based on chemical bond theory at microwave frequency. *J Alloys Compd* 2016, **688**: 416–421.

[281] Bi JX, Niu YJ, Wu HT. $Li_4Mg_3Ti_2O_9$: A novel low-loss microwave dielectric ceramic for LTCC applications. *Ceram Int* 2017, **43**: 7522–7530.

[282] Pan HL, Cheng L, Wu HT. Relationships between crystal structure and microwave dielectric properties of $Li_2(Mg_{1-x}Co_x)_3TiO_6$ ($0 \leqslant x \leqslant 0.4$) ceramics. *Ceram Int* 2017, **43**: 15018–15026.

[283] Fu ZF, Liu P, Ma JL, *et al*. Novel series of ultra-low loss microwave dielectric ceramics: $Li_2Mg_3BO_6$ (B = Ti, Sn, Zr). *J Eur Ceram Soc* 2016, **36**: 625–629.

[284] Bi JX, Xing CF, Yang CH, *et al*. Phase composition, microstructure and microwave dielectric properties of rock salt structured Li_2ZrO_3–MgO ceramics. *J Eur Ceram Soc* 2018, **38**: 3840–3846.

[285] Liu LT, Wang LG, Du JL, *et al*. Effects of $(Mg_{1/3}Sb_{2/3})^{4+}$ substitutions on the sintering behaviors and microwave

dielectric properties of $Li_2Mg_4Zr_{1-x}(Mg_{1/3}Sb_{2/3})_xO_7$ ceramics. *J Alloys Compd* 2021, **865**: 158942.

[286] Shi XL, Zhang HW, Zhang DN, *et al*. Effect of zirconium deficiency on structure characteristics, morphology and microwave dielectric properties of $Li_2Mg_3Zr_{1-x}O_6$ ceramics. *Ceram Int* 2021, **47**: 12567–12573.

[287] Wang G, Zhang DN, Gan GW, *et al*. Synthesis, crystal structure and low loss of $Li_3Mg_2NbO_6$ ceramics by reaction sintering process. *Ceram Int* 2019, **45**: 19766–19770.

[288] Xing CF, Bi JX, Wu HT. Effect of Co-substitution on microwave dielectric properties of $Li_3(Mg_{1-x}Co_x)_2NbO_6$ ($0.00 \leqslant x \leqslant 0.10$) ceramics. *J Alloys Compd* 2017, **719**: 58–62.

[289] Zhang P, Liu L, Xiao M, *et al*. A novel temperature stable and high *Q* microwave dielectric ceramic in $Li_3(Mg_{1-x}Mn_x)_2NbO_6$ system. *J Mater Sci*: *Mater Electron* 2017, **28**: 12220–12225.

[290] Zhang P, Sun KX, Xiao M, *et al*. Crystal structure, densification, and microwave dielectric properties of $Li_3Mg_2(Nb_{(1-x)}Mo_x)O_{6+x/2}$ ($0 \leqslant x \leqslant 0.08$) ceramics. *J Am Ceram Soc* 2019, **102**: 4127–4135.

[291] Wang G, Zhang DN, Huang X, *et al*. Crystal structure and enhanced microwave dielectric properties of Ta^{5+} substituted $Li_3Mg_2NbO_6$ ceramics. *J Am Ceram Soc* 2020, **103**: 214–223.

[292] Pei CJ, Li Y, Hou CD, *et al*. Sintering behavior and microwave dielectric properties of V^{5+} substituted $Li_3Mg_2SbO_6$ ceramics. *J Mater Sci*: *Mater Electron* 2019, **30**: 14495–14499.

[293] Pei CJ, Tan JJ, Li Y, *et al*. Effect of Sb-site nonstoichiometry on the structure and microwave dielectric properties of $Li_3Mg_2Sb_{1-x}O_6$ ceramics. *J Adv Ceram* 2020, **9**: 588–594.

[294] Li H, Zhang PC, Chen XQ, *et al*. Effect of Zn^{2+} substitution for Mg^{2+} in $Li_3Mg_2SbO_6$ and the impact on the bond characteristics and microwave dielectric properties. *J Alloys Compd* 2020, **832**: 155043.

[295] Zhang P, Hao MM, Mao XR, *et al*. Effects of W^{6+} substitution on crystal structure and microwave dielectric properties of $Li_3Mg_2NbO_6$ ceramics. *Ceram Int* 2020, **46**: 21336–21342.

[296] Wang G, Zhang DN, Li J, *et al*. Crystal structure, bond energy, Raman spectra, and microwave dielectric properties of Ti-doped $Li_3Mg_2NbO_6$ ceramics. *J Am Ceram Soc* 2020, **103**: 4321–4332.

[297] Zhang P, Sun KX, Mao XR, *et al*. Crystal structures and high microwave dielectric properties in Li^+/Ti^{4+} ions co-doped $Li_3Mg_2NbO_6$ ceramics. *Ceram Int* 2020, **46**: 8097–8103.

[298] Zhang P, Hao MM, Xiao M. Microwave dielectric properties of $Li_3Mg_2NbO_6$-based ceramics with $(M_xW_{1-x})^{5+}$ (M = Li^+, Mg^{2+}, Al^{3+}, Ti^{4+}) substitutions at Nb^{5+} sites. *J Alloys Compd* 2021, **853**: 157386.

[299] Wang G, Zhang HW, Huang X, *et al*. Crystal structure and enhanced microwave dielectric properties of non-stoichiometric $Li_3Mg_{2+x}NbO_6$ ceramics. *Mater Lett* 2019, **235**: 84–87.

[300] Chu X, Gan L, Ren SQ, *et al*. Low-loss and temperature-stable $(1-x)Li_2TiO_3-xLi_3Mg_2NbO_6$ microwave dielectric ceramics. *Ceram Int* 2020, **46**: 8413–8419.

[301] Zhang X, Tang B, Fang ZX, *et al*. Structural evolution and microwave dielectric properties of a novel $Li_3Mg_{2-x/3}Nb_{1-2x/3}Ti_xO_6$ system with a rock salt structure. *Inorg Chem Front* 2018, **5**: 3113–3125.

[302] Zhang X, Zhang X, Fang ZX, *et al*. Effects of lattice evolution and ordering on the microwave dielectric properties of tin-modified $Li_3Mg_2NbO_6$-based ceramics. *J Phys Chem C* 2020, **124**: 22069–22081.

[303] Qin F, Zhang S, Zuo RZ. Ultralow-loss and thermally stable $Li_4MgSn_{2-1.25x}Nb_xO_7$ microwave dielectric ceramics. *J Mater Sci*: *Mater Electron* 2020, **31**: 5567–5572.

[304] Li L, Chen XM. Frequency-dependent Qf value of low-loss $Ba_2Ti_9O_{20}$ ceramics at microwave frequencies. *Ceram Int* 2012, **38**: 6831–6835.

[305] Huang XL, Song Y, Wang FP. Microwave dielectric properties of $BaTi_4O_9$–$BaSm_2Ti_4O_{12}$ composite ceramics. *J Ceram Soc Japan* 2013, **121**: 880–883.

[306] Yang QH, Luo T, Yu T, *et al*. Improvement of microwave dielectric properties of $Ba_2Ti_9O_{20}$ ceramics using $[Zn_{1/3}Nb_{2/3}]^{4+}$ substitution for Ti^{4+}. *J Mater Sci*: *Mater Electron* 2020, **31**: 15184–15191.

[307] Jawahar IN, Mohanan P, Sebastian MT. $A_5B_4O_{15}$ (A = Ba, Sr, Mg, Ca, Zn; B = Nb, Ta) microwave dielectric ceramics. *Mater Lett* 2003, **57**: 4043–4048.

[308] Zheng JJ, Yang YK, Wu HT, *et al*. Structure, infrared spectra and microwave dielectric properties of the novel Eu_2TiO_5 ceramics. *J Am Ceram Soc* 2020, **103**: 4333–4341.

[309] Niu H, Gou HY, Ewing RC, *et al*. First-principles investigation of structural, elastic and electronic properties of lanthanide titanate oxides Ln_2TiO_5. *MRS Online Proc Libr* 2011, **1298**: 85–90.

[310] Ohsato H. Science of tungstenbronze-type like $Ba_{6-3x}R_{8+2x}Ti_{18}O_{54}$ (R = rare earth) microwave dielectric solid solutions. *J Eur Ceram Soc* 2001, **21**: 2703–2711.

[311] Suvorov D, Valant M, Kolar D. The role of dopants in tailoring the microwave properties of $Ba_{6-x}R_{8+2/3x}Ti_{18}O_{54}$ R = (La–Gd) Ceramics. *J Mater Sci* 1997, **32**: 6483–6488.

[312] Snashall AL, Norén L, Liu Y, *et al*. Phase analysis and microwave dielectric properties of BaO–Nd_2O_3–$5TiO_2$ composite ceramics using variable size TiO_2 reagents. *Ceram Int* 2012, **38**: S153–S157.

[313] Yao XG, Lin HX, Zhao XY, *et al*. Effects of Al_2O_3 addition on the microstructure and microwave dielectric properties of $Ba_4Nd_{9.33}Ti_{18}O_{54}$ ceramics. *Ceram Int* 2012, **38**: 6723–6728.

[314] Chen HT, Xiong Z, Yuan Y, *et al*. Dependence of microwave dielectric properties on site substitution in $Ba_{3.75}Nd_{9.5}Ti_{18}O_{54}$ ceramic. *J Mater Sci*: *Mater Electron*

2016, **27**: 10951–10957.

[315] Setasuwon P, Freer R, Azough F, *et al*. $(Ba_{1-y}Pb_y)_{3.75}Nd_{9.5}Ti_{18}O_{54}$ and $(Ba_{1-y}Sr_y)_{3.75}Nd_{9.5}Ti_{18}O_{54}$ microwave dielectric ceramics: Effect of Pb and Sr substitution on dielectric properties. *Br Ceram Trans* 2002, **101**: 237–241.

[316] Muhammad R, Iqbal Y, Rambo CR. Characterization of $Ba_{4.5}Re_9Ti_{18}O_{54}$ (Re = La, Nd) microwave dielectric ceramics. *J Mater Sci*: *Mater Electron* 2014, **25**: 1652–1656.

[317] Huang BY, Wang ZF, Chen T, *et al*. Microstructure and microwave dielectric properties of $Ba_{4.2}Nd_{9.2}Ti_{18-x}Sn_xO_{54}$ (x = 0, 0.25, 0.5, 1, 1.5, 2) ceramics. *J Mater Sci*: *Mater Electron* 2015, **26**: 3375–3379.

[318] Guo X, Tang B, Chen HT, *et al*. Microwave dielectric properties and microstructure of $(Ba_{0.98}Sr_{0.02})_{3.75}Nd_{9.5}Ti_{18-x}(Zn_{1/3}Nb_{2/3})_xO_{54}$ ceramics. *J Mater Sci*: *Mater Electron* 2015, **26**: 6182–6188.

[319] Guo X, Tang B, Liu JQ, *et al*. Microwave dielectric properties and microstructure of $Ba_{6-3x}Nd_{8+2x}Ti_{18-y}(Cr_{1/2}Nb_{1/2})_yO_{54}$ ceramics. *J Alloys Compd* 2015, **646**: 512–516.

[320] An SB, Jiang J, Wang JZ, *et al*. Microwave dielectric property modification of $Ba_4Nd_{9.33}Ti_{18}O_{54}$ ceramics by the substitution of $(Al_{0.5}Nb_{0.5})^{4+}$ for Ti^{4+} and the addition of $NdAlO_3$. *Ceram Int* 2020, **46**: 3960–3967.

[321] Xiong Z, Tang B, Fang ZX, *et al*. Crystal structure, Raman spectroscopy and microwave dielectric properties of $Ba_{3.75}Nd_{9.5}Ti_{18-z}(Al_{1/2}Nb_{1/2})_zO_{54}$ ceramics. *J Alloys Compd* 2017, **723**: 580–588.

[322] Zhou LL, Zhou HQ, Shao H, *et al*. Microstructure and microwave dielectric properties of $Ba_{6-3x}Sm_{8+2x}Ti_{18}O_{54}$ ceramics with various $Ba_xSr_{1-x}TiO_3$ additions. *J Rare Earths* 2012, **30**: 142–145.

[323] Xu Y, Fu RL, Agathopoulos S, *et al*. Synthesis and microwave dielectric properties of $BaO–Sm_2O_3–5TiO_2$ ceramics with $NdAlO_3$ additions. *Ceram Int* 2016, **42**: 14573–14580.

[324] Yao XG, Lin HX, Chen W, *et al*. Anti-reduction of Ti^{4+} in $Ba_{4.2}Sm_{9.2}Ti_{18}O_{54}$ ceramics by doping with MgO, Al_2O_3 and MnO_2. *Ceram Int* 2012, **38**: 3011–3016.

[325] Wang G, Fu QY, Shi H, *et al*. Novel thermally stable, high quality factor $Ba_4(Pr_{0.4}Sm_{0.6})_{28/3}Ti_{18-y}Ga_{4y/3}O_{54}$ microwave dielectric ceramics. *J Am Ceram Soc* 2020, **103**: 2520–2527.

[326] Wang G, Fu QY, Guo PJ, *et al*. A/B-site cosubstituted $Ba_4Pr_{28/3}Ti_{18}O_{54}$ microwave dielectric ceramics with temperature stable and high Q in a wide range. *Ceram Int* 2020, **46**: 11474–11483.

[327] Roth RS, Rawn CJ, Lindsay CG, *et al*. Phase equilibria and crystal chemistry of the binary and ternary barium polytitanates and crystallography of the barium zinc polytitanates. *J Solid State Chem* 1993, **104**: 99–118.

[328] Tang B, Yu SQ, Chen HT, *et al*. The influence of Cu substitution on the microwave dielectric properties of $BaZn_2Ti_4O_{11}$ ceramics. *J Alloys Compd* 2013, **551**: 463–467.

[329] Yu SQ, Tang B, Zhang SR, *et al*. Temperature stable high-Q microwave dielectric ceramics in $(1-x)BaTi_4O_{9-x}BaZn_2Ti_4O_{11}$ system. *Mater Lett* 2012, **67**: 293–295.

[330] Yu SQ, Tang B, Zhang X, *et al*. Improved high-Q microwave dielectric ceramics in CuO-doped $BaTi_4O_9–BaZn_2Ti_4O_{11}$ system. *J Am Ceram Soc* 2012, **95**: 1939–1943.

[331] Yu SQ, Zhang SR, Tang B, *et al*. Microwave dielectric properties of $BaO–2(1-x)ZnO–xNd_2O_3–4TiO_2$ (x = 0–1.0) ceramics. *Ceram Int* 2012, **38**: 613–618.

[332] Yang XY, Kyzzhibek T, Genevois C, *et al*. $Ba_8CoNb_{6-x}Ta_xO_{24}$ eight-layer shifted hexagonal perovskite ceramics with spontaneous Ta^{5+} ordering and near-zero τ_f. *Inorg Chem* 2019, **58**: 10974–10982.

[333] Sanoj MA, Reshmi CP, Sreena KP, *et al*. Sinterability and microwave dielectric properties of nano structured $0.95MgTiO_3–0.05CaTiO_3$ synthesised by top down and bottom up approaches. *J Alloys Compd* 2011, **509**: 3089–3095.

[334] Rajput SS, Keshri S. Structural, vibrational and microwave dielectric properties of $(1-x)Mg_{0.95}Co_{0.05}TiO_3–(x)Ca_{0.8}Sr_{0.2}TiO_3$ ceramic composites. *J Alloys Compd* 2013, **581**: 223–229.

[335] Rajput SS, Keshri S, Gupta VR. Microwave dielectric properties of $(1-x)Mg_{0.95}Zn_{0.05}TiO_3–(x)Ca_{0.6}La_{0.8/3}TiO_3$ ceramic composites. *J Alloys Compd* 2013, **552**: 219–226.

[336] Huang JB, Yang B, Yu CY, *et al*. Microwave and terahertz dielectric properties of $MgTiO_3–CaTiO_3$ ceramics. *Mater Lett* 2015, **138**: 225–227.

[337] Hsu CH, Chang CH. A temperature-stable and high-Q microwave dielectric ceramic of the $MgTiO_3–(Ca_{0.8}Sr_{0.2})(Zr_{0.1}Ti_{0.9})O_3$ system. *Ceram Int* 2015, **41**: 6965–6969.

[338] Li LX, Li S, Tian T, *et al*. Microwave dielectric properties of $(1-x)MgTiO_3–x(Ca_{0.6}Na_{0.2}Sm_{0.2})TiO_3$ ceramic system. *J Mater Sci*: *Mater Electron* 2016, **27**: 1286–1292.

[339] Chen CY, Peng ZJ, Xie LZ, *et al*. Microwave dielectric properties of novel $(1-x)MgTiO_3–xCa_{0.5}Sr_{0.5}TiO_3$ ceramics. *J Mater Sci*: *Mater Electron* 2020, **31**: 13696–13703.

[340] Hou GH, Wang ZH, Zhang F. Sintering behavior and microwave dielectric properties of $(1-x)CaTiO_3–xLaAlO_3$ ceramics. *J Rare Earths* 2011, **29**: 160–163.

[341] Liang F, Ni M, Lu WZ, *et al*. Microwave dielectric properties and crystal structures of $0.7CaTiO_3–0.3[La_xNd_{(1-x)}]AlO_3$ ceramics. *J Alloys Compd* 2013, **568**: 11–15.

[342] Li LX, Gao ZD, Liu YR, *et al*. Influence of $LaAlO_3$ additive to $MgTiO_3–CaTiO_3$ ceramics on sintering behavior and microwave dielectric properties. *Mater Lett* 2015, **140**: 5–8.

[343] Li LX, Li S, Lyu XS, *et al*. $LaAlO_3$ doped $(Mg_{0.95}Zn_{0.05})TiO_3–CaTiO_3$ ceramic system with

ultra-high-*Q* and temperature-stable characterization. *J Mater Sci*: *Mater Electron* 2015, **26**: 5871–5876.

[344] Zhang LZ, Lin HX, Zhao XY, *et al*. Investigation on microwave dielectric properties and microstructures of $(1-x)LaAlO_{3-x}Ca_{0.2}Sr_{0.8}TiO_3$ ceramics. *J Alloys Compd* 2015, **649**: 254–260.

[345] Dou ZM, Jiang J, Wang G, *et al*. Effect of Ga^{3+} substitution on the microwave dielectric properties of $0.67CaTiO_3$–$0.33LaAlO_3$ ceramics. *Ceram Int* 2016, **42**: 6743–6748.

[346] Weng MH, Liauh CT, Lin SM, *et al*. Sintering behaviors, microstructure, and microwave dielectric properties of $CaTiO_3$–$LaAlO_3$ ceramics using CuO/B_2O_3 additions. *Materials* 2019, **12**: 4187.

[347] Niu ST, Jiang J, Wang JZ, *et al*. The sintering behavior and microwave dielectric properties of $0.67CaTiO_3$–$0.33LaAlO_3$ ceramics sintered at medium temperatures with the additives of H_3BO_3–Li_2CO_3. *J Mater Sci*: *Mater Electron* 2020, **31**: 14879–14885.

[348] Wang SF, Wang YR, Hsu JC. Densification, microstructural evolution, and dielectric properties of $CaTiO_3$–$LaGaO_3$ microwave ceramics. *J Phys Chem Solids* 2011, **72**: 1011–1014.

[349]] Feteira A, Iddles D, Price T, *et al*. High-permittivity and low-loss microwave dielectric ceramics based on $(x)RE(Zn_{1/2}Ti_{1/2})O_3-(1-x)CaTiO_3$ (RE = La and Nd). *J Am Ceram Soc* 2011, **94**: 817–821.

[350] Li LX, Zhang MM, Liao QW, *et al*. Composite dielectrics $(1-y)(Mg_{1-x}Zn_x)_{1.8}Ti_{1.1}O_4-yCaTiO_3$ suitable for microwave applications. *J Alloys Compd* 2012, **531**: 18–22.

[351] Wang SF, Chen JH, Hsu YF, *et al*. Effects of $CaTiO_3$ addition on the densification and microwave dielectric properties of $BiSbO_4$ ceramics. *Ceram Int* 2013, **39**: 2857–2861.

[352] Chen YC, Yao SL. Influence of $Ca_{0.8}Sr_{0.2}TiO_3$ on the microstructures and microwave dielectric properties of $Nd(Mg_{0.4}Zn_{0.1}Sn_{0.5})O_3$ ceramics. *J Mater Sci*: *Mater Electron* 2012, **23**: 825–831.

[353] Yang XY, Wang XH, Yao GF, *et al*. Phase structures and microwave dielectric properties of $xCaTiO_3-(1-x)Sm_{0.9}Nd_{0.1}AlO_3$ ceramics. *J Mater Sci*: *Mater Electron* 2013, **24**: 4662–4668.

[354] Xu P, Yang J, Li JM, *et al*. Microstructure and microwave dielectric properties of $(1-x)Ca_{0.6}La_{0.267}TiO_{3-x}Ca(Mg_{1/3}Nb_{2/3})O_3$ ceramics. *Ceram Int* 2012, **38**: 3863–3867.

[355] Li JM, Han YX, Qiu T, *et al*. Effect of bond valence on microwave dielectric properties of $(1-x)CaTiO_{3-x}(Li_{0.5}La_{0.5})TiO_3$ ceramics. *Mater Res Bull* 2012, **47**: 2375–2379.

[356] Wang XC, Liu YW, Wang XH, *et al*. High permittivity and near-zero τεdielectrics $Ca_{0.36}Sr_{0.64}TiO_3$–$Li_{0.5}Nd_{0.5}TiO_3$ for multilayer ceramic capacitors. *Jpn J Appl Phys* 2015, **54**: 111501.

[357] Ning FF, Gan L, Yuan SF, *et al*. Correlation between vibrational modes of A-site ions and microwave dielectric properties in $(1-x)CaTiO_3-x(Li_{0.5}Sm_{0.5})TiO_3$ ceramics. *J Alloys Compd* 2017, **729**: 742–748.

[358] Yang XY, Wang XH, Huang M, *et al*. Synthesis and characterization of $CaTiO_3$–$(Sm,Nd)AlO_3$ microwave ceramics via sol−gel method. *J Sol Gel Sci Technol* 2014, **69**: 61–66.

[359] Qu JJ, Huang DL, Wei X, *et al*. Effect of $NdAlO_3$ on microstructure, dielectric properties and temperature-stable mechanism of $(Sr,Ca,Nd)TiO_3$ ceramics at microwave frequency. *J Mater Sci*: *Mater Electron* 2016, **27**: 11110–11117.

[360] Qu JJ, Liu F, Wei X, *et al*. Sintering behaviour and microwave dielectric properties of a new complex perovskite: $(1-x)(Sr_{0.3}Ca_{0.427}Nd_{0.182})TiO_3-xSmAlO_3$ ceramics. *Bull Mater Sci* 2016, **39**: 1645–1649.

[361] Zhang LM, Chang Y, Xin M, *et al*. Synthesis of $0.65CaTiO_3$–$0.35SmAlO_3$ ceramics and effects of La_2O_3/SrO doping on their microwave dielectric properties. *J Mater Sci*: *Mater Electron* 2018, **29**: 21205–21212.

[362] Yang XY, Zhang CY, Wu HY, *et al*. Structure and microwave dielectric properties of $CaSmAlO_4$–$CaTiO_3$–$Sm_{0.9}Nd_{0.1}AlO_3$ ceramics with medium to high permittivity. *J Ceram Soc Jpn* 2020, **128**: 756–760.

[363] Zhang LX, Gan L, Cheng HY, *et al*. Crystal structure, Raman spectra analysis and microwave dielectric properties optimization of $(Ca_{0.22}Li_{0.39}Sm_{0.39})TiO_3$ ceramics doped with $SmAlO_3$. *J Alloys Compd* 2020, **817**: 152708.

[364] Zhou SC, Luan XW, Hu S, *et al*. Sintering behavior, phase structure and microwave dielectric properties of CeO_2 added $CaTiO_3$–$SmAlO_3$ ceramics prepared by reaction sintering method. *Ceram Int* 2021, **47**: 3741–3746.

[365] Chen YC, You HM. Tuning the microwave dielectric properties of Zn_2SnO_4 ceramics by adding $Ca_{0.8}Sr_{0.2}TiO_3$. *Ceram Int* 2015, **41**: 9521–9526.

[366] Huang CL, Chien YH, Shih CF, *et al*. Crystal structure and dielectric properties of $xCa(Mg_{1/3}Nb_{2/3})O_3-(1-x)(Ca_{0.61}Nd_{0.26})TiO_3$ at the microwave frequency. *Mater Res Bull* 2015, **63**: 1–5.

[367] Yang XY, Wang XH, Li LT. Effect of MgO on microstructure and microwave dielectric properties of $0.84CaTiO_3-0.16Sm_{0.9}Nd_{0.1}AlO_3$ ceramics. *Mater Res Bull* 2015, **67**: 226–229.

[368] Reda AE, Ibrahim DM, Aziz DAA. Microwave dielectric properties of $(1-x)CaTiO_3$–$x(Na_{0.5}Nd_{0.5})TiO_3$ ceramics. *J Ceram Sci Tech* 2016, **7**: 243–248.

[369] Lin SH, Chen YB. Structure and characterization of B_2O_3 modified $yNd(Mg_{1/2}Ti_{1/2})O_3$–$(1-y)Ca_0.8Sr_{0.2}TiO_3$ ceramics with a near-zero temperature coefficient at microwave frequency. *Ceram Int* 2017, **43**: 2368–2371.

[370] Yang SW, Liang BL, Liu CH, *et al*. Microwave sintering and microwave dielectric properties of $(1-x)Ca_{0.61}La_{0.26}TiO_{3-x}Nd(Mg_{0.5}Ti_{0.5})O_3$ ceramics. *Materials* 2021, **14**: 438.

[371] Meng LF, Yuan CL, Liu X, *et al*. Electrical microstructures of $CaTiO_3$–$Bi_{0.5}Na_{0.5}TiO_3$ microwave ceramics with high

permittivity (ε_r^{max} ~487). *J Alloys Compd* 2019, **803**: 850–859.

[372] Zhou XJ, Zhou HF, Luan XW, *et al*. Structure and dielectric properties of novel series of $3CaO–RE_2O_3–2WO_3$ (RE = La, Nd and Sm) microwave ceramics and the adjustment of τ_f value. *J Mater Sci*: *Mater Electron* 2020, **31**: 14953–14960.

[373] Zhang XH, Chang N, Zhang J, *et al*. Low-loss $(1–x)Ba_{0.6}Sr_{0.4}La_4Ti_4O_{15}–xCaTiO_3$ microwave dielectric ceramics with medium permittivity. *J Alloys Compd* 2020, **819**: 153011.

[374] Zhou XJ, Wang KG, Hu S, *et al*. Preparation, structure and microwave dielectric properties of novel La_2MgGeO_6 ceramics with hexagonal structure and adjustment of its τ_f value. *Ceram Int* 2021, **47**: 7783–7789.

[375] Hsu CH, Chang CH. Microwave dielectric properties of $(Ca_{0.8}Sr_{0.2})(Sn_xTi_{1–x})O_3$ ceramics. *Mater Sci Eng*: *B* 2013, **178**: 354–357.

[376] Ravi GA, Azough F, Freer R. Structure and microwave dielectric properties of $Ca_{0.7}Ti_{0.7}La_{0.3}(Al_{0.3–x}Ga_x)O_3$ ceramics. *Adv Appl Ceram* 2012, **111**: 398–403.

[377] Lowndes R, Azough F, Cernik R, *et al*. Structures and microwave dielectric properties of $Ca_{(1–x)}Nd_{2x/3}TiO_3$ ceramics. *J Eur Ceram Soc* 2012, **32**: 3791–3799.

[378] Li JM, Qiu T. Microwave sintering of $Ca_{0.6}La_{0.2667}TiO_3$ microwave dielectric ceramics. *Int J Miner Metall Mater* 2012, **19**: 245–251.

[379] Iqbal Y, Muhammad R. Phase, microstructure and microwave dielectric properties of Nb and Ga doped $Ca_{0.6}La_{0.267}TiO_3$ ceramics. *J Mater Sci*: *Mater Electron* 2015, **26**: 10119–10122.

[380] Zhou CR, Chen GH, Cen ZY, *et al*. Structure and microwave dielectric characteristics of lithium-excess $Ca_{0.6}Nd_{0.8/3}TiO_3/(Li_{0.5}Nd_{0.5})TiO_3$ ceramics. *Mater Res Bull* 2013, **48**: 4924–4929.

[381] Hsu CH, Tsai PS, Tseng CF, *et al*. Microwave dielectric properties of $Ca_{0.4–x}Mg_xSm_{0.4}TiO_3$ ceramics. *J Alloys Compd* 2014, **582**: 355–359.

[382] Muhammad R, Iqbal Y. Microwave dielectric properties of $CaTi_{1–x}(Nb_{0.5}Ga_{0.5})_xO_3$ ceramics. *Mater Lett* 2015, **153**: 121–123.

[383] Xu Y, Fu RL, Agathopoulos S, *et al*. Sintering behavior, microstructure, and microwave dielectric properties of $Ca_{0.66}Ti_{0.66}Sm_{0.34}Al_{0.34}O_3$ ceramics. *Ceram Int* 2016, **42**: 19036–19041.

[384] Xu Y, Fu RL, Zhao P, *et al*. Sintering behavior, microwave dielectric properties of $Ca_{0.66}Ti_{0.66}Nd_{0.34}Al_{0.34}O_3$ ceramics revealed by microstructure and Raman scattering. *J Alloys Compd* 2019, **785**: 335–342.

[385] Chen GH, Chen JS, Kang XL, *et al*. Structural and microwave dielectric properties of new $CaTi_{1–x}(Al_{0.5}Nb_{0.5})_xO_3$ thermally stable ceramics. *J Alloys Compd* 2016, **675**: 301–305.

[386] Hameed I, Liu XQ, Li L, *et al*. Structure evolution and improved microwave dielectric characteristics in $CaTi_{1–x}(Al_{0.5}Nb_{0.5})_xO_3$ ceramics. *J Alloys Compd* 2020, **845**: 155435.

[387] Yan YX, Li ZM, Zhang ML, *et al*. Preparation and microwave dielectric properties of $Ca_{0.6}La_{0.8/3}(Sn_xTi_{1–x})O_3$ ceramics. *Ceram Int* 2017, **43**: 8534–8537.

[388] Wang XH, Mu ML, Jiang H, *et al*. Investigation on structure and microwave dielectric properties of novel high dielectric constant $Ca_{1–3x/2}Ce_xTiO_3$ ceramics sintered in nitrogen atmosphere. *J Mater Sci*: *Mater Electron* 2019, **30**: 1591–1599.

[389] Liu S, Tang B, Zhou MK, *et al*. Microwave dielectric characteristics of high permittivity $Ca_{0.35}Li_{0.25}Nd_{0.35}Ti_{1–x}(Zn_{1/3}Ta_{2/3})_xO_3$ ceramics (x = 0.00–0.12). *Ceram Int* 2019, **45**: 8600–8606.

[390] Xiong Z, Tang B, Luo FC, *et al*. Characterization of structure, chemical bond and microwave dielectric properties in $Ca_{0.61}Nd_{0.26}TiO_3$ ceramic substituted by chromium for titanium. *J Alloys Compd* 2020, **835**: 155249.

[391] Shi L, Peng R, Zhang HW, *et al*. Effects of Magnesium–tungsten co-substitution on crystal structure and microwave dielectric properties of $CaTi_{1–x}(Mg_{1/2}W_{1/2})_xO_3$ ceramics. *Ceram Int* 2021, **47**: 3354–3360.

[392] Zaman A, Uddin S, Mehboob N, *et al*. Structural investigation and improvement of microwave dielectric properties in $Ca(Hf_xTi_{1–x})O_3$ ceramics. *Phys Scr* 2020, **96**: 025701.

[393] Hu P, Jiao H, Wang CH, *et al*. Influence of thermal treatments on the low frequency conductivity and microwave dielectric loss of $CaTiO_3$ ceramics. *Mater Sci Eng*: *B* 2011, **176**: 401–405.

[394] Hsu CH, Chang CH. Microwave dielectric properties of new $(Ca_{0.8}Sr_{0.2})SnO_3$ ceramics. *Ceram Int* 2012, **38**: 4411–4413.

[395] Chen YC, Chen KC, Wu CY. Microwave dielectric properties of $(1−y)Nd_{1–2x/3}Ba_x(Mg_{0.5}Sn_{0.5})O_3–yCa_{0.8}Sr_{0.2}TiO_3$ ceramic. *J Mater Sci*: *Mater Electron* 2013, **24**: 819–826.

[396] Shi F, Fu GG, Xiao EC, *et al*. Lattice vibrational characteristics and dielectric properties of pure phase $CaTiO_3$ ceramic. *J Mater Sci*: *Mater Electron* 2020, **31**: 18070–18076.

[397] Tian CL, Yue ZX, Zhou YY. Microwave dielectric properties of $Ba[Ti_{0.4}Ga_{0.3}Nb_{0.3}(1−x)Sb_{0.3x}]O_3$ perovskite ceramics. *Mater Res Bull* 2013, **48**: 455–460.

[398] Liu F, Yuan CL, Liu XY, *et al*. Effects of structural characteristics on microwave dielectric properties of $(Sr_{0.2}Ca_{0.488}Nd_{0.208})Ti_{1–x}Ga_{4x/3}O_3$ ceramics. *Mater Res Bull* 2015, **70**: 678–683.

[399] Parida S, Rout SK, Subramanian V, *et al*. Structural, microwave dielectric properties and dielectric resonator antenna studies of $Sr(Zr_xTi_{1–x})O_3$ ceramics. *J Alloys Compd* 2012, **528**: 126–134.

[400] Wang JY, Zhou H, Liu JT, *et al*. Microstructure and dielectric tunable properties of $SrO(Sr_{1–x}Ba_xTiO_3)n$ microwave ceramics. *Ceram Int* 2012, **38**: 3503–3507.

[401] Zhang MW, Zhai JW, Shen B, *et al*. Microwave dielectric properties of low loss and highly tunable $Ba_{0.5}Sr_{0.5}Ti_{1-3y/2}W_yO_3$ ceramics. *J Mater Res* 2012, **27**: 910–914.

[402] Zhang JJ, Zhai JW, Wang JY. Structural and dielectric tunable properties of $Ba_{0.4}Sr_{0.6}Ti_{1-y}Si_yO_3$ microwave ceramics. *Sci China Technol Sci* 2012, **55**: 610–615.

[403] Tang LJ, Zhai JW, Shen B, *et al*. Property optimization of $Ba_{0.4}Sr_{0.6}TiO_3$–$BaMoO_4$ composite ceramics for tunable microwave applications. *Ceram Int* 2012, **38**: 4967–4971.

[404] Tang LJ, Zhai JW, Zhang HJ, *et al*. Microwave dielectric properties of tunable $Ba_{0.5}Sr_{0.5}TiO_3$ and scheelite $AMoO_4$ (A = Ba, Sr) composite ceramics. *J Alloys Compd* 2013, **551**: 556–561.

[405] Tang LJ, Wang JW, Zhai JW, *et al*. Dielectric tunable properties of $Ba_{0.5}Sr_{0.5}TiO_3$–$MgMoO_4$ composite ceramics for microwave applications. *J Mater Sci*: *Mater Electron* 2013, **24**: 2576–2580.

[406] Jiang HT, Zhai JW, Zhang MW, *et al*. Enhanced microwave dielectric properties of $Ba_{0.40}Sr_{0.60}TiO_3$–$Zr_{0.80}Sn_{0.20}TiO_4$ composite ceramics. *J Mater Sci* 2012, **47**: 2617–2623.

[407] Zhang QW, Zhai JW, Ben QQ, *et al*. Enhanced microwave dielectric properties of $Ba_{0.4}Sr_{0.6}TiO_3$ ceramics doping by metal Fe powders. *J Appl Phys* 2012, **112**: 104104.

[408] He YY, Zhao JY, Xu YB, *et al*. Microstructures and dielectric tunable properties of $Ba_{0.5}Sr_{0.5}TiO_3$–MgO–Mg_2TiO_4 composite ceramics. *J Mater Sci*: *Mater Electron* 2013, **24**: 2372–2378.

[409] He YY, Zhao JY, Xu YB, *et al*. Anomalous correlation between dielectric constant and tunability in (Ba,Sr)TiO_3–MgO–Mg_2SiO_4 composite ceramics. *J Am Ceram Soc* 2013, **96**: 1203–1208.

[410] Liu D, Pu YP, Shi X. Effects of Bi_2O_3 and $Cr_2Ti_3O_9$ co-doping on dielectric properties in $BaTiO_3$-based ceramics. *Vacuum* 2012, **86**: 1568–1571.

[411] Hu GX, Gao F, Liu LL, *et al*. Microstructure and dielectric properties of highly tunable $Ba_{0.6}Sr_{0.4}TiO_3$/MgO/Al_2O_3/ZnO composite. *J Alloys Compd* 2012, **518**: 44–50.

[412] Jiang K, Zhang JZ, Yu WL, *et al*. Manganese doping effects on interband electronic transitions, lattice vibrations, and dielectric functions of perovskite-type $Ba_{0.4}Sr_{0.6}TiO_3$ ferroelectric ceramics. *Appl Phys A* 2012, **106**: 877–884.

[413] Tseng CF, Lu SC. Microwave dielectric properties of $(Ba_{0.1}Mg_{0.9})(A_{0.05}Ti_{0.95})O_3$ (A = Zr, Sn) ceramics. *Ferroelectrics* 2013, **451**: 76–83.

[414] Liu F, Liu XY, Yuan CL, *et al*. Microstructures and microwave dielectric properties of $(1-x)(Sr_{0.4}Na_{0.3}La_{0.3})TiO_3$–$x$LnAlO$_3$ (Ln = Sm, Nd) ceramic systems. *J Eur Ceram Soc* 2015, **35**: 2091–2098.

[415] Xie WT, Jiang QX, Cao QL, *et al*. Effect of ZnO/WO_3 additives on sintering behavior and microwave dielectric properties of (Sr,Ca)TiO_3–(Sm,Nd)AlO_3 ceramics. *J Mater Sci*: *Mater Electron* 2018, **29**: 9745–9750.

[416] Singh J, Bahel S. Structural and dielectric properties of $(Ba_xMg_{1-x})(Ti_{0.95}Sn_{0.05})O_3$ (x = 0.025, 0.05, 0.075 and 0.1) solid solutions. *J Mater Sci*: *Mater Electron* 2019, **30**: 6500–6506.

[417] Ma PP, Liu XQ, Zhang FQ, *et al*. $Sr(Ga_{0.5}Nb_{0.5})_{1-x}Ti_xO_3$ low-loss microwave dielectric ceramics with medium dielectric constant. *J Am Ceram Soc* 2015, **98**: 2534–2540.

[418] Qu JJ, Liu F, Yuan CL, *et al*. Microwave dielectric properties of $0.2SrTiO_3$–$0.8Ca_{0.61}Nd_{0.26}Ti_{1-x}Al_{4x/3}O_3$ ceramics. *Mater Sci Eng*: *B* 2015, **191**: 15–20.

[419] Singh J, Bahel S. Synthesis and characterization of temperature stable low-loss $(1-x)Mg(Ti_{0.95}Sn_{0.05})O_3$–$(x)BaTiO_3$ ($0 \leqslant x \leqslant 0.1$) ceramics for microwave applications. *J Mater Sci* 2021, **56**: 10947–10964.

[420] Ullah B, Lei W, Cao QS, *et al*. Structure and microwave dielectric behavior of A-site-doped $Sr_{(1-1.5x)}Ce_xTiO_3$ ceramics system. *J Am Ceram Soc* 2016, **99**: 3286–3292.

[421] Tian CL, Yue ZX, Meng SQ, *et al*. Structures and microwave dielectric properties of $Ba[Ti_{1-x}(Co_{0.5}W_{0.5})_x]O_3$ (x = 0.40–0.90) perovskite ceramics. *J Am Ceram Soc* 2012, **95**: 1645–1650.

[422] Tian CL, Yue ZX, Zhou YY, *et al*. Crystal structures and microwave dielectric properties of Zn, W co-substituted $BaTiO_3$ perovskite ceramics. *J Solid State Chem* 2013, **197**: 242–247.

[423] Lin YJ, Wang SF, Chen SH, *et al*. Microwave dielectric properties of $(Ba_{1-x}Sr_x)(Mg_{0.5}W_{0.5})O_3$ ceramics. *Ceram Int* 2015, **41**: 8931–8935.

[424] Chen YC, Syu RY. Dielectric properties of $Ba_2Mg_{0.95}Zn_{0.05}WO_6$ ceramics at microwave frequency. *J Mater Sci*: *Mater Electron* 2016, **27**: 6979–6984.

[425] Bian JJ, Wu JY. Structure and microwave dielectric properties of B-site deficient double perovskite–$Ba[(Mg_{(1-x)/2}Y_{x/3}\square_{x/6})W_{1/2}]O_3$. *Ceram Int* 2016, **42**: 3290–3295.

[426] Ullah B, Lei W, Wang XW, *et al*. Structure instability and high microwave dielectric permittivity of nonstoichiometric $(Sr_{0.4}Ce_{0.4})_{1-x}Nd_xTi_{0.8}Mg_{0.2}O_3$ system for wireless communication. *J Materiomics* 2021, **7**: 25–33.

[427] Hu X, Huang XJ, Chen YH, *et al*. Phase evolution and microwave dielectric properties of $SrTiO_3$ added $ZnAl_2O_4$–Zn_2SiO_4–SiO_2 ceramics. *Ceram Int* 2020, **46**: 7050–7054.

[428] Liu F, Qu JJ, Yan HG, *et al*. Study on phase structures and compositions, microstructures, and dielectric characteristics of $(1-x)NdGaO_{3-x}Bi_{0.5}Na_{0.5}TiO_3$ microwave ceramic systems. *Ceram Int* 2020, **46**: 16185–16195.

[429] Jin X, Guo QH, Bian JJ. Structure and dielectric properties of A-site-deficient perovskite $Nd_{1-x/3}M_xNbO_3$ (M = Li, Ag; $0 \leqslant x \leqslant 0.20$) ceramics. *J Mater Sci* 2012, **47**: 6015–6024.

[430] Xiao M, Zhang QQ, Jia CR. The microstructure and properties of $Ag(Nb_{0.8}Ta_{0.2})_{1-x}(Mn_{0.5}W_{0.5})_xO_3$ ceramic system. *J Wuhan Univ Technol Mater Sci Ed* 2012, **27**:

735–739.

[431] Peng Y, Li LX, Cao LF, *et al*. Correlation between crystal structure and properties of ultra-high dielectric constant ceramics xSrCO$_3$–Bi$_2$O$_3$–Ag(Nb,Ta)O$_3$. *J Electroceramics* 2012, **28**: 209–213.

[432] Saleem M, Iqbal Y, Qin S, *et al*. Phase, microstructure and microwave dielectric properties of A-site deficient (La,Nd)$_{2/3}$TiO$_3$ perovskite ceramics. *Mater Sci Pol* 2015, **33**: 126–130.

[433] Zhang MM, Li LX, Xia WS, *et al*. Structure and properties analysis for MgTiO$_3$ and (Mg$_{0.97}$M$_{0.03}$)TiO$_3$ (M = Ni, Zn, Co and Mn) microwave dielectric materials. *J Alloys Compd* 2012, **537**: 76–79.

[434] Gogoi P, Sharma P, Pamu D. Microwave and broadband dielectric properties of Ni substituted MgTiO$_3$ ceramics. *J Mater Sci*: *Mater Electron* 2016, **27**: 9052–9060.

[435] Gogoi P, Singh LR, Pamu D. Characterization of Zn doped MgTiO$_3$ ceramics: An approach for RF capacitor applications. *J Mater Sci*: *Mater Electron* 2017, **28**: 11712–11721.

[436] Lin SH, Chen YB. Low dielectric loss characteristics of [(Mg$_{1-x}$Zn$_x$)$_{0.95}$Co$_{0.05}$]$_{1.02}$TiO$_{3.02}$ ceramics at microwave frequencies. *J Mater Sci*: *Mater Electron* 2017, **28**: 4154–4160.

[437] Li LX, Ding X, Liao QW. Structure and properties analysis for low-loss (Mg$_{1-x}$Co$_x$)TiO$_3$ microwave dielectric materials prepared by reaction-sintering method. *Ceram Int* 2012, **38**: 1937–1941.

[438] Gangwar RK, Singh SP, Choudhary M, *et al*. Microwave dielectric properties of (Zn$_{1-x}$Mg$_x$)TiO$_3$ (ZMT) ceramics for dielectric resonator antenna application. *J Alloys Compd* 2011, **509**: 10195–10202.

[439] Yu HT, Xue XM, Xu GL. Correlation between Sn substitution for Ti and microwave dielectric properties of magnesium titanate ceramics. *Int J Appl Ceram Technol* 2013, **10**: E186–E191.

[440] Santhosh Kumar T, Gogoi P, Perumal A, *et al*. Effect of cobalt doping on the structural, microstructure and microwave dielectric properties of MgTiO$_3$ ceramics prepared by semi alkoxide precursor method. *J Am Ceram Soc* 2014, **97**: 1054–1059.

[441] Gong ZJ, Wang ZF, Wang LX, *et al*. Microwave dielectric properties of high-Q Mg(Sn$_x$Ti$_{1-x}$)O$_3$ ceramics. *Electron Mater Lett* 2013, **9**: 331–335.

[442] Jia XB, Xu Y, Zhao P, *et al*. Structural dependence of microwave dielectric properties in ilmenite-type Mg(Ti$_{1-x}$Nb)O$_3$ solid solutions by Rietveld refinement and Raman spectra. *Ceram Int* 2021, **47**: 4820–4830.

[443] Wu HT, Jiang YS, Cui YJ, *et al*. Improvements in the sintering behavior and microwave dielectric properties of geikielite-type MgTiO$_3$ ceramics. *J Electron Mater* 2013, **42**: 445–451.

[444] Wang HP, Yang QH, Li DH, *et al*. Sintering behavior and microwave dielectric properties of MgTiO$_3$ ceramics doped with B$_2$O$_3$ by sol–gel method. *J Mater Sci Technol* 2012, **28**: 751–755.

[445] Tseng CF, Lu SC. Influence of SrTiO$_3$ modification on dielectric properties of Mg(Zr$_{0.05}$Ti$_{0.95}$)O$_3$ ceramics at microwave frequency. *Mater Sci Eng*: *B* 2013, **178**: 358–362.

[446] Yu HT, Cheng JL, Zhang WB, *et al*. Microwave dielectric properties of Mg(Zr$_{0.05}$Ti$_{0.95}$)O$_3$–SrTiO$_3$ ceramics. *J Mater Sci*: *Mater Electron* 2012, **23**: 572–575.

[447] Xue XM, Yu HT, Xu GL. Phase composition and microwave dielectric properties of Mg-excess MgTiO$_3$ ceramics. *J Mater Sci*: *Mater Electron* 2013, **24**: 1287–1291.

[448] Huang CL, Huang SH. Low-loss microwave dielectric ceramics in the (Co$_{1-x}$Zn$_x$)TiO$_3$ (x = 0–0.1) system. *J Alloys Compd* 2012, **515**: 8–11.

[449] Liou YC, Yang SL, Chu SY. Effects of MgO and Mg(OH)$_2$ on phase formation and properties of strontium-doped MgTiO$_3$ microwave dielectric ceramics. *J Alloys Compd* 2013, **576**: 161–169.

[450] Li H, Tang B, Li YX, *et al*. Effects of Mg$_{2.05}$SiO$_{4.05}$ addition on phase structure and microwave properties of MgTiO$_3$–CaTiO$_3$ ceramic system. *Mater Lett* 2015, **145**: 30–33.

[451] Tang B, Li YX, Li H, *et al*. Structure and microwave dielectric properties of (Zn$_{0.3}$Co$_{0.7}$)Ti$_{1-x}$Sn$_x$O$_3$ ceramics. *J Mater Sci*: *Mater Electron* 2015, **26**: 2795–2799.

[452] Huang XP, Liu F, Yuan CL, *et al*. Microstructures and microwave dielectric properties of Mg$_{n+1}$TinO$_{3n+1}$ ceramics with ultralow dielectric loss. *Mater Lett* 2016, **185**: 432–435.

[453] Chen CY, Peng ZJ, Xie LZ, *et al*. Effects of adding B$_2$O$_3$ on microwave dielectric properties of 0.9625MgTiO$_3$–0.0375(Ca$_{0.5}$Sr$_{0.5}$)TiO$_3$ composite ceramics. *Int J Appl Ceram Technol* 2020, **17**: 2545–2552.

[454] Yu T, Luo T, Yang QH, *et al*. Ultra-high quality factor of Mg$_6$Ti$_5$O$_{16}$-based microwave dielectric ceramics with temperature stability. *J Mater Sci*: *Mater Electron* 2021, **32**: 2547–2556.

[455] Chen KC, Chen YC, Chen MD. Microwave dielectric properties of Mg$_{1/3}$Nb$_{2/3}$SnO$_4$ ceramics. *Ferroelectr Lett Sect* 2012, **39**: 1–7.

[456] Bhuyan RK, Kumar TS, Pamu D, *et al*. Structural and microwave dielectric properties of Mg$_2$TiO$_4$ ceramics synthesized by mechanical method. *Int J Appl Ceram Technol* 2013, **10**: E18–E24.

[457] Bhuyan RK, Kumar TS, Goswami D, *et al*. Liquid phase effect of La$_2$O$_3$ and V$_2$O$_5$ on microwave dielectric properties of Mg$_2$TiO$_4$ ceramics. *J Electroceramics* 2013, **31**: 48–54.

[458] Bhuyan RK, Kumar TS, Goswami D, *et al*. Enhanced densification and microwave dielectric properties of Mg$_2$TiO$_4$ ceramics added with CeO$_2$ nanoparticles. *Mater Sci Eng*: *B* 2013, **178**: 471–476.

[459] Huang CL, Tseng YW, Chen JY, *et al*. Dielectric properties of high-Q (Mg$_{1-x}$Zn$_x$)$_{1.8}$Ti$_{1.1}$O$_4$ ceramics at microwave

frequency. *J Eur Ceram Soc* 2012, **32**: 2365–2371.

[460] Chen YB. Dielectric properties and crystal structure of Mg_2TiO_4 ceramics substituting Mg^{2+} with Zn^{2+} and Co^{2+}. *J Alloys Compd* 2012, **513**: 481–486.

[461] Cheng L, Liu P, Qu SX, *et al*. Microwave dielectric properties of Mg_2TiO_4 ceramics synthesized via high energy ball milling method. *J Alloys Compd* 2015, **623**: 238–242.

[462] Lyu XS, Li LX, Sun H, *et al*. A novel low-loss spinel microwave dielectric ceramic $CoZnTiO_4$. *J Mater Sci*: *Mater Electron* 2015, **26**: 8663–8666.

[463] Li H, Tang B, Li YX, *et al*. Relationships between Sn substitution for Ti and microwave dielectric properties of $Mg_2(Ti_{1-x}Sn_x)O_4$ ceramics system. *J Mater Sci*: *Mater Electron* 2015, **26**: 571–577.

[464] Chen YC, Syu RY. Enhancement quality factor of $ZnNiTiO_4$ microwave ceramics by substituting Ti^{4+} with Sn^{4+}. *J Mater Sci*: *Mater Electron* 2017, **28**: 673–678.

[465] Chen YC, Syu RY. Elucidating the microstructures and microwave dielectric properties of $ZnNiTiO_4$ ceramics. *J Mater Sci*: *Mater Electron* 2016, **27**: 8356–8362.

[466] Li H, Xiang R, Chen XQ, *et al*. Intrinsic dielectric behavior of Mg_2TiO_4 spinel ceramic. *Ceram Int* 2020, **46**: 4235–4239.

[467] Xiang R, Li H, Zhang PC, *et al*. Crystal structure and microwave dielectric properties of $Mg_2Ti_{1-x}Ga_{4/3x}O_4$ ($0.05 \leqslant x \leqslant 0.13$) ceramics. *Ceram Int* 2021, **47**: 8447–8452.

[468] Fang ZX, Tang B, Li YX, *et al*. Microstructures and microwave dielectric properties of $Na_{0.5}Nd_{0.2}Sm_{0.3}Ti_{1-x}Sn_xO_3$ ceramics (x = 0.00 to 0.50). *J Electron Mater* 2015, **44**: 4236–4242.

[469] Zhou L, Tang B, Zhang SR. Influence of Sn-substitution on microstructure and microwave dielectric properties of $Na_{1/2}Nd_{1/2}TiO_3$ ceramics. *J Mater Sci*: *Mater Electron* 2015, **26**: 424–428.

[470] Fang ZX, Tang B, Si F, *et al*. Effects of Zr-substitution on microwave dielectric properties of $Na_{0.5}Nd_{0.2}Sm_{0.3}Ti_{1-x}Zr_xO_3$ ceramics (x = 0.00–0.30). *J Electron Mater* 2016, **45**: 5198–5205.

[471] Fang ZX, Tang B, Zhang SR. Microwave dielectric properties of $Na_{1/2}Sm_{1/2}Ti_{1-x}(Cr_{1/2}Nb_{1/2})_xO_3$Ceramics ($x$ = 0–0.025). *IOP Conf Ser*: *Mater Sci Eng* 2017, **170**: 012029.

[472] Gan L, An SB, Yuan SF, *et al*. Sintering characteristics and microwave dielectric properties of $(1-x)Li_{0.5}Sm_{0.5}TiO_3$–$xNa_{0.5}Sm_{0.5}TiO_3$ (x = 0.35 to 0.45) ceramics. *J Electron Mater* 2019, **48**: 3624–3630.

[473] Zhou YY, Tian CL, Meng SQ, *et al*. Structural transitions and microwave dielectric properties of $Ba_{2-2x}Sr_{2x}SmSbO_6$ double perovskites. *J Am Ceram Soc* 2012, **95**: 1665–1670.

[474] Wu JY, Bian JJ. Structure stability and microwave dielectric properties of double perovskite ceramics–$Ba_2Mg_{1-x}Ca_xWO_6$ ($0.0 \leqslant x \leqslant 0.15$). *Ceram Int* 2012, **38**: 3217–3225.

[475] Chen YC, Wang YN, Syu RY. Effect of sintering temperature on microstructures and microwave dielectric properties of Ba_2MgWO_6 ceramics. *J Mater Sci*: *Mater Electron* 2016, **27**: 4259–4264.

[476] Diao CL, Wang CH, Luo NN, *et al*. First-principle calculation and assignment for vibrational spectra of $Ba(Mg_{1/2}W_{1/2})O_3$ microwave dielectric ceramic. *J Am Ceram Soc* 2013, **96**: 2898–2905.

[477] Li L, Zhang W, Chen XM, *et al*. Dielectric properties of $CaCu_3Ti_4O_{12}$, $Ba(Fe_{1/2}Nb_{1/2})O_3$, and $Sr(Fe_{1/2}Nb_{1/2})O_3$ giant permittivity ceramics at microwave frequencies. *J Appl Phys* 2012, **111**: 064108.

[478] Tay KW, Fu YP, Huang JF, *et al*. Effect of Bi_2O_3 and B_2O_3 additives on the sintering temperature, microstructure, and microwave dielectric properties for $Sm(Mg_{0.5}Ti_{0.5})O_3$ ceramics. *Ceram Int* 2011, **37**: 1025–1031.

[479] Chen YB. New dielectric material system of $Nd(Mg_{1/2}Ti_{1/2})O_3$–$SrTiO_3$ in the microwave frequency range. *J Alloys Compd* 2011, **509**: 2285–2288.

[480] Chen YC. Improving microwave dielectric properties of $La_{2.98/3}Sr_{0.01}(Mg_{0.5}Sn_{0.5})O_3$ ceramics with CuO additive. *Curr Appl Phys* 2012, **12**: 483–488.

[481] Hsu CH, Chang CH. Microwave dielectric properties of $Nd(Zn_{1/2}Ti_{1/2})O_3$ ceramics with V_2O_5 additives. *J Mater Eng Perform* 2013, **22**: 312–315.

[482] Chen YY, Chen YC, Liu HX, *et al*. Effect of Sm substitution on microwave dielectric properties of $Nd(Mg_{0.5}Sn_{0.5})O_3$ ceramics. *J Mater Sci*: *Mater Electron* 2013, **24**: 4600–4606.

[483] Chen YC, Yao SL, Wu CY. Microwave dielectric properties and microstructures of $Nd(Mg_{0.5-x}Co_xSn_{0.5})O_3$ ceramics. *J Mater Sci*: *Mater Electron* 2012, **23**: 1320–1326.

[484] Wang YN. Enhancing the microwave dielectric properties of $Nd(Mg_{0.5}Sn_{0.5})O_3$ ceramics by substituting Nd^{3+} with Ca^{2+}. *J Mater Sci*: *Mater Electron* 2013, **24**: 4510–4515.

[485] Chen YC, Wu CY. Effect of Sr substitution on microwave dielectric properties of $Nd(Mg_{0.5}Sn_{0.5})O_3$ ceramics. *Ceram Int* 2013, **39**: 1877–1883.

[486] Chen YC, Weng MZ, Chen YY. Influence of Ba^{2+} substitution on the microwave dielectric properties of $Nd(Mg_{0.5}Sn_{0.5})O_3$ ceramics. *J Mater Sci*: *Mater Electron* 2013, **24**: 2970–2975.

[487] Chen YC, Chen YY, Yao SL. Improved microwave dielectric properties of $Nd(Mg_{0.5}Sn_{0.5})O_3$ ceramics with Ni^{2+} substituting. *J Mater Sci*: *Mater Electron* 2013, **24**: 1150–1157.

[488] Chen YC, Chang KC, Yao SL. Improved microwave dielectric properties of $Nd(Mg_{0.5}Sn_{0.5})O_3$ ceramics by substituting Mg^{2+} with Zn^{2+}. *Ceram Int* 2012, **38**: 5377–5383.

[489] Chen YC, Tsai RJ, Wu CY. Microwave dielectric properties and microstructures of $Nd(Mg_{0.5}Sn_{0.5-x}Ti_x)O_3$ ceramics. *Ceram Int* 2012, **38**: 2927–2934.

[490] Chen YC, Chang KC, Tsai DY. A hybrid dielectric resonator antenna based upon novel complex perovskite microwave ceramic. *Ceram Int* 2013, **39**: 8043–8048.

[491] Li JM, Qiu T. Microwave dielectric properties of $Nd[(Zn_{1-x}Co_x)_{0.5}Ti_{0.5}]O_3$ ($0.025 \leqslant x \leqslant 0.1$) ceramics. *Ceram Int* 2012, **38**: 2597–2600.

[492] Li JM, Fan CG, Cheng ZX, *et al*. Influence of Zn nonstoichiometry on the phase structure, microstructure and microwave dielectric properties of $Nd(Zn_{0.5}Ti_{0.5})O_3$ ceramics. *J Alloys Compd* 2019, **793**: 385–392.

[493] Cao ZK, Xiao EC, Li XH, *et al*. Lattice vibrational characteristics, crystal structures and dielectric properties of non-stoichiometric $Nd_{(1+x)}(Mg_{1/2}Sn_{1/2})O_3$ ceramics. *J Materiomics* 2020, **6**: 476–484.

[494] Shi F, Xiao EC, Chen GH, *et al*. Lattice vibrational characteristics and structures-properties relationships of non-stoichiometric $Nd[Mg_{0.5}Sn_{0.5(1+x)}]O_3$ ceramics. *Appl Phys A* 2020, **126**: 1–14.

[495] Chen YC, Wang YN, Lee WC. Microstructures and microwave dielectric properties of $La_{1-x}B_x(Mg_{0.5}Sn_{0.5})O_3$ ceramics. *Curr Appl Phys* 2012, **12**: 726–731.

[496] Chen YC. Improved microwave dielectric properties of $La(Mg_{0.5}Sn_{0.5})O_3$ ceramics with Yb^{3+} doping. *Int J Appl Ceram Technol* 2012, **9**: 606–614.

[497] Wang YN, Chen MD. Improved microwave dielectric properties of $La(Mg_{0.5}Sn_{0.5})O_3$ ceramic with Ba^{2+} substitution. *J Mater Sci*: *Mater Electron* 2013, **24**: 3730–3735.

[498] Remya GR, Dhwajam DB, Thomas JK, *et al*. Dielectric and optical properties of ZnO and Eu_2O_3 doped $Pr_{0.22}Y_{0.78}TiTaO_6$ ceramic. *J Mater Sci*: *Mater Electron* 2012, **23**: 370–375.

[499] Chen YY, Chen YC, Chen MD. Tuning the microwave dielectric properties of $La(Mg_{0.4}Sr_{0.1}Sn_{0.5})O_3$ by introducing $Ca_{0.8}Sr_{0.2}TiO_3$. *J Mater Sci*: *Mater Electron* 2013, **24**: 3126–3131.

[500] Tseng CF, Huang CC. Microwave dielectric properties of $(1-x)Nd(Co_{1/2}Ti_{1/2})O_3$–$x(Ca_{0.8}Sr_{0.2})TiO_3$ composite ceramics. *J Mater Sci* 2012, **47**: 3982–3988.

[501] Wang YN, Chen MD. Improved microwave dielectric properties of $La(Mg_{0.5}Sn_{0.5})O_3$ ceramic with Sr^{2+} Substitution. *Ferroelectr Lett Sect* 2013, **40**: 121–129.

[502] Li JM, Qiu T. Microwave dielectric properties of $(1-x)Ca_{0.6}La_{0.267}TiO_3$–$xCa(Sm_{0.5}Nb_{0.5})O_3$ ceramics. *Ceram Int* 2012, **38**: 4331–4335.

[503] Fan J, Zhao Q, Du K, *et al*. Lattice structure and microwave dielectric properties of $La[Al_{1-x}(Mg_{0.5}Ti_{0.5})_x]O_3$ (x = 0–0.2)-based ceramics. *J Am Ceram Soc* 2020, **103**: 3231–3237.

[504] Yang HC, Zhang SR, Yang HY, *et al*. Vibrational spectroscopic and crystal chemical analyses of double perovskite Y_2MgTiO_6 microwave dielectric ceramics. *J Am Ceram Soc* 2020, **103**: 1121–1130.

[505] Chen CT, Huang CY, Lin YM, *et al*. Structure and microwave dielectric property relations in Barium cobalt magnesium niobate ceramics. *Jpn J Appl Phys* 2011, **50**: 091503.

[506] Wang SF, Wang YR, Liu CY, *et al*. Microwave dielectric properties of multi-ions $Ba(Zn,Ta)O_3$-based perovskite ceramics. *Ceram Int* 2012, **38**: 1127–1132.

[507] Ning PF, Li LX, Zhang P, *et al*. Raman scattering, electronic structure and microwave dielectric properties of $Ba([Mg_{1-x}Zn_x]_{1/3}Ta_{2/3})O_3$ ceramics. *Ceram Int* 2012, **38**: 1391–1398.

[508] Chen CT, Huang CY, Lin HJ, *et al*. Effect of small amount of cobalt substitution on structure and microwave dielectric properties of Barium magnesium niobate ceramics. *J Eur Ceram Soc* 2012, **32**: 2373–2380.

[509] Sun TL, Li L, Mao MM, *et al*. Effects of postdensification annealing on microwave dielectric properties of $Ba([Mg_{1-x}Co_x]_{1/3}Nb_{2/3})O_3$ ceramics. *Int J Appl Ceram Technol* 2013, **10**: E210–E218.

[510] Ma PP, Yi L, Liu XQ, *et al*. Effects of postdensification annealing upon microstructures and microwave dielectric characteristics in $Ba((Co_{0.6-x/2}Zn_{0.4-x/2}Mg_x)_{1/3}Nb_{2/3})O_3$ ceramics. *J Am Ceram Soc* 2013, **96**: 3417–3424.

[511] Ma PP, Yi L, Liu XQ, *et al*. Effects of Mg substitution on order/disorder transition, microstructure, and microwave dielectric characteristics of $Ba((Co_{0.6}Zn_{0.4})_{1/3}Nb_{2/3})O_3$ complex perovskite ceramics. *J Am Ceram Soc* 2013, **96**: 1795–1800.

[512] Diao CL, Shi F. Effect of sintering temperature on dielectric properties, vibrational modes and crystal structures of $Ba[(Ni_{0.7}Zn_{0.3})_{1/3}Nb_{2/3}]O_3$ ceramics. *J Mater Sci* 2012, **47**: 5438–5445.

[513] Wang J, Lu WZ, Lei W. Effects of Ba deficiency on ion ordering, grain growth, and microwave dielectric properties of $Ba_{1-x}Zn_{1/3}Nb_{2/3}O_3$ ceramics. *Jpn J Appl Phys* 2012, **51**: 041501.

[514] Diao CL, Shi F. Correlation among dielectric properties, vibrational modes, and crystal structures in $Ba[Sn_xZn_{(1-x)/3}Nb_{2(1-x)/3}]O_3$ solid solutions. *J Phys Chem C* 2012, **116**: 6852–6858.

[515] Shi F, Diao CL. Evaluation of dielectric properties, vibration modes, and crystal structures in $Ba[Zn_{1-x/3}Ni_{x/3}Nb_{2/3}]O_3$ ceramics. *Metall Mater Trans A* 2013, **44**: 381–387.

[516] Fu MS, Ni L, Chen XM. Abnormal variation of microwave dielectric properties in A/B site co-substituted $(Ca_{1-0.3x}La_{0.2x})[(Mg_{1/3}Ta_{2/3})_{1-x}Ti_x]O_3$ complex perovskite ceramics. *J Eur Ceram Soc* 2013, **33**: 813–823.

[517] Sun TL, Mao MM, Chen XM. Structure and microwave dielectric properties of $Ba[(Mg_{1-x}Ni_x)_{1/3}Nb_{2/3}]O_3$ ceramics. *Mater Res Bull* 2015, **72**: 291–298.

[518] Sindam B, James Raju KC. Influence of sintering temperature on microwave dielectric properties, structure and lattice modes of $Ba(Zn_{1/3}Ta_{2/3})O_3$ resonators. *J Mater Sci*: *Mater Electron* 2015, **26**: 3997–4004.

[519] Sun TL, Zhao YF, Chen XM. Improvement of microwave dielectric properties for $Ba(Ni_{1/3}Nb_{2/3})O_3$ ceramics by

Zr-substitution. *Ceram Int* 2015, **41**: 5872–5880.

[520] Sun TL, Chen XM. Tailoring the order-disorder transition and microwave dielectric properties of $Ba[(Ni_{0.6}Zn_{0.4})_{1/3}Nb_{2/3}]O_3$ ceramics by Mg-substitution. *Mater Chem Phys* 2015, **165**: 142–149.

[521] Wang ZF, Huang BY, Wang LX, *et al*. Low loss $(Ba_{1-x}Sr_x)(Co_{1/3}Nb_{2/3})O_3$ solid solution: Phase evolution, microstructure and microwave dielectric properties. *J Mater Sci*: *Mater Electron* 2015, **26**: 4273–4279.

[522] Zhou XH, Zhang YQ, Yang XS, *et al*. Effects of Y_2O_3 substitution on microwave dielectric properties of $Ba(Co_{0.6}Zn_{0.38})_{1/3}Nb_{2/3}O_3$ ceramics. *J Mater Sci*: *Mater Electron* 2015, **26**: 7683–7689.

[523] Zhang YQ, Zhou XH, Yang XS, *et al*. Effects of Y_2O_3/CeO_2 co-doping on microwave dielectric properties of $Ba(Co_{0.6}Zn_{38})_{1/3}Nb_{2/3}O_3$ ceramics. *J Alloys Compd* 2016, **679**: 247–253.

[524] Rodrigues JEFS, Castro PJ, Pizani PS, *et al*. Structural ordering and dielectric properties of $Ba_3CaNb_2O_9$-based microwave ceramics. *Ceram Int* 2016, **42**: 18087–18093.

[525] Ni LZ, Li LX, Du MK. Ultra-high-*Q* and wide temperature stable $Ba(Mg_{1/3}Ta_x)O_3$ microwave dielectric ceramic for 5G-oriented dielectric duplexer adhibition. *J Alloys Compd* 2020, **844**: 156106.

[526] Jinga SI, Stoleriu S, Busuioc C. Microwave dielectric properties of $Ba(Zn_{1/3}Ta_{2/3})O_3$ ceramics doped with Nb_2O_5, MnO_2 or V_2O_3. *Mater Res Bull* 2012, **47**: 3713–3718.

[527] Wang ZF, Huang BY, Wang LX, *et al*. Sintering characteristics and microwave dielectric properties of $Ba(Co_{1/3}Nb_{2/3})O_3$–MnO_2 ceramics. *J Mater Sci*: *Mater Electron* 2015, **26**: 1107–1112.

[528] Tang B, Fang ZX, Li YX, *et al*. Microwave dielectric properties of $Ba(Co_{0.56}Y_{0.04}Zn_{0.35})_{1/3}Nb_{2/3+x}O_3$ ($x = -0.004 \sim 0.008$) ceramics. *J Mater Sci*: *Mater Electron* 2015, **26**: 6585–6591.

[529] Sindam B, James Raju KC. Microwave dielectric properties of $Ba(Zn_{1/3}Ta_{2/3})O_3$ for application in high power waveguide window. *Eur Phys J B* 2016, **89**: 92.

[530] Peng S, Xu JM, Li H. Microstructure and microwave dielectric properties of $Ba([Mg_{1-x}Zn_x]_{1/3}Ta_{2/3})O_3$ solid solution ceramics. *J Mater Sci*: *Mater Electron* 2020, **31**: 20423–20430.

[531] Peng S, Wu MQ, Xu JM, *et al*. Effect of La_2O_3 addition on the microwave dielectric properties of $Ba(Mg_{1/3}Ta_{2/3})O_3$ ceramics. *J Mater Sci*: *Mater Electron* 2017, **28**: 3349–3355.

[532] Peng S, Xu JM, Li F. Influence of Ca^{2+} substitution for Ba^{2+} on the crystal structure and microwave dielectric properties of $Ba_{1-x}Ca_x(Mg_{1/3}Ta_{2/3})O_3$ ceramics. *J Mater Sci*: *Mater Electron* 2020, **31**: 15822–15828.

[533] Peng S, Wu MQ, Xu JM, *et al*. Microwave dielectric properties of $Ba[Mg_{1-x/3}Sn_xTa_{2(1-x)/3}]O_3$ (x = 0–0.25) ceramics. *J Mater Sci*: *Mater Electron* 2017, **28**: 174–179.

[534] Ni LZ, Li LX, Du MK, *et al*. Wide temperature stable $Ba(Mg_xTa_{2/3})O_3$ microwave dielectric ceramics with ultra-high-*Q* applied for 5G dielectric filter. *Ceram Int* 2021, **47**: 1034–1039.

[535] Guevarra J, van Smaalen S, Rotiroti N, *et al*. Crystal structure of $Ca_5Nb_5O_{17}$. *J Solid State Chem* 2005, **178**: 2934–2941.

[536] Joseph T, Anjana PS, Letourneau S, *et al*. Structure and microwave dielectric properties of $Ca_5A_4TiO_{17}$ (A = Nb, Ta) ceramics. *Mater Chem Phys* 2010, **121**: 77–82.

[537] Manan A, Iqbal Y. Influence of Sm substitution on the phase, microstructure and microwave dielectric properties of $SrLa_4Ti_5O_{17}$. *J Mater Sci*: *Mater Electron* 2011, **22**: 1848–1854.

[538] Iqbal Y, Manan A, Reaney IM. Low loss $Sr_{1-x}Ca_xLa_4Ti_5O_{17}$ microwave dielectric ceramics. *Mater Res Bull* 2011, **46**: 1092–1096.

[539] Iqbal Y, Manan A. Phase, microstructure and microwave dielectric properties of Zr-doped $SrLa_4Ti_{5-x}Zr_xO_{17}$. *J Mater Sci*: *Mater Electron* 2012, **23**: 536–541.

[540] Li CC, Wei XY, Yan HX, *et al*. Microwave dielectric properties of CaO–La_2O_3–Nb_2O_5–TiO_2 ceramics. *J Mater Sci*: *Mater Electron* 2013, **24**: 1947–1954.

[541] Li CC, Wei XY, Yan HX, *et al*. Microwave dielectric properties of $La_3Ti_2TaO_{11}$ ceramics with perovskite-like layered structure. *J Eur Ceram Soc* 2012, **32**: 4015–4020.

[542] Manan A, Reaney IM. The effect of processing conditions on the phase, microstructure and dielectric properties of $SrCa_4Nb_4TiO_{17}$ and $Ca_5Nb_4TiO_{17}$ microwave ceramics. *Mater Sci Pol* 2012, **30**: 98–104.

[543] Iqbal Y, Muhammad R. Phase, microstructure, and microwave dielectric properties of $NaCa_{4-x}Sr_xNb_5O_{17}$ (x = 0 to 4) ceramics. *J Electron Mater* 2013, **42**: 452–457.

[544] Muhammad R, Iqbal Y. Preparation and characterization of K-substituted $NaCa_4Nb_5O_{17}$ microwave dielectric ceramics. *J Mater Sci*: *Mater Electron* 2013, **24**: 2322–2326.

[545] Rejini R, Subodh G, Sebastian MT. $Ca_4La_2Ti_5O_{17}$: A novel low loss dielectric ceramics in the CaO–La_2O_3–TiO_2 system. *J Mater Sci*: *Mater Electron* 2008, **19**: 1153–1155.

[546] Chen GH, Di JC, Xu HR, *et al*. Microwave dielectric properties of $Ca_4La_2Ti_{5-x}(Mg_{1/3}Nb_{2/3})_xO_{17}$ ceramics. *J Am Ceram Soc* 2012, **95**: 1394–1397.

[547] Di JC, Chen GH, Hou MZ, *et al*. Low loss and middle permittivity of $(1-x)Ca_4La_2Ti_5O_{17-x}NdAlO_3$ dielectric resonators with near-zero temperature coefficient of the resonant frequency. *J Mater Sci* 2012, **47**: 2271–2277.

[548] Chen GH, Di JC, Li M, *et al*. Synthesis, microstructure and microwave dielectric properties of $Ca_{4-x}Mg_xLa_2Ti_5O_{17}$ ceramics. *J Mater Sci*: *Mater Electron* 2012, **23**: 746–752.

[549] Fang L, Li CC, Peng XY, *et al*. $Sr_{4-m}La_mTi_{m-1}Ta_{4-m}O_{12}$ (m = 1, 2, 3): A novel series of $A_4B_3O_{12}$-type microwave ceramics with a high Q and low τ_f. *J Am Ceram Soc* 2010, **93**: 1884–1887.

[550] Fang L, Li CC, Peng XY, *et al*. Two novel $A_4B_3O_{12}$-type microwave ceramics with high-*Q* and near-zero τ_f. *J Mater Res* 2010, **25**: 1239–1242.

[551] Suresh MK, John A, Thomas JK, *et al*. Structural, spectroscopic and dielectric investigations on $Ba_8Zn(Nb_{6-x}Sb_x)O_{24}$ microwave ceramics. *Mater Res Bull* 2010, **45**: 1389–1395.

[552] Suresh MK, John A, Thomas JK, *et al*. Structural analysis and properties of thermally stable $Ba_8Mg(Nb_{6-x}Sb_x)O_{24}$ microwave ceramics. *J Alloys Compd* 2011, **509**: 2401–2406.

[553] Solomon S, Suresh MK, Thomas JK, *et al*. Synthesis, structural analysis and dielectric properties of $Ba_8(Mg_{1-x}Zn_x)Nb_6O_{24}$ hexagonal perovskites. *Ceram Int* 2012, **38**: 6487–6494.

[554] Fang L, Su CX, Wei ZH, *et al*. Phase structure, band gap and microwave dielectric properties of $Ba_8Ti_3Nb_{4-x}Sb_xO_{24}$ ceramics. *Ceram Int* 2013, **39**: 579–583.

[555] Tian CL, Yue ZX, Zhou YY. Microstructures and microwave dielectric properties of $Ba_4LiNb_3O_{12}$–$BaWO_4$ composite ceramics. *Mater Sci Eng*: *B* 2013, **178**: 178–182.

[556] Zhou HF, Liu XB, Chen XL, *et al*. $Ba_4LiNb_{3-x}Sb_xO_{12}$: Phase evolution, microstructure and optimized microwave dielectric properties. *Mater Lett* 2013, **96**: 199–202.

[557] Tang Y, Fang WS, Fang L, *et al*. Phase transformation and microwave dielectric properties of $Ba_4LiTa_{3-x}Sb_xO_{12}$. *Ceram Int* 2015, **41**: 6653–6656.

[558] Liao W, Fang L, Xiang F, *et al*. Effect of Sb^{5+} substitution on the dielectric properties of $Ba_3LiTa_3Ti_5O_{21}$ ceramics. *J Mater Sci*: *Mater Electron* 2013, **24**: 272–276.

[559] Fang L, Liao W, Wu MX, *et al*. Microwave dielectric properties of $Ba_3LiNb_{3-x}Sb_xTi_5O_{21}$ (x = 0−3) ceramics. *Mater Lett* 2012, **76**: 73–76.

[560] Fang L, Wu MX, Liu QW, *et al*. High ε_r and low loss microwave dielectric ceramics $Ba_3LiNb_{3-x}Ta_xTi_5O_{21}$. *Mater Chem Phys* 2012, **136**: 599–603.

[561] Wang KG, Zhou HF, Luan XW, *et al*. Microwave dielectric properties of $LiSmTa_4O_{12}$ ceramics with A-site deficient perovskite structure. *Mater Lett* 2020, **274**: 128020.

[562] Fan XC, Chen XM, Liu XQ. Structural dependence of microwave dielectric properties of $SrRAlO_4$ (R = Sm, Nd, La) ceramics: Crystal structure refinement and infrared reflectivity study. *Chem Mater* 2008, **20**: 4092–4098.

[563] Fan XC, Mao MM, Chen XM. Microstructures and microwave dielectric properties of the $CaSmAlO_4$-based ceramics. *J Am Ceram Soc* 2008, **91**: 2917–2922.

[564] Yuan HX, Chen XM, Mao MM. Structure and microwave dielectric characteristics of $Ca_{1+x}Nd_{1-x}Al_{1-x}Ti_xO_4$ ceramics. *J Am Ceram Soc* 2009, **92**: 2286–2290.

[565] Mao MM, Fan XC, Chen XM. Effect of A-site ionic radius on the structure and microwave dielectric characteristics of $Sr_{1+x}Sm_{1-x}Al_{1-x}Ti_xO_4$ ceramics. *Int J Appl Ceram Technol* 2010, **7**: E156–E162.

[566] Zhang C, Yi L, Chen XM. Improvement of microwave dielectric characteristics in $SrNdAlO_4$ ceramics by Ca-substitution. *Ceram Int* 2014, **40**: 6077–6082.

[567] Xiao Y, Chen XM, Liu XQ. Microstructures and microwave dielectric characteristics of $CaRAlO_4$ (R = Nd, Sm, Y) ceramics with tetragonal K_2NiF_4 structure. *J Am Ceram Soc* 2004, **87**: 2143–2146.

[568] Mao MM, Chen XM. Infrared reflectivity spectra and microwave dielectric properties of $(Sr_{1-x}Ca_x)SmAlO_4$ ($0 \leqslant x \leqslant 1$) ceramics. *Int J Appl Ceram Technol* 2011, **8**: 1023–1030.

[569] Mao MM, Chen XM, Liu XQ. Structure and microwave dielectric properties of solid solution in $SrLaAlO_4$–Sr_2TiO_4 system. *J Am Ceram Soc* 2011, **94**: 3948–3952.

[570] Mao MM, Liu XQ, Chen XM. Structural evolution and its effects on dielectric loss in $Sr_{1+x}Sm_{1-x}Al_{1-x}Ti_xO_4$ microwave dielectric ceramics. *J Am Ceram Soc* 2011, **94**: 2506–2511.

[571] Liu B, Yi L, Liu XQ, *et al*. Structure and microwave dielectric properties of $SrSmAlO_4$–Sr_2TiO_4 solid solutions. *J Electroceramics* 2015, **34**: 114–121.

[572] Liu B, Li L, Liu XQ, *et al*. Structural evolution of $SrLaAl_{1-x}(Zn_{0.5}Ti_{0.5})_xO_4$ ceramics and effects on their microwave dielectric properties. *J Mater Chem C* 2016, **4**: 4684–4691.

[573] Ren GR, Zhu JY, Li L, *et al*. $SrLa(R_{0.5}Ti_{0.5})O_4$ (R = Mg, Zn) microwave dielectric ceramics with complex K_2NiF_4-type layered perovskite structure. *J Am Ceram Soc* 2017, **100**: 2582–2589.

[574] Yan H, Chen GY, Li L, *et al*. Microwave dielectric properties of $SrLa[Ga_{1-x}(Mg_{0.5}Ti_{0.5})_x]O_4$ and $SrLa[Ga_{1-x}(Zn_{0.5}Ti_{0.5})_x]O_4$ (x = 0.2–0.8) ceramics. *Int J Appl Ceram Technol* 2020, **17**: 790–796.

[575] Manan A, Ullah R, Iqbal Y, *et al*. Tailoring the microwave dielectric properties of $Sr_{0.6}Ca_{0.4}LaAlO_4$ ceramic by TiO_2 addition. *J Aust Ceram Soc* 2020, **56**: 1013–1019.

[576] Liu B, Li L, Liu XQ, *et al*. $Sr_{n+1}Ti_nO_{3n+1}$ (n = 1, 2) microwave dielectric ceramics with medium dielectric constant and ultra-low dielectric loss. *J Am Ceram Soc* 2017, **100**: 496–500.

[577] Yuan ZQ, Liu B, Liu XQ, *et al*. Structure and microwave dielectric characteristics of $Sr(La_{1-x}Sm_x)_2Al_2O_7$ ceramics. *RSC Adv* 2016, **6**: 96229–96236.

[578] Liu B, Liu XQ, Chen XM. $Sr_2LaAlTiO_7$: A new Ruddlesden–Popper compound with excellent microwave dielectric properties. *J Mater Chem C* 2016, **4**: 1720–1726.

[579] Yi L, Li L, Liu XQ, *et al*. Structure evolution and enhanced microwave dielectric characteristics of $(Sr_{1-x}Ca_x)La_2Al_2O_7$ ceramics. *J Am Ceram Soc* 2014, **97**: 3531–3536.

[580] Yi L, Liu XQ, Li L, *et al*. $SrLn_2Al_2O_7$ (Ln = La, Nd, Sm) microwave dielectric ceramic new materials. *Int J Appl Ceram Technol* 2013, **10**: E177–E185.

[581] Dias A, Viegas JI, Moreira RL. Synthesis and μ-Raman scattering of Ruddlesden–Popper ceramics $Sr_3Ti_2O_7$, $SrLa_2Al_2O_7$ and $Sr_2LaAlTiO_7$. *J Alloys Compd* 2017, **725**: 77–83.

[582] Hameed I, Liu B, Li L, *et al*. $(Sr_{1-x}Ca_x)_2TiO_4$ microwave

dielectric ceramics with R-P structure (x = 0–0.15). *Int J Appl Ceram Technol* 2019, **16**: 2040–2046.

[583] Liu B, Huang YH, Song KX, *et al*. Structural evolution and microwave dielectric properties in $Sr_2(Ti_{1-x}Sn_x)O_4$ ceramics. *J Eur Ceram Soc* 2018, **38**: 3833–3839.

[584] Hameed I, Wu SY, Li L, *et al*. Structure and microwave dielectric characteristics of $Sr_2[Ti_{1-x}(Al_{0.5}Nb_{0.5})_x]O_4$ ($x \leqslant$ 0.50) ceramics. *J Am Ceram Soc* 2019, **102**: 6137–6146.

[585] Xie MQ, Song XQ, Du K, *et al*. Improved microwave dielectric properties of the $(Sr_{1-3x/2}La_x)_2Ti_{1-y}Ce_yO_4$ ceramics. *J Mater Sci*: *Mater Electron* 2020, **31**: 13541–13548.

[586] Dai QL, Zuo RZ. A novel ultralow-loss Sr_2CeO_4 microwave dielectric ceramic and its property modification. *J Eur Ceram Soc* 2019, **39**: 1132–1136.

[587] Wang Y, Tang TL, Li MX, *et al*. $Ce_{0.75}Y_{0.25}O_{1.875}$: New temperature-stable microwave dielectric ceramics with high Q values for microwave application. *Ceram Int* 2020, **46**: 6984–6986.

[588] Ullah A, Liu HX, Manan A, *et al*. Microwave dielectric properties of $Bi_2(Li_{0.5}Ta_{1.5})O_7$–$TiO_2$-based ceramics for 5G cellular base station resonator application. *Ceram Int* 2021, **47**: 8416–8423.

[589] Wang ZJ, Chen Y. Structures and microwave dielectric properties of Ti-doped CeO_2 ceramics with a near-zero temperature coefficient of resonant frequency. *J Alloys Compd* 2021, **854**: 157270.

[590] Du C, Guo HH, Zhou D, *et al*. Dielectric resonator antennas based on high quality factor $MgAl_2O_4$ transparent dielectric ceramics. *J Mater Chem C* 2020, **8**: 14880–14885.

[591] Qin TY, Zhong CW, Qin Y, *et al*. The structure evolution and microwave dielectric properties of $MgAl_{2-x}(Mg_{0.5}Ti_{0.5})_xO_4$ solid solutions. *Ceram Int* 2020, **46**: 19046–19051.

[592] Liu B, Song KX. Vibrational spectroscopy and microwave dielectric properties of two novel $Ca_3Ln_2W_2O_{12}$ (Ln = La, Sm) tungstate ceramics. *Mater Res Bull* 2021, **133**: 111022.

[593] Hu S, Zhou HF, Zhou XJ, *et al*. Phase structure, sintering behaviour and microwave dielectric properties of Ln_2MoO_6 (Ln = La and Y) ceramics. *Ceram Int* 2020, **46**: 24552–24556.

[594] Kim E, Huang K, Jegelka S, *et al*. Virtual screening of inorganic materials synthesis parameters with deep learning. *npj Comput Mater* 2017, **3**: 53.

[595] Raccuglia P, Elbert KC, Adler PDF, *et al*. Machine-learning-assisted materials discovery using failed experiments. *Nature* 2016, **533**: 73–76.

[596] Weng BC, Song ZL, Zhu RL, *et al*. Simple descriptor derived from symbolic regression accelerating the discovery of new perovskite catalysts. *Nat Commun* 2020, **11**: 3513.

[597] Kim C, Pilania G, Ramprasad R. Machine learning assisted predictions of intrinsic dielectric breakdown strength of ABX_3 perovskites. *J Phys Chem C* 2016, **120**: 14575–14580.

[598] Xue D, Balachandran PV, Yuan R, *et al*. Accelerated search for $BaTiO_3$-based piezoelectrics with vertical morphotropic phase boundary using Bayesian learning. *PNAS* 2016, **113**: 13301–13306.

[599] Sun YT, Bai HY, Li MZ, *et al*. Machine learning approach for prediction and understanding of glass-forming ability. *J Phys Chem Lett* 2017, **8**: 3434–3439.

[600] Kim C, Pilania G, Ramprasad R. From organized high-throughput data to phenomenological theory using machine learning: The example of dielectric breakdown. *Chem Mater* 2016, **28**: 1304–1311.

[601] Qin JC, Liu ZF, Ma MS, *et al*. Machine learning approaches for permittivity prediction and rational design of microwave dielectric ceramics. *J Materiomics* 2021, https://doi.org/10.1016/j.jmat.2021.02.012.

[602] Qin J, Liu Z, Ma M, *et al*. Structure and microwave dielectric properties of gillespite-type $ACuSi_4O_{10}$ (A = Ca, Sr, Ba) ceramics and quantitative prediction of the $Q \times f$ value via machine learning. *ACS Appl Mater Interfaces* 2021, **13**: 17817–17826.